



UNIVERSITÀ  
DEGLI STUDI  
FIRENZE

DIPARTIMENTO DI  
MEDICINA Sperimentale  
E Clinica

## **DOTTORATO DI RICERCA IN SCIENZE BIOMEDICHE**

**CICLO XXIX**

**COORDINATORE Prof. Persio Dello Sbarba**

**Novel molecular tools in cancer therapy: diagnostic and therapeutic applications  
of antibodies targeting ion channels and receptors.**

Settore Scientifico Disciplinare MED/04

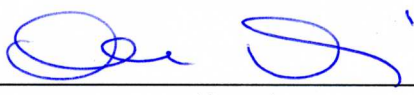
**Dottorando**

Dott. Duranti Claudia

  
(firma)

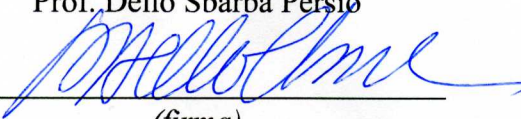
**Tutore**

Prof. Arcangeli Annarosa

  
(firma)

**Coordinatione**

Prof. Dello Sbarba Persio

  
(firma)

Anni 2013/2016

**ABSTRACT**

Immunotherapy has had a revolutionary impact on cancer treatment, providing valuable tools to be used in combination or as an alternative to chemotherapy (Weiner G.J., 2015).

Such wide success has been demonstrated by the fact that, since 1997, twelve monoclonal antibodies have been approved by the FDA for the treatment of a variety of solid tumors and haematological malignancies, along with an increasing number of new antibodies that are now being tested at different stages of clinical trials ([ClinicalTrials.gov](http://ClinicalTrials.gov)). Nevertheless, there are limitations to the use of monoclonal antibodies mainly due to their big size, which is detrimental especially for their applications in clinics and diagnostics. For these reasons, the arise of recombinant antibodies, which conjugate small size with antigen specificity has represented a big achievement in the oncological setting.

Another crucial point is the identification of cell antigens, which can be exploited to target cancer cells. To this purpose, we have focused on ionotropic Glutamate Receptor 4 (iGluR4), which is involved in many CNS pathological conditions and, moreover, has recently emerged to be implicated in many aspects of cancer progression (Stepulak A. et al., 2011; Stepulak A. et al., 2014; Ribeiro MP *et al.*, 2016). We have also focused on hERG1 voltage-gated ion channel, that it is known to be a role player in cancer progression (Bianchi L. *et al.*, 1998; Lastraioli E. *et al.*, 2015). More recently, it has emerged as a novel target for cancer therapy and as a marker for patients' stratification (Arcangeli A. *et al.*, 2009; Pointer KB *et al.*, 2016). Moreover, it has been demonstrated that hERG1 forms complexes in particular with  $\beta 1$  subunit of integrin receptors, thus mediating its effects in cancer cell behavior (Crociani et al. 2013).

The present work has focused on developing new antibodies, that have demonstrated their potential from a diagnostic or a therapeutic point of view.

We have produced two clones B5 and C4 of a monoclonal antibody directed against ionotropic Glutamate Receptor 4 (iGluR4), providing evidences that this molecule is able to recognize the antigen, also in a pathological scenario such as that of *tuberous sclerosis complex* (TSC) disease. Moreover, C4 anti-iGluR4 clone has emerged as a

possible positive allosteric modulator of the receptor; such behavior will be better characterized in the future, to exploit its potential application as a channel regulator (Stepulak A. et al., 2014).

We are also assembling a construct for the production of a scFv-iGluR4 directed against the same antigen as the monoclonal antibody, to overcome the problems related to the passage of the blood brain barrier (BBB). In fact, it is known that recombinant protein therapeutics are too large to cross the BBB, however, recombinant proteins can be reengineered as BBB-penetrating IgG fusion proteins, where the IgG part is a genetically engineered monoclonal antibody (MAb) (Pardridge WM and Boado RJ, 2012). The recombinant antibody we have produced will be conjugated with NPs (already capable to cross an *in vitro* model of BBB), to set up a *drug-delivery system*.

In parallel, we have developed a *single-chain variable fragment* antibody, scFv-hERG1-G3 (scFv-hERG1 construct), that has already been validated, after labelling with Alexa 488 fluorophore, as a tool for optical *in vivo* imaging (Lastraioli E. et al., 2016). Moreover, we have produced a new antibody scFv-hERG1-D8-Cys (scFv-hERG1-Cys construct) (via mutagenesis of the scFv-hERG1 construct), in which we have reintroduced one of the cysteine that is in a fundamental position for the formation of the disulfide bonds, within the VH chain of the scFv antibody. In fact, scFv-hERG1-G3 antibody, in this position, showed a phenylalanine amino acid. We have given evidence that the restoration of the Cys deeply affects the protein yield, without affecting the antibody binding capacities. scFv-hERG1-D8-Cys has also demonstrated to have effects on cell growth and invasiveness, as demonstrated by the viability experiments performed on 2D tumour cell lines and on 3D spheroid tumour cell cultures (patent in preparation).

In the third part of this work, we have focused on the expression and characterization of a scDb bispecific antibody directed against hERG1- $\beta$ 1 oncogenic unit. The antibody has been also characterized with IF experiments performed on different substrates, showing the capacity to recognize hERG1- $\beta$ 1 complex.

These evidences allow us to conclude that both scFv-hERG1-D8-Cys and anti-scDb-hERG1- $\beta$ 1, after a proper validation, will represent valuable tools for cancer therapy.

<b>1. INTRODUCTION.....</b>	<b>1</b>
<b>1.1 CANCER IMMUNOTHERAPY.....</b>	<b>1</b>
1.1.1 Passive immunotherapy.....	2
1.1.1.1 Monoclonal antibodies for cancer therapy.....	2
1.1.1.2 Antibody structure.....	7
1.1.1.3 Antibody engineering.....	9
1.1.1.4 Single-chain variable fragment antibodies (scFv).....	10
1.1.1.5 Bispecific antibodies.....	11
1.1.1.6 Recombinant antibody expression systems.....	14
<b>1.2 ION CHANNELS.....</b>	<b>19</b>
1.2.1 Glutamate Receptor Ion channels.....	20
1.2.1.1 AMPA-type Glutamate Receptors.....	21
1.2.1.2 Ionotropic Glutamate Receptors in CNS diseases and cancer.....	23
1.2.1.3 Tuberous Sclerosis Complex (TSC).....	24
1.2.2 hERG1 Potassium channel.....	26
1.2.2.1 hERG1 structure.....	26
1.2.2.2 hERG1 physiological expression and function.....	27
1.2.2.3 hERG1 and cancer.....	28
1.2.2.4 hERG1- $\beta$ 1 integrin complex in cancer.....	30
<b>2. AIMS OF THE STUDY.....</b>	<b>32</b>
<b>3. MATERIALS AND METHODS.....</b>	<b>34</b>
3.1 ANTI- IGLUR4 MONOCLONAL ANTIBODY DEVELOPMENT.....	34
3.2 PRODUCTION AND CHARACTERIZATION OF ANTI-SCFV-HERG1 ANTIBODIES .....	47
3.3 PRODUCTION AND CHARACTERIZATION OF ANTI-HERG1- $\beta$ 1 SINGLE CHAIN DIABODY (SCDB).....	56
<b>4. RESULTS.....</b>	<b>57</b>
4.1 DEVELOPMENT AND CHARACTERIZATION OF A MONOCLONAL ANTIBODY DIRECTED AGAINST IONOTROPIC GLUTAMATE RECEPTOR 4 (iGLUR4)....	57
4.1.1 Monoclonal antibody development.....	58
4.1.2 Anti-iGluR4 clones screening and characterization.....	64
4.1.3 Anti-iGluR4 antibody testing in immunocytochemistry (ICC) and immunohistochemistry (IHC).....	68
4.1.4 anti-iGluR4 monoclonal antibody engineering.....	74
4.2 PRODUCTION AND CHARACTERIZATION OF ANTI- HERG1 SINGLE CHAIN VARIABLE FRAGMENTS ANTIBODIES.....	77
4.2.1 anti-scFv-hERG1-G3 expression and characterization as an in vivo imaging tool	77

4.2.2 scFv-hERG1-D8Cys production and characterization as a potential antitumor agent	87
4.3 PRODUCTION AND CHARACTERIZATION OF HERG1-B1 BISPECIFIC SINGLE CHAIN DIABODY (SCDB).....	104
4.3.1 anti-hERG1- $\beta$ 1-scDb antibody production.....	104
5. DISCUSSION.....	111
5.1 ANTI- iGLUR4 MONOCLONAL ANTIBODY DEVELOPMENT.....	111
5.2 PRODUCTION AND CHARACTERIZATION OF ANTI SCFV-HERG1 ANTIBODIES	113
5.3 PRODUCTION AND CHARACTERIZATION OF HERG1-B1 BISPECIFIC SINGLE CHAIN DIABODY (SCDB).....	116
6. REFERENCES.....	118

# **1. INTRODUCTION**

## **1.1 Cancer immunotherapy**

Cancer immunotherapy has been particularly improved in the last fifteen years, as mechanisms related to the anti-tumor immune response have been elucidated and novel technological platforms for the production of active anti-cancer compounds, along with innovative advances to quantify clinical responses, have led to enhanced immunotherapeutic protocols for patients' treatment in the clinical setting (Papaioannou NE *et al*, 2016).

Cancer immunotherapy involves the exploitation of the immune system's to recognize, target and destroy cancer cells. The idea of using the immune system against cancer is based, among others, on the fact that immune cells:

- provide constant surveillance throughout the body;
- are specifically stimulated against tumors, which are by definition antigenic and often immunogenic; and
- protect against tumor relapse, due to induction of specific and long-lasting memory.

Nevertheless, tumors escape from immunosurveillance through a well described process termed "cancer immunoediting", which consists of elimination, balance, escape, and, eventually, leads to cancer growth (Koebel CM *et al*, 2007).

It is possible to classify cancer immunotherapy in two main groups of intervention: passive and active (Fig 1)

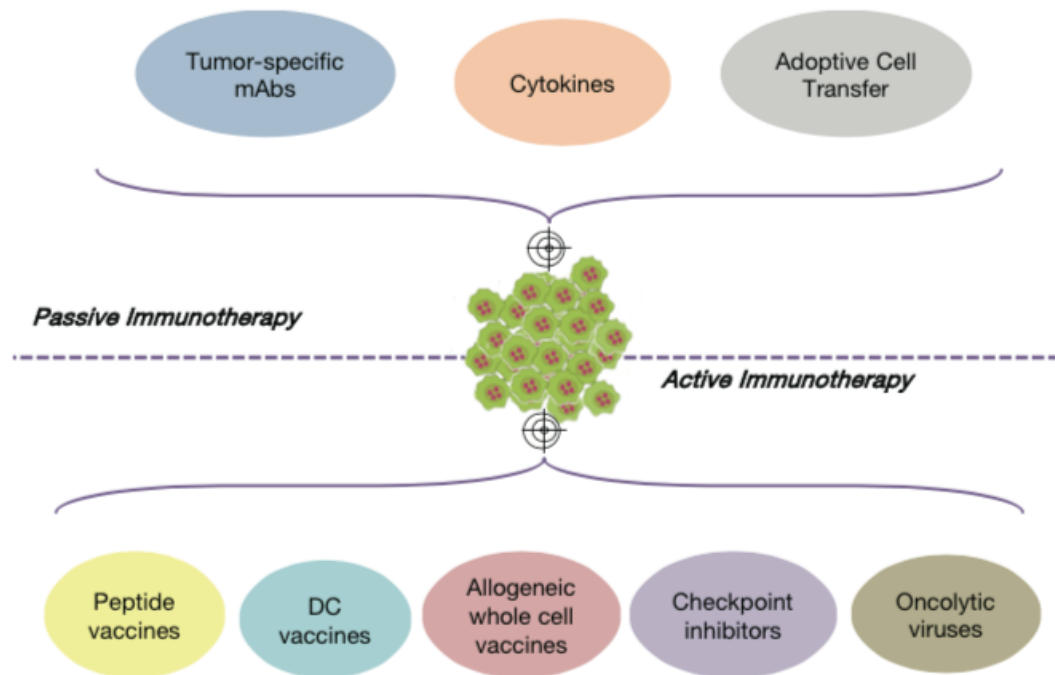


Fig. 1 Schematization of cancer immunotherapy approaches: passive and active. Dc: dendritic cells vaccines (Papaioannou NE *et al*, 2016).

Such classification is made considering the kind of therapeutic agent used alongside with the patient's immune system: *passive immunotherapy* includes the infusion of tumor-specific antibodies, the administration of recombinant cytokines and the adoptive transfer of immune cells pre-activated to lyse tumors *in vivo*. *Active immunotherapy*, instead, aims to stimulate effector functions *in vivo*. This represents the main reason why to succeed in such approach the patient's immune system should be able to respond upon challenge, in order to mediate effector functions. It includes vaccination strategies with tumor peptides or allogeneic whole cells, the use of autologous dendritic cells as vehicles for tumor antigen delivery and the infusion of antibodies targeting crucial checkpoints of T cell activation.

### ***1.1.1 Passive immunotherapy***

#### ***1.1.1.1 Monoclonal antibodies for cancer therapy***

The first *monoclonal antibodies* (mAbs) evaluated in the clinic as cancer treatments were murine mAbs, thus problems associated with administering murine mAbs to humans limited their clinical utility. These problems included the development of an

immune response against the therapeutic mAb itself (HAMA, human anti-mouse antibody response), the rapid clearance of the mAb and a not completely satisfactory ability of the murine mAb to interact with the human immune system in a manner that leads to immune destruction of the cancer.

Advances in antibody engineering have led to improvements and, nowadays, antibodies are chimeric, humanized or fully human.

The most commonly used mAbs in cancer immunotherapy are of the IgG class due to their long half-life and stability in serum. Naked anti-cancer mAbs mediate their function through directly inducing programmed cell death upon binding to tumor targets and by antibody-dependent cellular cytotoxicity (ADCC), complement-mediated cytotoxicity (CMC) (Fig.2a) and/or antibody-dependent cellular phagocytosis (ADCP). mAbs can also have direct effects on target cells by blocking the binding of an activating ligand that is responsible for the survival of the cancer cell, inhibiting the dimerization of a receptor, thereby blocking an activation signal or inducing an apoptotic signal by crosslinking a receptor. Such crosslinking of a receptor can be enhanced when a mAb is bound to Fc receptor-expressing cells (Fig.2b).

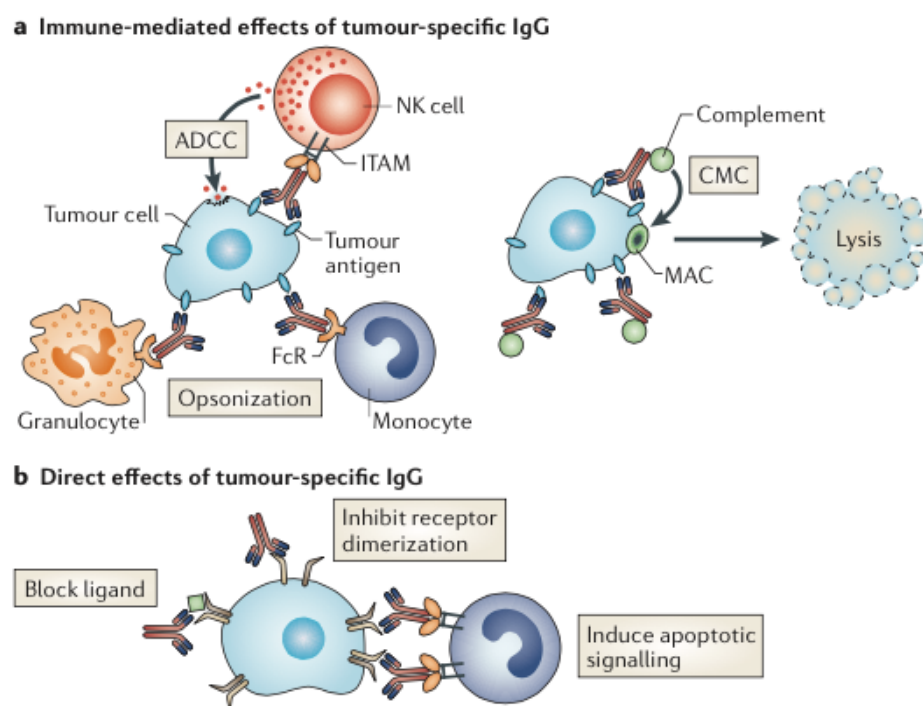


Fig.2 Mechanisms of action exploited by monoclonal antibodies to target cancer cells (Weiner. G.J., 2015).

These mechanisms are routinely identified *in vitro* but their relative contribution to clinical responses to mAb therapy is difficult to determine. mAbs can mediate ADCC by immune effector cells that express immunoreceptor tyrosine-based activation motifs (ITAMs), such as natural killer (NK) cells, monocytes, macrophages and granulocytes. Fixation of complement can trigger the *opsonization* of the target cell and thereby enhance phagocytosis and lysis by monocytes and granulocytes. CMC can directly result in target cell death through the development of a membrane attack complex (MAC). The biggest challenge remains to understand which one of these mechanisms could be the most relevant for a candidate mAb in a clinical scenario.

Many efforts have been devoted to the study of a variety of mAbs-based approaches for cancer therapy, considering different strategies (Fig. 3), which include both passive and active immunotherapy approaches (Table 1).

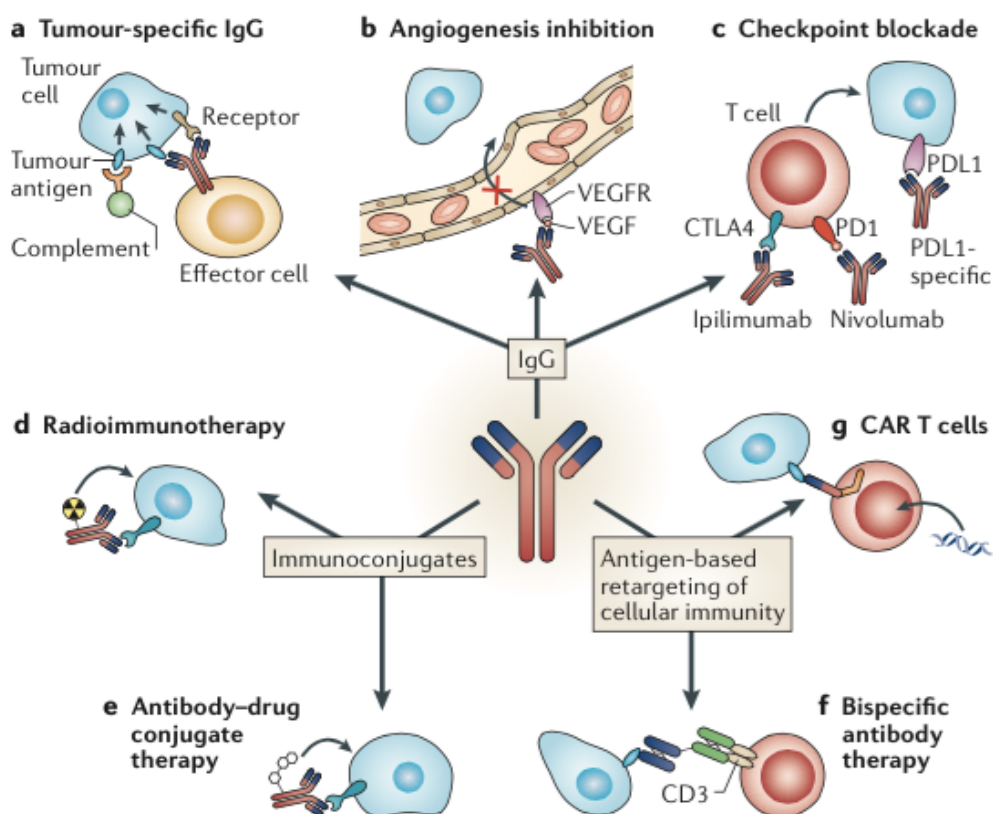


Fig. 3 Mechanisms of action exploited by monoclonal antibodies to target cancer cells - ADCC, antibody dependent cellular cytotoxicity; CMC, complement-mediated cytotoxicity; ITAMs, immunoreceptor tyrosine-based activation motifs, NK, natural killer; MAC, membrane attack complex (Weiner. G.J., 2015).

mAb-based therapeutic	Structure	Characteristics of target antigen	Example of major ongoing research questions
Antitumour mAbs	Unmodified IgG or IgG modified to mediate enhanced ADCC	Tumour-associated surface antigen	Are IgGs with enhanced affinity for Fc receptors more clinically effective than unaltered IgG?
Angiogenesis inhibition	Unmodified IgG	Host molecules that control angiogenesis	What is the best way to evaluate clinical response in patients treated with angiogenesis inhibitors?
T cell checkpoint blockade	IgG1 (blocks checkpoint and mediates ADCC) or IgG4 (blocks checkpoint without mediating extensive ADCC)	Molecules that limit the anticancer T cell response	How should we combine checkpoint blockade mAbs with each other, with other immunotherapeutics and with other anticancer agents?
Radioimmunotherapy	Unmodified IgG or mAb fragment	Tumour-associated antigen that is not shed or present in the circulation	How can the logistics of administering successful radioimmunotherapeutic agents be simplified to enhance their clinical utility?
Antibody–drug conjugate	IgG modified with cleavable linker and drug	Highly specific tumour-associated antigen that can internalize when bound by a mAb	What is the best combination of linkers and drugs with each mAb and target antigen?
Bispecific antibody	Variable regions from cancer-specific mAbs linked to variable regions specific for activating receptors on T cells	Tumour-associated antigen that is not commonly absent in antigen-loss-resistant cancer variants	Can effective bispecific constructs that have modified kinetics (thereby avoiding the logistic complexities of continuous infusion) be developed?
Chimeric antigen receptor T cell	Gene therapy approach to modifying T cells by inserting DNA coding for the mAb variable region fused to DNA coding for signalling peptides	Highly tumour-specific antigen that is not commonly absent in antigen-loss-resistant cancer variants	Can very promising preliminary results be extended to solid tumours, or will toxicity be associated even with low levels of target antigen expression by benign cells?

ADCC, antibody-dependent cellular cytotoxicity; IgG, immunoglobulin G; mAb, monoclonal antibody.

Table 1 Various strategies to target cancer directly, including using immunoglobulin G (IgG), alter the host response to cancer, deliver cytotoxic substances to cancer and retarget the cellular immune response towards cancer (Weiner G.J., 2015).

Along with the aforementioned mechanisms regarding IgG molecules that bind to target cancer cells, such as the direct signalling-induced death of cancer cells, as it is for example for herceptin and rituximab (Fig.3, a); IgG mAbs can also be used to inhibit angiogenesis (Fig. 3, b), as it is for example for bevacizumab, which prevents binding of vascular endothelial growth factor (VEGF) to its receptors and inhibits angiogenesis. **Bevacizumab** is applied for the treatment of some solid tumors (e.g. colorectal cancer and metastatic colorectal cancer), in combination with chemotherapy (Ellis L.M. *et al.*, 2008).

Another approach is represented by the block of inhibitory signals (Fig.3, C), thereby resulting in a stronger anti-tumor T cell response (for example, ipilimumab and nivolumab). **Ipilimumab** (Yervoy, Bristol-Myers Squibb) is a fully human IgG1 mAb that blocks the interaction of CTLA-4 and B7- 1/2. Since February 2016, ipilimumab has been approved for treating unresectable or metastatic melanoma, where it demonstrated significant survival advantage (Hodi FS *et al.*, 2010; Robert C. *et al.*, 2011). Currently, 120 open clinical studies are or will be recruiting patients with various types of cancer, who will receive ipilimumab as monotherapy (e.g. for recurrent

platinum-sensitive ovarian cancer; NCT01611558) or as a combinatorial treatment (e.g. with chemoradiation for locally advanced cervical cancer; NCT01711515).

**Pembrolizumab** (Keytruda, Merck) is a humanized IgG4 mAb that targets PD-1, thus disrupting its inhibitory interaction with PD-L1/2. Since February 2016, pembrolizumab is approved for the treatment of advanced melanoma progressed on ipilimumab, and BRAF mutant melanoma progressed on a BRAF inhibitor (e.g. dabrafenib, vemurafenib). It is also approved for treating metastatic PD-L1<sup>+</sup> NSCLC, after progression on platinum-containing chemotherapy and/or on EGFR/ALK-targeted medication (e.g. erlotinib, gefitinib, ceritinib) for tumors bearing EGFR or ALK mutations (Hamid O. *et al.*, 2013; Patnaik A. *et al.*, 2015; Ribas A. *et al.*, 2015)

**Nivolumab** (Opdivo, Bristol-Myers Squibb) is a fully human IgG4 anti-PD-1 mAb with the same mode of action as pembrolizumab, but with 10-fold reduced affinity for PD-1 compared to pembrolizumab. As of February 2016, it is approved for the treatment of metastatic melanoma.

Radioimmunoconjugates (Fig. 3, D) (for example, <sup>131</sup>I tositumomab and ibritumomab tiuxetan) deliver radioisotopes to the cancer cells, whereas antibody–drug conjugates (Fig. 3, E) (for example, brentuximab vedotin and trastuzumab emtansine) deliver highly potent toxic drugs to the cancer cells. mAb variable regions are also used to retarget immune effector cells towards cancer cells through the use of bispecific mAbs that recognize cancer cells with one arm and activating antigens on immune effector cells with the other arm (Fig.3, F) (for example, blinatumomab). Bispecific mAbs have also shown promise actions by bridging immune effectors to cancer cells and promoting tumor cell eradication. A new class of such mAbs, the recombinantly produced bispecific T cell engagers (BiTEs), that can induce T cell-mediated tumor elimination in the absence of T cell receptor (TCR)-MHC interactions.

**Blinatumomab** is currently the only Food and Drug Administration (FDA) approved BiTE for treating refractory or relapsed Philadelphia chromosome-negative B-acute lymphocytic leukemia (Suryadevara C.M. *et al.*, 2015).

Another gene therapy approach implies that the DNA for a mAb variable region is fused to signalling peptides and is transferred to T cells, thereby rendering them chimeric

antigen receptor (CAR) T cells (Fig.3, G) specific for the tumor (Barrett, D. M. *et al.*, 2014).

In the following table are shown mAbs currently approved (up to February 2016) for treatment of several malignancies (Table 2).

Monoclonal antibodies and conjugates approved for the treatment of cancer in humans (February 2016)				
Antibody	Trade name (company)	Target	Antibody type	Cancer type
Alemtuzumab	Campath (Genzyme)	CD52	Humanized	Chronic lymphocytic leukemia
Bevacizumab	Avastin (Roche)	VEGFA	Humanized	CRC, NSCLC, RCC, glioblastoma
Cetuximab	Erbix (Bristol-Myers Squibb/Lilly)	EGFR	Chimeric	CRC, breast, lung
Denosumab	Xgeva/Prolia (Amgen)	RANK ligand	Human	Solid tumor bony metastases
Gemtuzumab ozogamicin	Mylotarg (Wyeth)	CD33	Humanized	Acute myeloid leukemia
Nimotuzumab	Theraloc/TheraCIM (YM Biosciences)	EGFR	Humanized	Head and neck
Ofatumumab	Arzerra (GlaxoSmithKline)	CD20	Human	Chronic lymphocytic leukemia
Panitumumab	Vectibix (Amgen)	EGFR	Human	CRC
Pertuzumab	Perjeta (Roche)	HER2	Humanized	Breast
Rituximab	Rituxan/MabThera (Biogen, Roche)	CD20	Chimeric	Non-Hodgkin's lymphoma
Tositumomab and <sup>131</sup> I-tositumomab	Bexxar (GlaxoSmithKline)	CD20	Mouse	Lymphoma
Trastuzumab	Herceptin (Roche)	HER2	Humanized	Breast

Table 2 Monoclonal antibodies approved for human cancer treatment (up to February 2016) (Papaioannou *et al.*, 2016).

### 1.1.1.2 Antibody structure

Vertebrates express five classes (or isotypes) of antibodies called immunoglobulins (Igs): alpha (IgA), delta (IgD), epsilon, (IgE), gamma (IgG,) and mu (IgM).

IgGs represent the most abundant Igs in human blood (85% of Ig in serum) and are the most widely used Igs for therapeutic and diagnostic applications (Maynard and Georgiou, 2000).

From a structural point of view, IgG molecules are heterotetramers composed of two identical  $\gamma$  heavy chains and two identical light chains that are joined by a series of disulfide bonds. Any single human IgG molecule is composed of a constant region (Fc) and a fragment antigen-binding region (Fab); within the Fab region, there are two  $\gamma$  heavy chains of subclasses 1, 2, 3 or 4, and either two  $\kappa$  or  $\lambda$  light chains. Each light chain contains one variable domain (VL) and one constant domain (CL), while heavy chains contain one variable domain (VH) and three constant domains (i.e. CH1, CH2

and CH3). The variable regions, at the N-terminus of the Fab fragment, are responsible of the specificity, diversity and affinity of antigen binding, instead the Fc domains are responsible for mediating antibody structure and effector functions and for determining IgG *in vivo* half-life (Fig. 4).

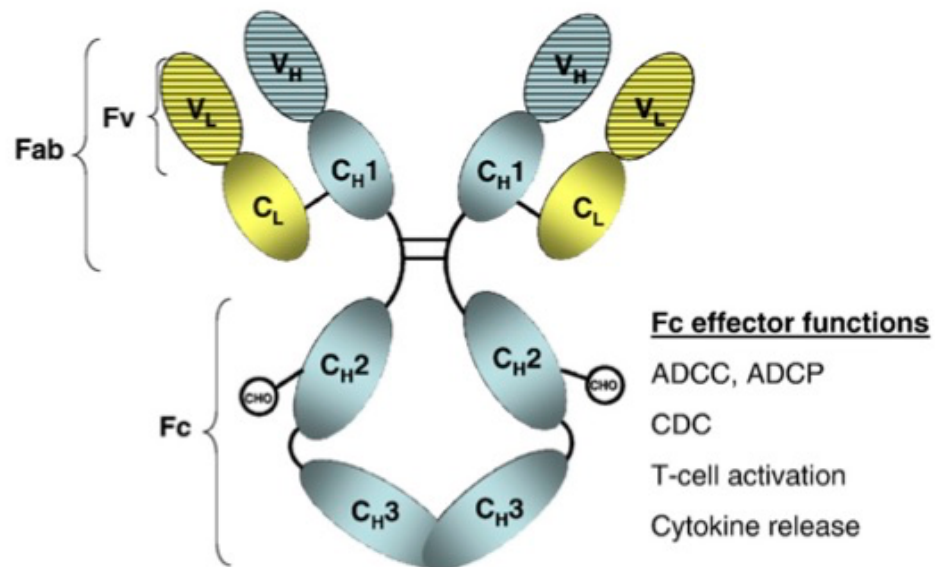


Fig.4 Schematic structure of a Ig molecule. Heavy chains are shaded in blue and light chains are shaded yellow with the lined regions representing the variable domains (N.E. Weissner and J.C. Hall, 2009).

V<sub>H</sub>-region antigen specificity results from recombination of variable (V), diversity (D) and junctional (J) gene segments, whereas V<sub>L</sub> region antigen specificity results from recombination of the VJ gene segments that occurs during B-cell maturation to generate the DNA encoding the unique Ab combining site. Within each V<sub>H</sub> and V<sub>L</sub> domain are three hypervariable regions where sequence variability is concentrated and loops are formed. These regions are responsible for the antigen recognition and are also called complementary determining regions (CDRs). CDRs are separated by domains that exhibit far less variation; these portions are referred to as the framework regions which act as a scaffold to support the loops. The constant C<sub>H</sub>1 and C<sub>L</sub> domains function to extend the Fab arms of the IgG to facilitate interaction with the antigen and increase the maximum rotation of the Fab arms (Weissner NE *et al.*, 2009).

### ***1.1.1.3 Antibody engineering***

It is without a doubt that full length mAbs can be used in many successful therapeutic applications, even though some limitations still remain, particularly due to the unwanted Fc-induced effector functions (e.g. cytokine inactivation, receptor blockade, viral neutralization and/or faster clearance rates). These issues have been overcome by recombinant Ab fragment (rAb) molecules. These molecules, lacking the Fc region, possess unique characteristics suitable for various therapeutic applications (Holliger and Hudson, 2005). The first molecules lacking of the Fc regions were generated by proteolytic treatment with papain or pepsin, to yield Fab and F(ab')<sub>2</sub> fragments, respectively (Porter, 1959). However, proteolysis is generally non-specific and does not yield molecules smaller than Fab fragments. Smaller rAb fragments are being investigated as alternatives to mAbs as they retain the target specificity, with the fundamental characteristic of the small size, usually five to six-fold smaller than the intact IgG molecule. For such reasons, among others, the use of antibody fragments in therapy exerts several advantages over whole antibodies, especially in therapy targeting solid tumor in which there is a remarkable advantage concerning the speed of penetration between a fragment versus the full length antibody. For instance, in 1988, it was established that an intact molecule of IgG took fifty-four hours to penetrate 1 mm into a solid tumor, while a Fab fragment managed the same distance in sixteen hours (Jain, 1987). Currently, scFvs are the most popular rAb fragment format and have been engineered into several types of scFv-based multimeric or scFv-conjugate fragments for a range of therapeutic and diagnostic applications (Fig.5) (Weisser N.E. and Hall J.C., 2009).

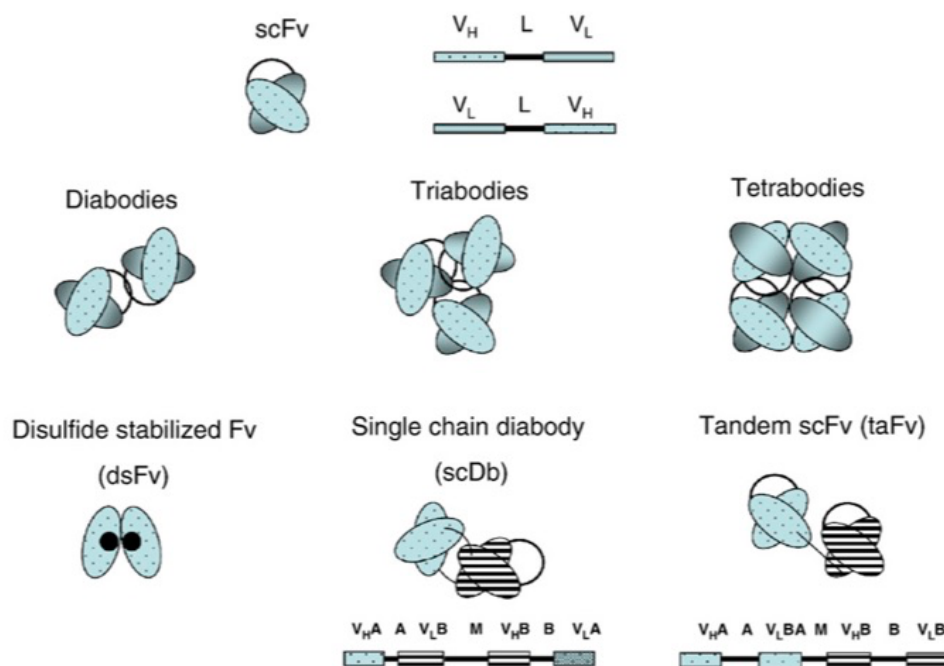


Fig.5 scFv and scFv-based rAb fragments structure (N.E. Weissner and J.C. Hall, 2009).

#### 1.1.1.4 Single-chain variable fragment antibodies (scFv)

scFvs Abs have a molecular weight around 28–30 kDa and are composed of V<sub>H</sub> and V<sub>L</sub> chains, joined via a flexible peptide linker (Maynard and Georgiou, 2000). The first scFv molecules were developed independently by Huston *et al.* (1988) and Bird *et al.* (1988) and represent the smallest functional V<sub>H</sub>–V<sub>L</sub> domains of an Ab necessary for high-affinity binding of antigen. scFvs were originally derived from genes isolated from murine hybridoma cell lines and are capable of binding the target antigens with an affinity similar to that of the parent mAb (Bird *et al.*, 1988). Peptide linkers are fundamental for the constitution of scFv antibodies, as they join the V<sub>H</sub> and V<sub>L</sub> chains and usually vary from 10 to 25 amino acids in length, typically including hydrophilic amino acids; the most common linker is the decapenta-peptide (Gly<sub>4</sub>Ser)<sub>3</sub>. Multimer formation is primarily determined by linker length in which shorter linkers (0–12 amino acids) favor the formation of dimers or trimers (reviewed in Todorovska *et al.* (2001)). The variable regions can be connected in either the V<sub>H</sub>-linker-V<sub>L</sub> or V<sub>L</sub>-linker-V<sub>H</sub> orientation, usually the most common is the V<sub>H</sub>-linker-V<sub>L</sub> connection, and these orientations can affect expression efficiency (Merk *et al.*, 1999), stability, and antigen binding activity (Desplancq *et al.*, 1994).

*In vivo* studies have provided confirmation that size is an important parameter in pharmacokinetics and biodistribution of mAbs molecules in particular when used for cancer therapy. One of the main disadvantages of scFv antibodies is that they monovalently bind their target antigen and dissociation occurs quickly, limiting retention times and being cleared rapidly, especially in the non-equilibrium conditions of the body (Hollinger and Hudson, 2005).

Such issues could be overcome by the use of intermediate-sized multivalent molecules, such as bivalent diabodies (55 kDa) which provide rapid tissue penetration, high target retention and rapid blood clearance (Fig.6).

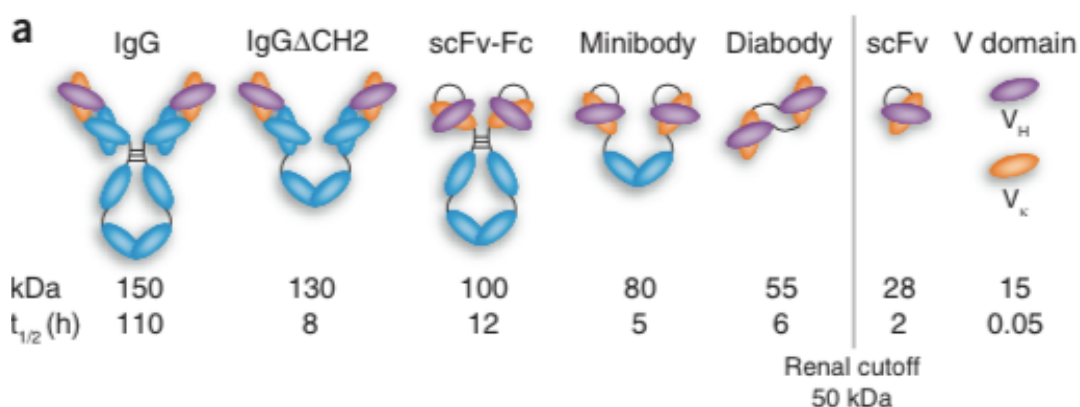


Fig. 6 Renal cutoff for clearance of rAbs (Hollinger and Hudson, 2005).

#### 1.1.1.5 Bispecific antibodies

Bispecific antibodies (bsAbs) have recently raised a lot of attention as potential cancer therapeutic agents because they offer several advantages:

- bsAbs can redirect specific immune cells towards tumor cells, thereby enhancing tumor killing;
- bsAbs can simultaneously block two different targets in different pathways that carry out unique or overlapping functions in pathogenesis;
- bsAbs can potentially increase binding specificity by interacting with two different cell-surface antigens instead of one.

The development of bispecific antibodies (bsAbs) has experienced many difficulties, mainly due to the manufacturing problems, poor yields, instability and immunogenicity (Spiess C. *et al*, 2015).

Concerning the methodology for bsAbs production, they are primarily produced by three methods, which include:

- quadroma technology, based on the somatic fusion of two different hybridomas cell lines;
- chemical conjugation, through the use of chemical cross-linkers;
- genetic approaches utilizing recombinant DNA technology.

Bispecific antibodies can be roughly divided into two main subgroups: immunoglobulin G (IgG)-like molecules and non-IgG-like molecules (Fig.7) and so far there are over 30 bsAbs in clinical development with two, Catumaxomab and Blinatumomab, already approved for the market.

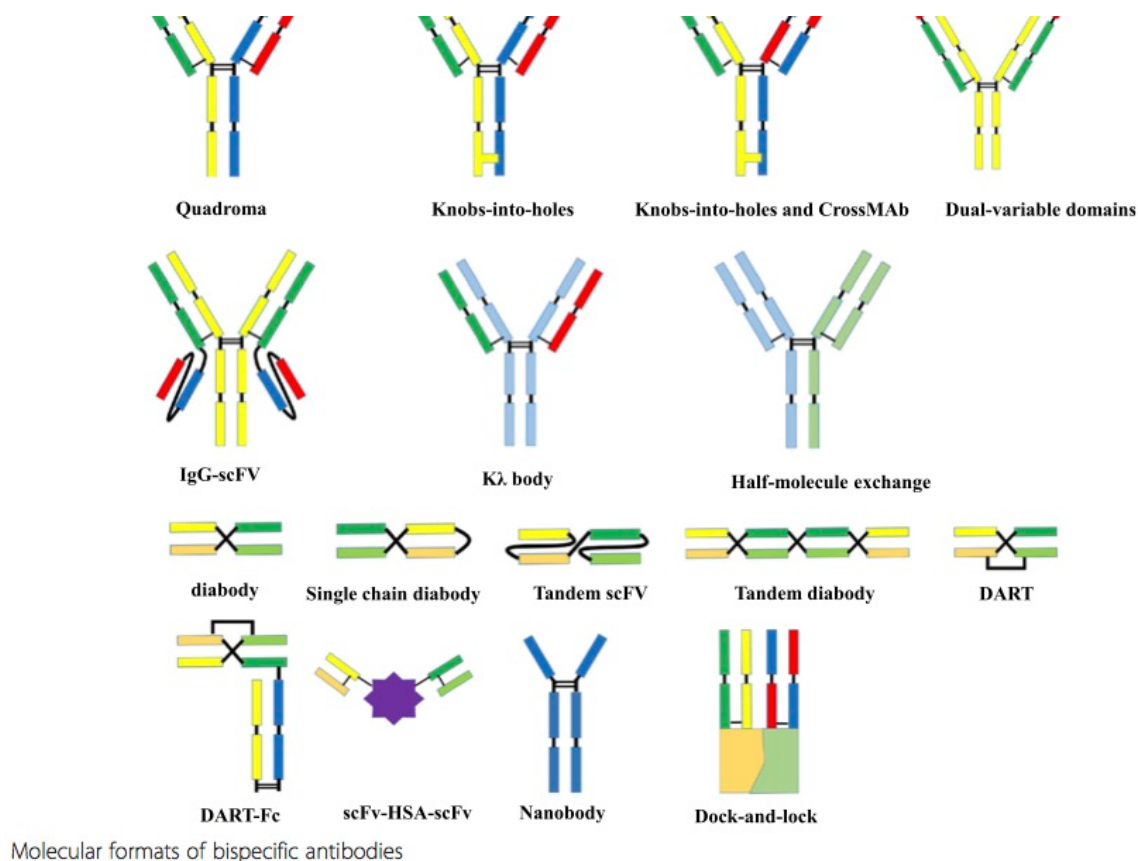


Fig. 7 Different formats of bispecific antibodies (Fan G. *et al.*, 2015).

IgG-like bsAbs retain Fc-mediated effector functions such as ADCC, CDC and antibody-dependent cellular phagocytosis (ADCP).

Non-IgG-like include mainly scFv-based bsAbs and nanobodies. It is known that scFvs can become dimers, trimers, or tetramer depending on linker length, antibody sequence and other factors (Le Gall F. *et al.*, 1999). Such format is favored and has many possible clinical applications. Among scFv-based bsAbs formats there are:

- ***Tandem scFvs***, which consist of two scFvs connected by a flexible peptide linker, such as glycine-serine repeat motifs in a tandem orientation. The famous bispecific T cell engager (BiTE) technology is based on this format (Chames P. *et al.*, 2009).
- ***Diabody format***, in which the variable domains of two different antibodies are connected by two linkers. These have the function to increase the stability of the diabody.
- ***Single-chain diabolies***, the diabody format can be converted into a single-chain diabody by adding an additional connection linker between the chains
- ***Tandem diabolies (TandAbs)*** are formed by two pairs of VL and VH domains, connected in a single polypeptide chain, forming a tetravalent TandAb.
- ***Dual-affinity retargeting molecules (DARTs)*** DARTs are created by the association of the VH of a first variable region linked to the VL on a second chain, and the VH of the second variable region linked to the VL on the first chain in a  $VL_A - VH_B + VL_B - VH_A$  configuration. Due to their small size, DARTs are prone to elimination (Moore P.A. *et al.*, 2011).

scFv-based bsAbs present many advantages including the ease of manufacturing and enhanced tissue penetration, moreover they offer the possibility to bind epitopes that can be sterically inaccessible to antibodies in complete IgG format.

Nevertheless, there are weaknesses mainly due to their short half-lives, such as rapid blood clearance, fast off-rates and poor retention times in targeted sites, characteristics that are important, particularly, considering clinical applications, such as tumor targeting (Kontermann R.E., 2011). To overcome this disadvantages, various strategies

have been explored to extend serum half-life, such as the covalent or non-covalent attachment of polyethylene glycol (PEG) polymer chains, so called PEGylation; fusion with human serum albumin (HSA) or an album-binding moiety; Fc fragment fusion; multimerization.

bsAbs have many possible clinical applications and one of the most recent strategies in which bispecific antibodies are used successfully is redirecting T cells to tumor cells (Satta A *et al.*, 2013). In fact, tumor-specific T-cell responses are limited by immune escape mechanisms utilized by tumor cells during immunoediting. One strategy to harness the immune cells is to take advantage of bsAbs to kill tumor cells and Triomabs, BITEs and DARTs bispecific antibodies have been developed for this purpose.

Several BsAbs are in preclinical development such as those for crossing the blood-brain barrier (BBB). In fact, one of the promising application of bsAbs is to cross the blood-brain barrier to target pathogenesis mediators in neurological diseases (Stanimirovic D *et al.*, 2014). The BBB forms a forbidden zone for monospecific antibody therapy. One of the strategies used to overcome this problem is to bind the transferrin receptor (TfR). TfR is highly expressed on the surface of brain endothelium and, after the binding with the TfR, the circulating bsAb is transported into the brain via receptor-mediated transcytosis. The affinity between the bsAb and TfR is weak; therefore, bsAb can be released from the endothelium and enter the brain to target their second antigen with the other binding arm (Couch JA *et al.*, 2013).

In this scenario, it is reasonable to propose that bAbs in near future might improve treatment options against cancer, autoimmune diseases and inflammatory diseases. Nevertheless, several critical points still remain to be solved, such as the simplification of the structure, the production procedures and, above all, the identification of target pairs and bsAbs with potential synergistic effect, which represents overall one of the biggest challenge (Fan G. *et al.*, 2015).

#### **1.1.1.6 Recombinant antibody expression systems**

One of the detrimental factors that affects antibody production is the choice of a proper expression system; different kinds of hosts have been used, including prokaryotes, such as *E. coli* (Martin *et al.*, 2006) and *B. subtilis*, and eukaryotes, including *S. cerevisiae*

(Hackel *et al.*, 2006), *Pichia pastoris* (Ren *et al.*, 2008), insect cells (Bruenke *et al.*, 2004), plant cells (Mayfield *et al.*, 2003), plants (Makvandi-Nejad *et al.*, 2005) and mammalian cells (Natsume *et al.*, 2006). The application of antibody fragments for both therapeutic and diagnostic application is strictly linked to the development of platforms for efficient and cost effective production of these molecules (Andersen and Reilly, 2004). Such goal is influenced by many factors, as protein expression is variable and yields vary for each rAb fragment and/or fragment type. Usually, rAb expression differs in yield and activity, as it is affected by several factors such as protein size, solubility, stability and amino acid sequence; thus expression of each protein must be optimized. The optimal expression system depends on the type of rAb fragments being expressed, as well as, the required purity and quantity of the final product. The most common expression systems used up to now include: bacterial cells, yeast and filamentous fungi, transgenic plants and mammalian cells.

- **Bacterial cells.** The most widely used bacterial expression system is *E. coli*, which is suitable for the production of small non-glycosylated rAb fragments, including scFvs (Wang *et al.*, 2008). In fact, compared to mammalian cells, expression in *E. coli* is faster with satisfactory expression levels (Andersen and Reilly, 2004; Chen *et al.*, 2004). Nevertheless, *E. coli* is not capable of post-transcriptional modifications, such as protein glycosylation. Expression of rAbs in bacterial cells can be directed to different cell compartments such as extracellular and periplasmic spaces, inner and outer membrane or within the cytoplasm. High-level expression can be induced with IPTG but often the reducing bacterial environment results in the formation of inclusion bodies, that require solubilization (with denaturing reagents, such as Urea 8M) and refolding. It must be taken into account that refolding efficiency varies depending on the type of antibody (You *et al.*, 2003).
- **Expression in yeast and filamentous fungi.** Recombinant antibody production in yeast and fungi combines the advantages eukaryotic expression, including protein processing, folding, and post translational modifications. In yeasts, proteins are expressed into the culture supernatant allowing faster and easier purification, which results in better quality purified proteins, with less contaminating endotoxins as compared to the bacterially expressed counterparts. Moreover, scFvs that tend to

accumulate in inclusion bodies in *E. coli* are often expressed in soluble form in yeasts. scFv-based fragments, including diabody and diabody-immunotoxin conjugates (Kim *et al.*, 2007) and scFv-Fcs (Powers *et al.*, 2001; Ren *et al.*, 2008), have been produced in yeast and filamentous fungal species including *S. cerevisiae* (Hackel *et al.*, 2006), *P. pastoris* (Ren *et al.*, 2008), *Aspergillus awamori* (Sotiriadis *et al.*, 2001) and *Kluyveromyces lactis* (Swennen *et al.*, 2002). One of the most widely used species of yeast is *Pichia pastoris*. The mechanism exploited for protein expression by this methylotrophic yeast employs a promoter obtained from the methanol regulated alcohol oxidase I gene. This promoter is tightly regulated at a transcriptional level and allows high extracellular expression rates which are produced by either fed-batch or continuous culture methods. Induction of protein expression in methylotrophic yeast exploits a unique methanol utilization pathway

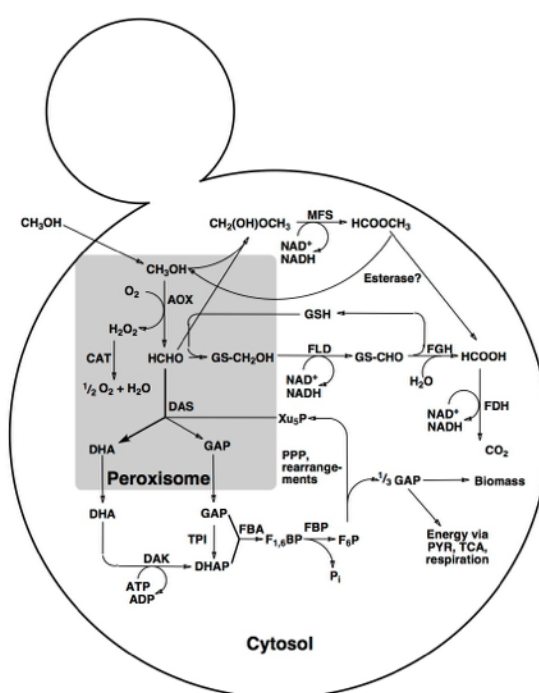


Fig.8 Methanol utilization pathway (MUT) in methylotrophic yeast. The main pathways and the respective enzymes working in the methanol metabolism in methylotrophic yeasts are shown. AOX: alcohol oxidase, CAT: catalase, FLD: formaldehyde dehydrogenase, FGH: S-formylglutathione hydrolase, FDH: formate dehydrogenase, DAS: dihydroxyacetone synthase, TPI: triosephosphate isomerase, DAK: dihydroxy-acetone kinase, FBA: fructose 1,6-bisphosphate aldolase, FBP: fructose 1,6-bisphosphatase, MFS: methylformate synthase; DHA: dihydroxyacetone, GAP: glyceraldehyde 3-phosphate, DHAP: dihydroxyacetone phosphate, F<sub>1,6</sub>BP: fructose 1,6-bisphosphate, F<sub>6</sub>P: fructose 6-phosphate, P<sub>i</sub>: phosphate, Xu<sub>5</sub>P: xylulose 5-phosphate, GSH: glutathione, PYR: pyruvate; PPP: pentose phosphate pathway, TCA: tricarboxylic acid cycle. (Hartner F.S. and Glieder A., 2013)

(MUT) pathway (Ellis S.B. *et al.*, 1985; Cregg J.M. *et al.*, 1989; Sakai Y. *et al.*, 1992; Roggenkamp R. *et al.*, 1984). Since a part of the MUT pathway takes place in the peroxisomes, these organelles proliferate massively upon methanol induction. After induction, they can account for up to 80% of the cytoplasmic space (Gleeson M.A. and Sudbery P.E., 1988). During the first step of methanol utilization, methanol is oxidised to formaldehyde and hydrogen peroxide by alcohol oxidases (AOX, EC 1.1.3.13). The toxic H<sub>2</sub>O<sub>2</sub> is broken down to oxygen and water by the action of catalase (CAT). Both enzymes are sequestered in peroxisomes (Fig.8) (Gellissen G., 2002; Stewart M.Q. *et al.*, 2001; Johnson M.A. *et al.*, 1999). The expression of the methanol pathway genes is repressed by glucose and ethanol and strongly induced by methanol. Ethanol and glucose act via two distinct mechanism to repress the MUT pathway (Parpinello G. *et al.*, 1998; Sakai Y. *et al.*, 1987; Alamae T. *et al.*, 1998).

Moreover, it is worth noting that the remarkable advances in continuous culture methods have increased the productivity of antibody fragments (Yamawaki *et al.*, 2007) along with improvements regarding opportunities coming from the reengineering of *P. pastoris*, especially in the field of biopharmaceutical production. Tailor-made expression systems have been set up by modifying transcription, translation, post-translational modifications (PTMs) and designing synthetic regulatory networks (Lynch S.A., 2012). Yeasts can perform typical eukaryotic PTMs, but final glycosylation patterns of yeasts and humans differ significantly. Thus, there have been efforts to humanize yeast glycosylation which has been accomplished in *P. pastoris* (De Pourcq K. *et al.*, 2010; Hamilton S.R. *et al.*, 2010). Also, hypermannosylation is less pronounced in *P. pastoris* and terminal  $\alpha$ -1,3-mannose linkages are not observed (Choi B-K. *et al.*, 2003). Thus, glycoengineered strains provide humanized N-glycosylation patterns, synthetic promoters allow the fine-tuning of expression levels and various tools for strain engineering and metabolic modeling are available (Fig.9) (Vogl T. *et al.*, 2013)

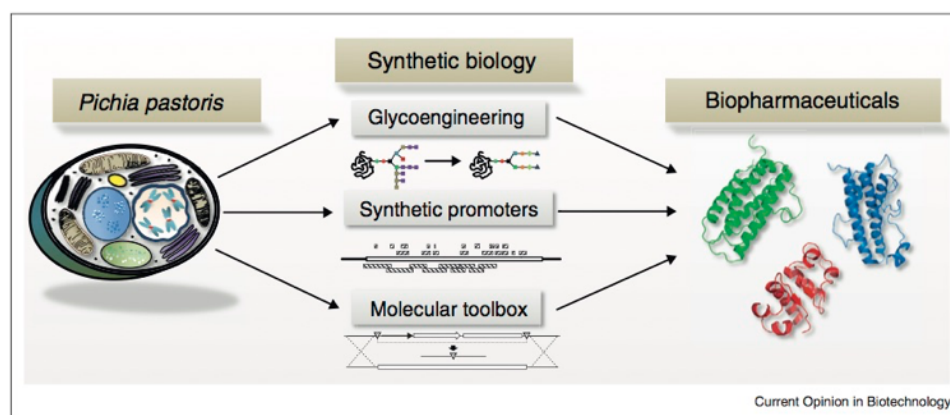


Fig. 9 Current synthetic biology approaches to improve biopharmaceutical yields and quality in *P. pastoris* (Vogl T. *et al.*, 2013)

- **Plant expression.** scFvs have been also expressed in transgenic plants (Ma *et al.*, 2005). Plants present several advantages regarding antibody production, including lower cost and the ability to alter production levels based on market needs, but also the lack of mammalian pathogens and a reduction in endotoxin contamination compared to the bacterial expression system. However, there are disadvantages that include the long initial lead time for production, uncertain regulatory mechanisms, and questions about the suitability of plant glycans in human therapeutics (Andersen and Reilly, 2004). Taken together, these factors explain why no commercial plant derived products are currently available (Pujol *et al.*, 2005).
- **Mammalian cells expression.** The most common mammalian host cell systems used to generate recombinant proteins are CHO and non-secreting (NSO) cells. The expression of scFv fragments in mammalian cells has primarily been done with minibody type fragments, such as bispecific antibodies (Natsume *et al.*, 2006), that require PTMs and expression of scFvs in CHO cells has been tested as an alternative to bacterial cells expression for those antibodies that have inefficient refolding from inclusion bodies and in application where lower levels of contaminating endotoxin are desired.

## 1.2 Ion channels

It is well known that ion channels play a crucial role in many pathological conditions, including cancer. In fact, different types of ion channels are involved at different levels in each of the six cancer hallmarks (Prevarskaya *et al.*, 2010). Such evidences have put light on novel potential exploitations of ion channels as targets for the development of therapeutic agents (D'Amico M. *et al.*, 2013). Ion channels are integral membrane proteins that allow the passive passage of certain ions into and out of the cell. Depending on their gating mechanism, ion channels can be divided into two main groups:

- ***Voltage-gated channels***, which can be opened by changing in the membrane potential and, when they are active, are responsible for the passage of specific ions.
- ***Ligand-gated channels***, which are opened by ligands and conduct cations or anions without high selectivity.

In physiological conditions, ion channels contribute to many different processes such as, electric signalling, gene expression, synaptic transmission, learning and memory (Fiske *et al.*, 2006; Madden D.R., 2002).

Pathological conditions related to miss-functions of ion channels (channelopathies) are characterize by an abnormal activity of these proteins, whose aberrant expression can also sustain growth and proliferation of tumor cells (Kunzelmann, 2005; Li and Xiong, 2011).

We will focus on Glutamate Receptor ion channels and hERG1 potassium channels, as increasing evidences have emerged regarding their involvement in a wide variety of pathologic conditions, and, in particular, in different aspects of cancer progression. In this scenario, they have been identified as novel molecular target to be exploited both for diagnostic and therapeutic purposes.

### 1.2.1 Glutamate Receptor Ion channels

Glutamate is the most abundant excitatory neurotransmitter in the vertebrate brain and it targets two receptor families: *ionotropic glutamate receptors (iGluRs)* and *metabotropic glutamate receptors (mGluRs)*.

*iGluRs* belong to the superfamily of ligand-gated ion channels. They are responsible for both synaptic transmission and synaptic plasticity and they are deeply involved in molecular mechanisms of learning and memory. They form tetrameric ligand-gated ion channel pores that allow the influx of  $\text{Na}^+$  and  $\text{Ca}^{2+}$  when glutamate binds to the extracellular ligand-binding domain (LBD). *iGluRs* can be further subdivided into:

- N-methyl-D-aspartate, *NMDA receptors*,
- $\alpha$ -amino-3-hydroxy-5-methyl-4-isoxazolepropionic acid, *AMPA receptors* and
- *kainate receptors* (Traynelis *et al.*, 2010) (Fig. 10, A)

All subtypes of *iGluRs* are permeable to both  $\text{Na}^+$  and  $\text{K}^+$ , which keeps the reversal potential close to 0 mV. Some subtypes, especially NMDAR, have also high permeability to  $\text{Ca}^{2+}$ . Glutamate receptor subunits are modular structures that contain four discrete semiautonomous domains: the extracellular amino-terminal domain (ATD), the extracellular ligand-binding domain (LBD), the transmembrane domain (TMD), and an intracellular carboxyl-terminal domain (CTD) (Fig. 10, B). Apart from the CTD and the M4 transmembrane segment, each of the individual domains exhibits low sequence homology to bacterial proteins with known structures and, in some instances, a related function (O'Hara *et al.*, 1993; Wo and Oswald, 1995; Wood *et al.*, 1995; Paas, 1998; Kuner *et al.*, 2003). Figure 10, C shows the crystal structure at 3.6 Å of the membrane-spanning tetrameric GluR2 AMPA receptor. Detailed crystallographic structures have been described for a membrane-spanning tetrameric glutamate receptor (Sobolevsky *et al.*, 2009), as well as the isolated ATDs and LBDs in complex with various agonists, antagonists, and modulators. These data, along with functional and biochemical experiments, have begun to define the relationship between receptor structure and function.

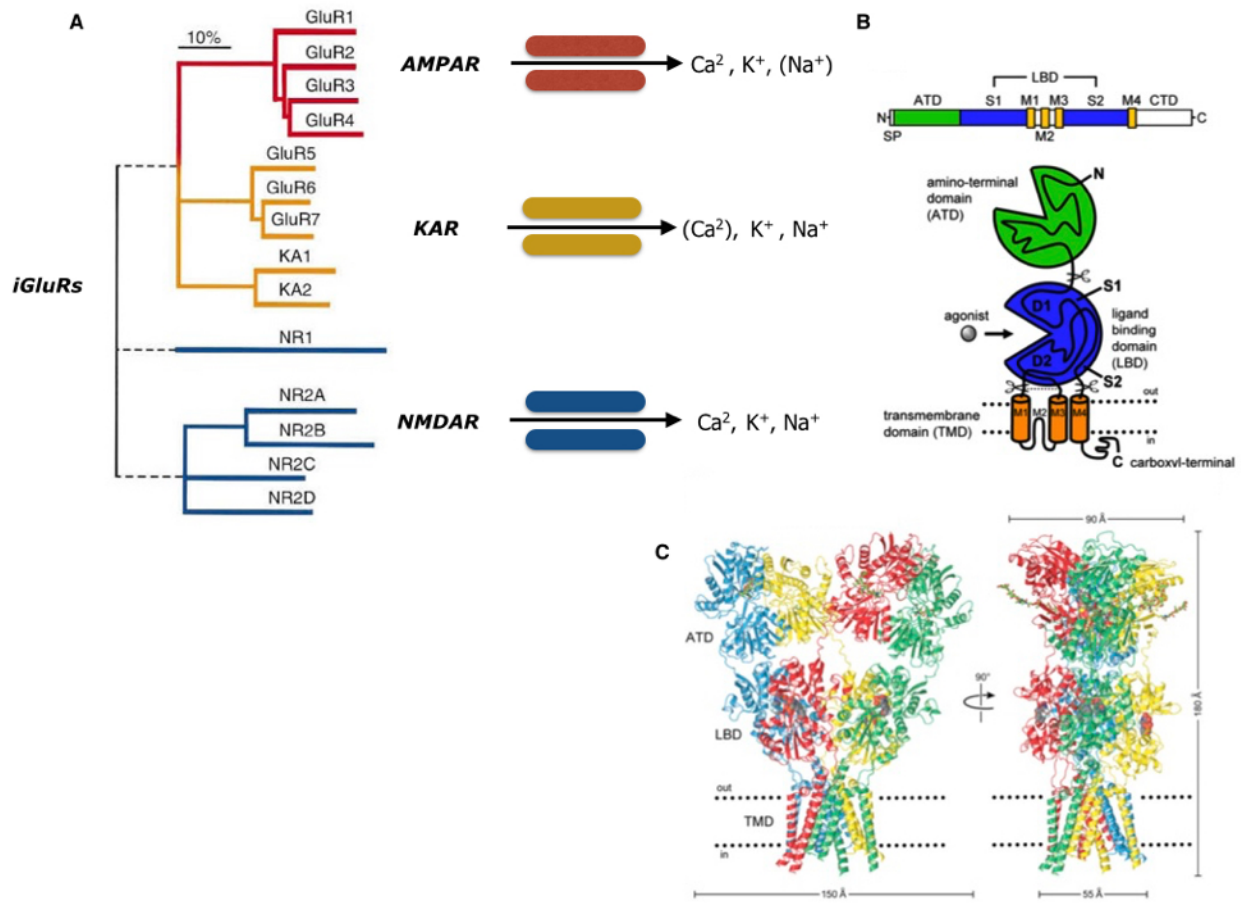


Fig.10 Glutamate receptors ion channels classification; (A) Linear representation of the subunit polypeptide chain and schematic illustration of the subunit topology, (B). Crystal structure at 3.6 Å of the membrane-spanning tetrameric AMPA receptor; (C) (modified from Traynelis S.F. *et al.*, 2010).

### 1.2.1.1 AMPA-type Glutamate Receptors

AMPA receptors are homo- and heterotetramers composed by four different subunits (GluR1, GluR2, GluR3, and GluR4; also named GluA1–A4), which allow sodium influx in response to ligand binding, triggering a fast excitatory postsynaptic response in neurons (Traynelis SF *et al.*, 2010; Palmer CL *et al.*, 2005). The electrophysiological properties of the AMPAR channels rely on the receptor molecular composition. GluR2 subunit determines AMPARs permeability to calcium and zinc. The genomic DNA of GluR2 codifies a glutamine (Q) residue at amino acid 607; however, after RNA editing by the enzyme adenosine deaminase acting on RNA 2 (ADAR2), the glutamine codon is

converted to an arginine (R) codon. AMPARs containing the GluR2(R) subunit are calcium impermeable since this arginine residue, positively charged at physiological pH, lies in the domain lining the channel pore. The receptors containing GluR2(Q) or lacking GluR2 are calcium and zinc permeable. Although the majority of AMPARs in the brain contain the GluR2(R) subunit and thus are calcium impermeable, emerging evidences point out a key role for  $\text{Ca}^{2+}$ -permeable AMPARs both in synaptic plasticity and disease (Liu SJ *et al.*, 2007; Hideyama T *et al.*, 2011; Weiss JH, 2011; Wright A., 2012).

AMPA receptors gating mechanism is based on the binding of agonists, including glutamate and the synthetic amino acids AMPA and kainate, to the D1 (domain 1) of LBD, thus allowing the flexible D2 (domain 2) to move toward D1. This movement is transmitted through the linkers to the transmembrane domain leading to a conformational change ('gating' of the channel) permitting flow of ions.  $\text{Na}^+$  is illustrated entering the cell through the central pore, which leads to depolarization. Binding of non-competitive antagonists stabilizes the closed conformation, thus preventing gating of the channel when agonist is bound to the ligand-binding domain (L B D ) (Rogawski MA, 2013) (Fig. 11).

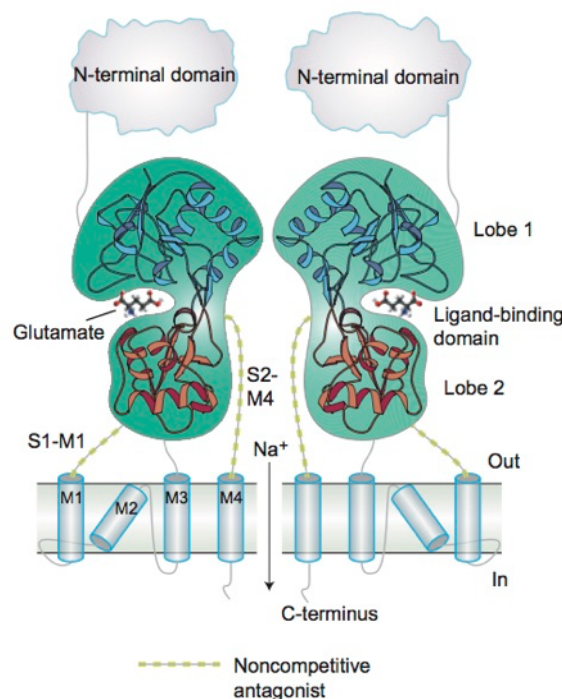


Fig. 11 Model of the AMPA receptor illustrating the domain structure of two subunits with linker segments that bind non-competitive antagonists (Rogawski M.A., 2013)

### ***1.2.1.2 Ionotropic Glutamate Receptors in CNS diseases and cancer***

Abnormal glutamate signalling is involved in the pathogenesis of conditions of acute brain injuries, such as stroke, epilepsy, and head trauma, and in chronic neurodegenerative diseases, including amyotrophic lateral sclerosis, Parkinson's and Alzheimer's disease (Chen H.S. *et al.*, 2006; Cavalheiro E.A. *et al.*, 2001). Many *in vitro* and *in vivo* studies, in the last decades, have demonstrated the potential utility of AMPA receptors as a target for seizure protection (Rogawski M.A., 1999). Since perampanel approval, in 2012, as a new and unique seizure medication that blocks the action of glutamate at AMPA receptors in the brain, which is used as adjunctive treatment in patients with focal epilepsy, AMPA receptors have been validated as novel targets for epilepsy therapy, arising interest concerning the investigation of other drugs that target AMPA receptors for the treatment of epilepsy and of other CNS disorders.

Beside its role in CNS pathological conditions, glutamate also exerts an important trophic function in the development of the CNS, regulating the proliferation and migration of neuronal progenitors (Chen H.S. *et al.*, 2006). In fact, stimulation of AMPAR and NMDAR in neuronal cultures has been linked to the activation of the mitogen-activated protein kinase (MAPK) and phosphoinositide-3-kinase (PI3-K) pathways (Perkinton M.S. *et al.*, 1999; Platenik J. *et al.*, 2000; Mao L. *et al.*, 2004), which are implicated in neural progenitor survival and proliferation (Fournier N.M. *et al.*, 2012)

The expression of iGluRs subunits have been demonstrated in tumor cells derived from nervous tissue, such as glioma, glioblastoma, medulloblastoma, and neuroblastoma cells (Yoshioka A. *et al.*, 1996; Aronica E. *et al.*, 2001; Ishiuchi S *et al.*, 2002), thus leading to further investigation regarding the role of glutamate on tumor cell proliferation. Interestingly, glutamate seems to play a central role in the malignant phenotype of gliomas via two main mechanisms:

1. the glutamate produced and released from glioma cells causes excitotoxic damage in the surrounding neurons, which facilitates the expansion of tumor cells;

2. glutamate also activates iGluR and mGluR present on glioma cells (Ye Z.C. *et al.*, 1999; Takano T. *et al.*, 2001; de Groot J. *et al.*, 2001), which contributes to survival signalling.

Interestingly, glioblastoma-tumor initiating cells express high levels of functional, calcium-permeable AMPA receptors, containing GluR1 and GluR4 subunits, when compared with the differentiated tumor cultures consisting of non-stem cells derived from the same tumor tissues (Oh M.C. *et al.*, 2012). These findings suggest that functional AMPA receptors can be formed in specific areas of the tumor. In the last decade, emerging evidences have arisen regarding the role of glutamate as a signal mediator involved in the stimulation of non-neuronal cell proliferation (Rzeski W. *et al.*, 2001; Skerry T.M. *et al.*, 2001; Hinoi E. *et al.*, 2004).

Differential expression of mRNA for iGluR subunits have been found in different types of cancer: thyroid, lung and breast carcinomas, multiple myeloma, colon adenocarcinoma, T cell leukemia (Stepulak A. *et al.*, 2009), larynx (Stepulak A. *et al.*, 2011), and gastric cancer cells (Watanabe K. *et al.*, 2008), as well as in osteosarcoma (Kalariti N. *et al.*, 2004).

Moreover, gene silencing of GluR4 modulated the mRNA expression of various tumor-suppressor genes, oncogenes and other genes involved in invasion, adhesion and metastatic capabilities (such as SNCG and MYC, MMP-2 and MTA-2, IGTB3), which resulted in significant increase of cell viability of human rhabdomyosarcoma/medulloblastoma (TE671) and human multiple myeloma RPMI8226 cells. Additionally, silencing of GluR4 stimulated migration of TE671 cells (Luksch *et al.*, 2011).

These data reinforce the evidence that iGluR subunits are expressed in the central nervous system and peripheral tumors, and correlations with prognosis have been established, thus leading to new opportunities for the development of therapies targeting glutamate signalling in cancer therapy (Ribeiro MP *et al.*, 2016)

### **1.2.1.3 Tuberous Sclerosis Complex (TSC)**

TSC is an autosomal dominant disorder caused by inactivating mutations in either the *TSC1* or *TSC2* gene (van Slegtenhorst M. *et al.*, 1997). It is characterized by the widespread development of benign tumors, termed hamartomas, in multiple organ systems including the kidneys (Neumann *et al.*, 1998), lungs (Vicente *et al.*, 2004),

heart (Jozwiak *et al.*, 2005), skin (Roach and Sparagana, 2004), and central nervous system (CNS) (Gomez, 1999) (Table 3).

*Clinical manifestations of tuberous sclerosis complex (Pan et al., 2004)*

---

Brain: cortical tubers, subependymal nodules (SENs), subependymal giant cell astrocytomas (SEGAs)
Eye: retinal hamartomas
Heart: cardiac rhabdomyomas
Kidney: benign angiomyolipomas, cysts, malignant angiomyolipomas, renal cell carcinoma
Lung: lymphangiomyomatosis (LAM), multifocal micronodular pneumocyte hyperplasia
Skin: hypomelanotic macules, shagreen patches, periungual or subungual fibromas, facial angiofibromas
Behavior: mental retardation, autism, bipolar disorder

---

Table 3 Clinical manifestations of tuberous sclerosis complex (Pan *et al.*, 2004)

CNS pathological manifestations (Table 3) include cortical tubers, subependymal nodules (SEN), and subependymal giant cell astrocytomas (SEGA) (Shepherd *et al.*, 1991; Mizuguchi and Takashima, 2001). The CNS manifestations of TSC are the most disabling and include seizures, mental retardation, and behavioral disorders such as autism (Sparagana and Roach, 2000). Epilepsy has been identified as the most common neurological symptom in TSC, 60-90% of individuals diagnosed with tuberous sclerosis complex develop epilepsy during their lifetime (Webb *et al.*, 1991; Gomez, 1999; Cross, 2005). Seizures occurred in 96% of patients aged 9–14 years referred to a child neurological clinic (Jozwiak *et al.*, 2000). Epilepsy in children with TSC tends to be progressive, with increasing seizure frequency and pharmacological intractability over time (Holmes G.L. *et al.*, 2007). The hallmark of TSC is represented by cortical tubers, that are pathognomonic of this pathology (Gomez, 1999). Tubers consist of abnormal cells with both neuronal and glial marker proteins, suggesting that they arise early in tissue development. The histopathological features of cortical tubers include disorganized, hamartomatous regions of cortex with abnormal cellular morphology, dysplastic neurons, giant cells (cytomegaly), heterotopic neurons, aberrant dendritic arbors, aberrant axonal projections, and astrocytic proliferation (White *et al.*, 2001). Many factors are involved in seizure development, but, ultimately, seizures arise due to

an imbalance between excitation and inhibition in a given cortical region. Particularly, glutamate receptors govern neuronal excitability and are developmentally regulated. When dysplastic neurons or giant cells within tubers were analyzed specifically, dysplastic neurons had increased GluR3, GluR4, GluR6, NR2B and NR2C mRNA, while giant cells had up-regulated NR2D mRNA. Moreover, Talos and colleagues have analyzed surgically resected human cortical tubers and have found a strong increase in GluR1 and GluR4 expression in the dendritic process of dysplastic neurons of this tissue, compared to normal neurons, suggesting that the increased calcium permeability engendered by these receptor subunit alterations could promote increased epileptogenesis (Talos M.D. *et al.*, 2003). A more recent study has corroborated this evidence, in fact immunocytochemical analysis of cortical tuber human specimen has demonstrated a low expression of GluR4 in normal-sized and dysplastic neurons, instead GluR4 was consistently increased in giant cells (balloon cells), dysplastic astroglia and reactive astrocytes, which are known as hallmarks features of TSC (Talos M.D. *et al.*, 2008).

### **1.2.2 *hERG1 Potassium channel***

hERG1 (also named Kv11.1) belongs to an evolutionarily conserved multigenic family of voltage-activated, outward rectifying  $K^+$  channels, the EAG family. *KCNH2* gene (formerly indicated as *hERG1*) was cloned in 1994 from a human hippocampal cDNA library and it is localized on chromosome 7, in q35-36 position (Warmke and Ganetzky, 1994). From a physiological point of view, hERG1 channels are responsible for the potassium current ( $I_{Kr}$ ) that mediates the rapid repolarizing phase following cardiac action potential.

#### **1.2.2.1 *hERG1 structure***

hERG1 channel is composed of 1159 amino acids, and both amino- and carboxy-terminals are located in the cytoplasm. The pore region of hERG1 channel is delimited by four  $\alpha$ -subunits, each composed by 6 transmembrane domains (S1-S6) (Fig. 12).

S1-S4 segments constitute the voltage sensor domain. S5, the P-loop, and S6 domains of each subunit contribute to the pore of the channel, determining potassium selectivity. In the large P-loop (residues 573-637) there are 2 consensus sites for N-glycosylation:

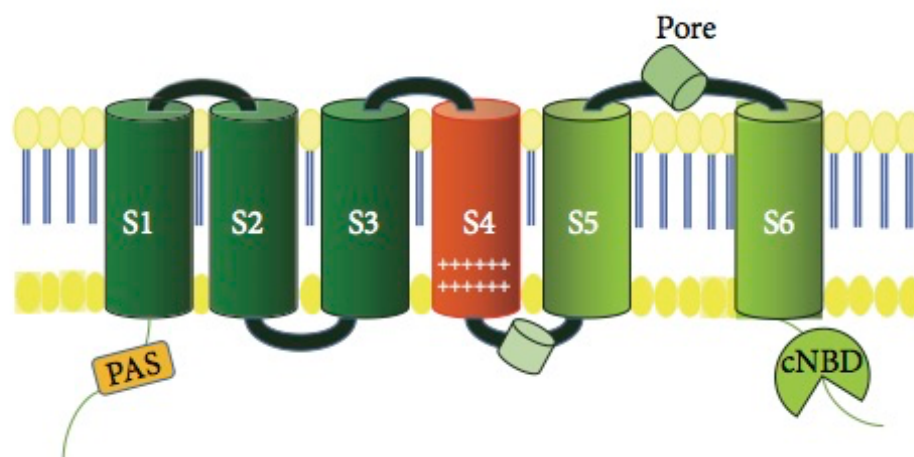


Fig.

Fig. 12 Structure of hERG1 potassium channel. PAS: PAS (acronym of Per Art Sim) domain; cNBD (cyclic nucleotide binding domain) (Lastraioli E. *et al.*, 2015).

N598 and N629; although it was demonstrated that only N596 is effectively glycosylated (Petrecca *et al.*, 1999). In addition to the transmembrane segments, each subunit has large cytoplasmic N-terminal and C-terminal regions. The N-terminal region contains: the N-tail (residues 1-25), the Per-Arnt-Sim (PAS) domain (residues 26-135), that defines the *ether-a-go-go* subfamily of VGK channels (678) (Morais Cabral *et al.*, 1998; Warmke and Ganetzky, 1994) and the proximal N-tail (residues 136-376). The C-terminal region is composed by: the C-linker (residues 666-748), the cyclic nucleotide binding domain (cNBD) (residues 749-872), which seems to play a role in regulation of deactivation gating (Al-Owais *et al.*, 2009) and the distal C-tail (residues 873-1159).

#### 1.2.2.2 hERG1 physiological expression and function

hERG1 channel expression has been demonstrated in the heart, various brain regions, smooth muscle cells, endocrine cells, as well as tumor primary samples and tumor cell lines (Arcangeli *et al.* 2009; Jehle *et al.* 2011).

In physiological conditions, hERG1 channel is responsible of the rapid component of the delayed rectifier potassium current,  $I_{Kr}$ , which terminates the plateau phase and regulates repolarisation of the cardiac action potential. Reduction of hERG currents causes lengthening of the cardiac action potential. Mutations in KCNH2 gene or Kv11.1

blockade are associated to chromosome-7-linked congenital long QT syndrome (LQTS-2) and acquired long QT syndrome, respectively.

### 1.2.2.3 *hERG1* and cancer

Different types of ion channels and transporters have been found to be functionally expressed in different types of cancer cells, and to regulate different aspects of tumor cell behavior (cell proliferation, apoptosis, migration, invasiveness etc.). Figure 13 reports an overview regarding the functional role of ion channels and transporters in some of the most diffuse solid cancers (Lastraioli *et al.*, 2015).

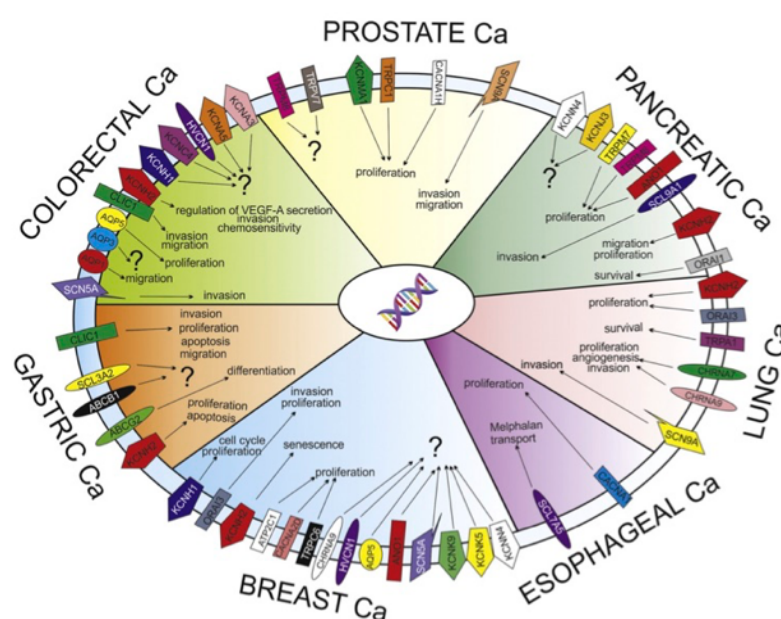


Fig. 13 Ion channels and transporters (ICT) profile and role in the solid cancers (Breast, Prostate, Lung, Colorectal, Esophageal, Pancreatic and Gastric). This figure summarizes the main roles exerted by ICT in cancer biology (Lastraioli E. *et al.*, 2014)

Many studies in the last decades have extensively demonstrated the expression of *hERG1* in several types of cancer (Bianchi S. *et al.*, 1998) and its interaction with many oncoproteins (Lin *et al.*, 2007). *Kv11.1* was found over-expressed in a variety of tumors with different histogenesis: colorectal cancer (Lastraioli E. *et al.*, 2004; Lastraioli *et al.*, 2012; Crociani *et al.*, 2013), esophageal adenocarcinoma (Lastraioli E. *et al.*, 2006), gastric cancer (Shao *et al.* 2005; Lastraioli E. *et al.* 2005; Crociani O. *et al.*, 2014), glioblastoma multiforme (Masi A. *et al.*, 2005), endometrial adenocarcinoma (Cherubini A. *et al.*, 2000), neuroblastoma (Arcangeli A. *et al.*, 1993), melanoma (Afrasiabi *et al.*,

2010; Arcangeli *et al.*, 2013) and both Acute Myeloid and Acute Lymphoblastic Leukaemia (AML and ALL) (Pillozzi S. *et al.* 2007; Pillozzi S. and Arcangeli A., 2010). hERG1 channel can thus be considered a marker for malignant transition and its expression usually correlates to poor prognosis (Lastraioli E. *et al.*, 2004; Pillozzi S. *et al.*, 2007; Ding *et al.*, 2010; Lastraioli E. *et al.*, 2012; Arcangeli A. *et al.*, 2013). It has been also demonstrated that hERG1 is expressed in precancerous lesions, such as Barrett's esophagus. In this pathological setting, hERG1 expression marks a higher risk to develop adenocarcinoma, thus being proposed as a prognostic marker useful for patients' stratification (Lastraioli E. *et al.*, 2016).

hERG1 channel was found implicated in many aspect of tumor progression: enhanced cell proliferation, cell survival, invasiveness, angiogenesis, lymph node dissemination and metastasis (Arcangeli A. *et al.*, 2009).

hERG1 channel, also, plays a role in the development of new vasculature necessary for solid tumors growth. Increased neoangiogenesis, another hallmark of malignant tissue growth, has been reported for glioblastoma, as well as for human gastric cancer. In such tumors, the generation of blood vessels was stimulated by hERG1-dependent secretion of vascular endothelial growth factor (Masi A. *et al.*, 2005; Crociani O. *et al.*, 2013; Crociani O. *et al.*, 2014).

Moreover, many studies report the effect of specific hERG1 blockers on tumor progression. In various leukemia cell lines, treatment with the hERG1 blocker E-4031 reduces their proliferation rate (Smith *et al.*, 2002). hERG1 channel blocking with E-4031 and silencing using specific siRNA prevent proliferation and cell migration in melanoma cell line MDA-MB-435S (Afrasiabi *et al.*, 2010).

Kv11.1 blockers have shown proapoptotic effects on cancer cell lines and on reconstituted systems like transfected HEK293, such phenomenon is mainly related to the inhibition signalling pathways in which hERG1 is involved. In fact, hERG1 channel is capable of triggering many intracellular signalling pathways. The channel was indeed found in macromolecular complexes on the surface of plasma membrane of cancer cells, together with integrin subunits (Arcangeli *et al.*, 1993; Hofmann *et al.*, 2001; Cherubini *et al.*, 2005; Pillozzi *et al.*, 2007; Crociani *et al.*, 2013), growth factors receptors (e.g.

vascular endothelial growth factor receptor-1 (FLT-1) (Pillozzi *et al.*, 2007)) or chemokines receptors (e.g. chemokine CXC receptor-4 (CXCR-4) (Pillozzi *et al.*, 2011)).

#### 1.2.2.4 hERG1- $\beta$ 1 integrin complex in cancer

Integrins encompass a family of 24 heterodimeric ( $\alpha$ - and  $\beta$ -subunits) transmembrane receptors involved in mediating cell-cell and extracellular matrix (ECM)-cell interactions (Hynes 2002), transducing signals bidirectionally across the cell membrane. Each subunit is composed by a large extracellular domain, a single spanning transmembrane domain and a small cytoplasmic tail (Fig. 14, A).

Many types of cancer are characterized by the interaction between hERG1 channel and integrin receptors (Fig. 14, C). This phenomenon has been described for neuroblastoma (Arcangeli *et al.*, 1993), colon cancer (Crociani *et al.*, 2013), leukemia cells (Hofmann *et al.*, 2001; Pillozzi *et al.*, 2007; Pillozzi *et al.*, 2011) and in reconstituted models of transfected HEK293 (Cherubini *et al.*, 2005). From a molecular point of view, integrin activates hERG1 channel (Arcangeli *et al.*, 1993), and hERG1 channel modulates integrin downstream signalling (Cherubini *et al.*, 2005; Arcangeli and Becchetti 2006; Pillozzi *et al.*, 2007; Pillozzi *et al.*, 2011; Crociani *et al.*, 2013).

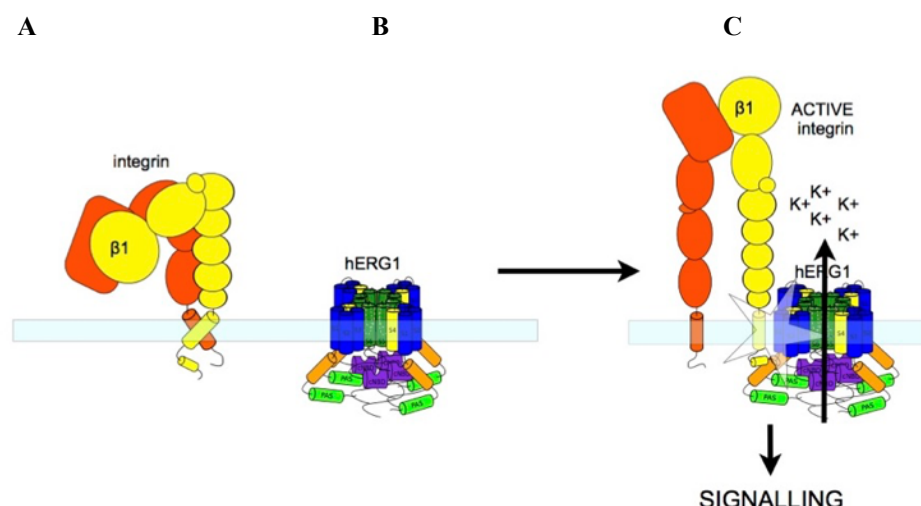


Fig. 14 Schematic representation of hERG1 and  $\beta$ 1 integrin complex formation.  $\beta$ 1 integrin structure in its inactive state (panel A), hERG1 tetrameric structure (panel B); hERG1/ $\beta$ 1 integrin complex interaction (Panel C) (Crescioli S., 2014)

It has been demonstrated that hERG1 blockers inhibit FLT1- $\beta$ 1integrin-hERG1 complex related effects, inhibiting signalling and migration in acute myeloid leukemia cells (Pillozzi *et al.*, 2007) and acting on CXCR4- $\beta$ 1integrin-hERG1 complex in acute lymphoblastic leukemia (Pillozzi *et al.*, 2011). In subcutaneous tumor models of colorectal cancer, selective hERG1 blockers disrupt  $\beta$ 1integrin-hERG1 complex related signalling, resulting in the inhibition of cell growth, angiogenesis and metastatic spread (Crociani *et al.*, 2013).

For these reasons, targeting hERG1 channel in specific macromolecular complexes selectively expressed on cancer cells, such as hERG1/ $\beta$ 1integrin complex, could be a valid strategy for cancer therapy.

## **2. AIMS OF THE STUDY**

Cancer is currently the second leading cause of death in the United States, and is expected to surpass heart diseases as the leading cause of death in the next few years (Siegel R.L., 2015).

Immunotherapy has demonstrated to be a valuable approach to treat cancer and monoclonal antibodies have been applied with success in therapy protocols (Weiner G.J., 2015).

Many interests were raised by the development of recombinant antibodies (scFvs and bispecific antibodies), which conjugate antigen specificity with the invaluable advantage of small size, thus resulting in enhanced capacity to penetrate effectively the tumor mass (Verhaar *et al.*, 1995). These molecules have been exploited to be used both for diagnostic and therapeutic purposes.

The aim of the present study is the development of monoclonal and recombinant antibodies directed against targets on the plasma membrane surface, which are relevant in the oncological setting. We have focused on the production and characterization of the following molecules to be used for diagnostic and therapeutic purposes:

1. a monoclonal antibody against ionotropic Glutamate Receptor 4 (iGluR4), to exploit as a diagnostic tool; moving forward from the anti-iGluR4 monoclonal antibody, we have developed a *single-chain variable fragment* antibody directed against the same antigen for conjugation with nanoparticles (NPs) to set up a *drug-delivery system*, overcoming problems related to the passage of the blood-brain barrier (BBB). After accomplishment of VL and VH characterization, the next step will be the assembly of the scFv-iGluR4 construct by SOE (Splicing by Overlapping Regions) PCR. The construct will be cloned into a proper vector for expression in *Pichia pastoris* yeast cells. In the meanwhile, we have studied the problem related to the conjugation of the scFv antibody to PLGA-PEG Rhodamine B-G7 (NPs). To this purpose, we have exploited a single chain antibody (scFv) already produced in our laboratory, directed against hERG1 protein. scFv-hERG1-

D8 antibody characterization will be described in details in the second part of the present thesis.

2. a single-chain variable fragment antibody directed against hERG1 channel; the antibody was produced and characterized (patent N° FI2014A000189) and as it has shown great promise as a molecular tool for optical *in vivo* imaging applications. Moving from the original antibody sequence, we have produced a new antibody (via mutagenesis), scFv-hERG1-D8Cys, which has been expressed and characterized, showing promises as a possible novel candidate for therapeutic applications;
3. a bispecific antibody, anti-hERG1- $\beta$ 1-scDb, directed against hERG1 channel and  $\beta$ 1 integrin, which has demonstrated to be able to bind the oncogenic unit hERG1- $\beta$ 1.

### 3. MATERIALS AND METHODS

#### 3.1 Anti- iGluR4 monoclonal antibody development.

##### IMMUNIZATION

Hybridomas were produced according to Köhler and Milstein (1975) standard protocol. Three six week old female Balb/c mice were immunized according to the protocol reported in Table 1 (*Current Protocols in Molecular Biology*, 1994), using the selected anti-iGluR4 peptide conjugated with Ovalbumin (Primm Srl).

DAY	OVA-CONJUGATED ANTI-GLUR4 PEPTIDE
1	100µg carrier-conjugated peptide+ Complete Freund's Adjuvant Intraperitoneal injection
21	50 µg carrier-conjugated peptide+ Incomplete Freund's Adjuvant Intraperitoneal injection
35	50 µg carrier-conjugated peptide+ Incomplete Freund's Adjuvant Intraperitoneal injection
49	50 µg carrier-conjugated peptide+ Incomplete Freund's Adjuvant Intraperitoneal injection
63	100 µg carrier-conjugated peptide+ Incomplete Freund's Adjuvant Intravenous injection

Table 1. Female Balb/c mice immunization protocol

##### CELL FUSION

Three days after the final intravenous injection, mice were sacrificed by cervical dislocation and spleens were surgically resected.

To obtain spleen cell suspension, spleens were minced in a sterile Petri dish, using a surgical scalpel, then they were homogenized in 2 ml of DMEM culture medium (Euroclone) using a glass tissue homogenizer.

B-lymphocytes isolated from a spleen after the homogenization procedure were fused with aminopterin sensitive myeloma cells (NS0) using the polyethylene glycol (PEG) (Sigma) method (Galfrè and Milstein 1981) .

NS0 cells were maintained in logarithmic phase growth for 7 days before cell fusion. An equal number ( $10^8$  cells) of B-lymphocytes and NS0 cells were mixed together in 30 ml of DMEM + 4 mM L-Gln and centrifuged at 700 g for 5 min. Supernatant was discarded and the tube with cell pellet was placed in a beaker with 37°C water. The cell fusion protocol follows.

1. Add 1 ml of 37°C preheated PEG in 1 minutes, stirring;
2. Stir for 2 minutes;
3. Add 1 ml of 37°C preheated DMEM + 4 mM L-Gln in 1 minutes, stirring;
4. Repeat C;
5. Add 1 ml of 37°C preheated DMEM + 4 mM L-Gln in 30 sec, stirring;
6. Repeat E;
7. Add 6 ml of 37°C preheated DMEM + 4 mM L-Gln in 2 minutes, stirring;
8. Add 12 ml of 37°C preheated DMEM + 4 mM L-Gln drop to drop, stirring;
9. Centrifuge at 800 g for 5 minutes and discard supernatant.

The fusion product was resuspended in DMEM + 4 mM L-Gln supplemented with 20% FetalClone I serum (Hyclone) and HAT, (Hypoxanthine, Aminopterin, Timidine) (Sigma).

B-cell/NS0 hybrid selection requires the use of a selective agent, added to the medium, which is HAT. HAT contributes to selection, exploiting the following mechanism: NS0 myeloma cells lack of the expression of Hypoxanthine-Guanine PhosphoRibosyl Transferase (HGPRT) enzyme. HGPRT is an enzyme that catalyses the conversion of hypoxanthine to inosine monophosphate and guanine to guanosine monophosphate, transferring the 5-phosphoribosyl group from 5-phosphoribosyl 1-pyrophosphate (PRPP) to the purine, thus playing a central role in the generation of purine nucleotides through the purine *salvage pathway*. Cells that do not express this enzyme can produce

purine nucleotides only through the *de novo* pathway; but the latter is blocked by aminopterin.

The cell fusion product was resuspended in 48 ml of selective complete DMEM medium and aliquoted, according to the following dilutions 1:2, 1:4, 1:8 and 1:8 in 24-well multi-well plates (2 ml for well). The plates were incubated in a humidified incubator at 37°C, 5% CO<sub>2</sub>. After two weeks the selected hybridomas formed visible colony-like clusters.

Hybridomas were analyzed for their capacity to bind the antigen by Enzyme-Linked Immunosorbent Assay (ELISA) in order to select the best population for soft agar cloning.

### ***ELISA ASSAY***

An ELISA assay was performed using the iGluR4-peptide, previously used for immunization. The antigen was diluted to 10 µg/ml in 100 mM Na<sub>2</sub>CO<sub>3</sub> buffer and aliquoted 100 µl/well in a 96-well plate. Each following step was preceded by three washes with 200 µl 0.05% Tween-20 in PBS. After incubation overnight at 4°C, wells were quenched by addition of 200 µl/well blocking solution (3% BSA in 0.05% Tween-20 in PBS) and incubated for one hour at room temperature. Each supernatant was dispensed in duplicate, 100 µl/well. After incubation for two hours at room temperature, anti-mouse secondary antibody (Sigma) diluted in blocking solution 1:500 (10 µg/ml) was dispensed 100 µl/well and incubated for one hour at room temperature. The assay was developed by addition of 100 µl/well TMB (3,3',5,5'-Tetramethylbenzidine) substrate (Sigma) and the reaction stopped with 100 µl/well 0,5 M HCl. Plates were analyzed measuring the absorbance at 450 nm.

### ***SOFT AGAR CLONING***

For monoclonal antibody production, clonal isolation of hybridomas was achieved after two subsequent cloning processes: manual colony picking and soft agar cloning.

Colonies obtained from cell fusion, grown after HAT selection in 24-well multi-well plates, were picked and transferred each one into a new well. The supernatant of those clones was assayed by ELISA in order to choose the best hybridomas for soft agar cloning.

Hybridomas were plated (10000, 5000, 2500, 1250 cells per 60 mm dishes) in soft agar to allow the formation of colonies from single cells. Soft agar plates were composed of a Base Layer (0.5% low melting point agarose in DMEM supplemented with 4 mM L-Gln, 20% Fetal Clone I serum and 1x HAT) and a Top Layer (cells in 0.25% low melting point agarose in DMEM supplemented with 4 mM L-Gln, 20% Fetal Clone I serum and 1x HAT). After about 15 days, the clones were picked up, seeded in a 24-well multi-well plate, amplified and adapted to grow in an aminopterin free medium. Aminopterin remains inside the cells even if HAT is removed from the culture medium, continuing to exploit its inhibitory effect on the *de novo* synthesis of nucleotide bases. For this reason aminopterin was diluted from the culture by several passages of the cells in hypoxanthine-thymidine (HT) (Sigma) supplemented medium (approximately 2-3 weeks) before transfer into normal hybridoma growth medium: DMEM High Glucose, added with 4 mM L-Gln and 10% FetalClone I (Hyclone).

#### ***ISOTYPE TEST***

The isotype test was performed using IsoQuick for Mouse Monoclonal Isotyping (Sigma) following the manufacturer's instructions.

#### ***CELL CULTURE AND TRANSFECTION***

All cell lines were routinely cultured in a humidified incubator at 37°C with 5% CO<sub>2</sub>. HEK 293 cells were cultured in Dulbecco's Modified Eagle Medium (DMEM) High Glucose (Euroclone) supplemented with 4 mM L-Gln and 10% FBS serum (Euroclone).

HEK 293 were stably cotransfected with iGluR4 cDNA in pRK5 plasmid, kindly gifted by Prof. Huganir (Johns Hopkins Medicine Brain Science Institute at the Johns Hopkins University School of Medicine, Baltimore, USA), after linearization with BglII restriction endonuclease, and pcDNA 3.1(+) with a 1:6 ratio. Cotransfection was necessary because iGluR4-pRK5 doesn't carry the eucaryotic gene for antibiotic resistance. Cells, after cotransfection, carried G418 resistance which was exploited for cell selection.

Cotransfection was performed using Lipofectamine 2000 (Thermo Fisher Scientific), following the manufacturer's instructions, and cells were selected using G418 (Gibco for Thermo Fisher Scientific).

### ***TOTAL RNA EXTRACTION***

Total RNA was extracted from cells, using a solution of phenol and guanidine isothiocyanate (TRIzol® Reagent, Ambion®). RNA concentrations were determined by measuring the optical density (OD) at 260 and 280 nm. An OD<sub>260</sub>=1 is equivalent to 40 µg/ml RNA. The concentration in µg/ml can be calculated from the absorbance value:

$$A_{260} \times \text{dilution factor} \times 40 \text{ µg/ml}$$

The ratio of the absorbance values at 260 nm and 280 nm (A<sub>260</sub>/A<sub>280</sub>) provides an estimate of the purity of RNA with respect to contaminants that absorb in the UV spectrum, such as protein. Pure RNA has an A<sub>260</sub>/A<sub>280</sub> ratio of 1.8 to 2.1, ideally. RNA samples with an A<sub>260</sub>/A<sub>280</sub> ratio between 1.7 and 2 were considered to be sufficiently pure for further experiments.

### ***RNA REVERSE TRANSCRIPTION (RT-PCR)***

Reverse transcription polymerase chain reaction (RT-PCR) is a technique where a RNA strand is reverse transcribed into its complementary DNA (cDNA) using the reverse transcriptase enzyme. mRNA was reverse transcribed to cDNA using Random Primers:

COMPONENTS	STOCK CONCENTRATION	FINAL CONCENTRATION	VOLUME µl
Random primers	3 µg/µl	300 ng	2
RNA	————	————	1
dNTP	10 mM	0,5 mM	1
ddH <sub>2</sub> O	————	————	8

The mix was incubated in a thermal cycler at 70°C for five minutes, and then immediately placed on ice for five minute. Then, the following was added to the tube:

COMPONENTS	VOLUME $\mu$ l
<b>5X First-Strand Buffer</b>	4
<b>SuperScript II Reverse Transcriptase (Invitrogen)</b>	1
ddH <sub>2</sub> O	3

The mix was incubated in the thermocycler as follows:

<u>Steps</u>	<u>Temperature</u>	<u>Time (min)</u>
1	25°C	10
2	42°C	50
3	70°C	15

### ***END POINT PCR***

End Point-PCR was performed using the following primers designed to amplify a portion of the cDNA of the AMPA-type iGluR4.

<b>GLUR4 FORWARD PRIMER</b>	ACAAACGCCTTCTGTTCCCA
<b>GLUR4 REVERSE PRIMER</b>	GCTCCACCATGTATAAACCTCTC

COMPONENTS	STOCK CONCENTRATION	FINAL CONCENTRATION	VOLUME $\mu$ l
DNA	—	—	2
Forward primer	20 $\mu$ M	200 nM	0,25
Reverse primer	20 $\mu$ M	200 nM	0,25
Platinum PCR Supermix (Invitrogen)	—	—	22,5

The mix was incubated in the thermocycler as follows:

<u>Steps</u>	<u>Temperature</u>	<u>Time</u>
1	94°C	2 min
2	94°C	30 sec
3	54°C	40 sec
4	72°C	30 sec
5	72°C	10 min

Steps 2-4 were repeated 34 times.

### ***CYTOFLUORIMETRIC ANALYSIS***

10<sup>5</sup> HEK293-iGluR4 and HEK293-MOCK cells were incubated with antibody supernatants (diluted in PBS 1:2 or 1:4) at room temperature for 15 minutes. After incubation, cells were centrifuged and FITC secondary antibody (1:100) was incubated for other 15 minutes. After secondary antibody incubation, cells were centrifuged, resuspended in 300 µl of PBS and analyzed using a FACS Canto (BD Biosciences)

### ***IMMUNOFLUORESCENCE***

Cells were grown on glass coverslips and fixed with 4% methanol-free formaldehyde (Thermo Scientific) in PBS for 15 minutes. Nonspecific sites were blocked with 10% BSA for 2 hours. Primary antibody (hybridoma supernatants) was incubated overnight at 4°C. Glass coverslips were washed 3 times in PBS and the secondary antibody, anti-mouse IgG-Alexa 488 (1:500) (Invitrogen) was incubated for 1 hour at room temperature in the dark. Glass coverslips were washed as above, nuclei were stained with Hoechst (1:1000) for 30 minutes and then mounted on slides using ProLong Gold Antifade Reagent (Life Technologies) following manufacturer's instructions. Cells were visualized on a confocal microscope (Nikon, C1).

### ***IG G ANTIBODY PURIFICATION***

Purification of IgG B5 and C4 anti-iGluR4 mAb supernatants was performed by Affinity Chromatography, using ÄKTA Pure Protein Purification System (GE Healthcare, Life Sciences) using HiTrap Protein A HP 1 ml columns (GE Healthcare, Life Sciences). Wash steps and equilibration were performed according to the manufacturer's instructions, using a buffer composed of 20 mM sodium phosphate, pH 8 and elution was performed using a buffer composed of 0.1 M citrate buffer pH 4.5, adjusted with Tris 1M pH 9. Analysis and quantification was accomplished using UNICORN 7.0 software.

### ***COOMASSIE STAINING***

After SDS-PAGE, proteins were stained on the gel with Coomassie Brilliant Blue method. The gel was incubated for 30 minutes at room temperature (RT) with

Coomassie Staining Solution (0.05% Brilliant Blue R-250, 50% methanol, 10% acetic acid, 40% H<sub>2</sub>O) and then with Destaining Solution (methanol 40%, acetic acid 10%, H<sub>2</sub>O 50%) until bands with a blue color became clearly visible.

### ***IMMUNOCYTOCHEMISTRY (ICC)***

Cells were grown on glass coverslips, fixed with 90% ethanol for 10 minutes and then incubated with H<sub>2</sub>O<sub>2</sub> 0,1% in PBS for 15 minutes at RT. Non-specific sites were blocked with Ultra V block (Thermo Fisher Scientific) incubated for 20 minutes at RT. Cells were washed and incubated with primary antibody (or antibody supernatants, 1:10) diluted in Ultra V block/PBS overnight at 4°C. The following day immunostaining was performed with a commercially available kit (PicTure Plus kit and DAB; Zymed, Carlsbad, CA) according to the manufacturer's instructions.

### ***IMMUNOHISTOCHEMISTRY (IHC)***

The slides were de-waxed in Histoclear and hydrated through graded ethanol solution to H<sub>2</sub>O. The endogenous peroxidase were blocked using H<sub>2</sub>O<sub>2</sub> 1% solution in PBS. Antigen retrieval was performed by treatment with proteinase K (5 µg/ml). Purified antibodies B5 and C4 anti-GuR4 (1:100) were incubated 2 hours at 37°C. The following day immunostaining was performed with a commercially available kit (PicTure Plus kit and DAB; Zymed, Carlsbad, CA) according to the manufacturer's instructions.

### ***CELL VIABILITY***

Cell viability was evaluated performing a Trypan blue assay; 10<sup>3</sup> cells/well were seeded in a 96-well plate. After 24 hours, the medium was replaced by 100 µl of fresh medium containing different concentrations of B5 and C4 anti-iGluR4 antibodies (1:10; 1:20; 1:100). Cells were cultured 24 hours in a humidified incubator at 37°C and 5% CO<sub>2</sub>.

After treatment cells were detached and viable cells were counted. Experiments were performed in triplicate.

### ***ELECTROPHYSIOLOGICAL RECORDING***

Whole cell patch-clamp data were recorded at room temperature (about 25°C) by using a Multiclamp 700A amplifier (Axon Instruments, Molecular Devises, USA).

Micropipettes (3-5 M $\Omega$ ) were pulled from borosilicates glass capillaries (Harvard Apparatus, Holliston, MA), with a PC-10 pipette puller (Narishige, Tokio). Currents,z were low-pass filtered at 2 kHz and digitized online at 10 kHz, with a Digidata 1322A and pClamp 8.2 (Axon Instruments, Molecular Devises, USA). Data were analyzed off-line with pClamp and Origin 8.0 (Microcal, Inc. Northampton, MA) software.

The external solution contained 130 mM NaCl, 3 mM KCl, 2 mM CaCl<sub>2</sub>, 1 mM MgCl<sub>2</sub>, 25 mM Glucose; pH 7.4.

The pipette ('intracellular') solution contained: 125 mM Cs-gluconate, 6 mM CsCl, 10 mM HEPES, 2 mM MgCl<sub>2</sub> and 0.2 mM EGTA, pH 7.3. The whole cell inward currents were evoked by pressure application of 10 mM glutamate and recorded at a holding of -70 mV (Stepulak A. *et al.*, 2009). Solutions were applied using a 700  $\mu$ l capillary, which has been positioned next to the cells we wanted to analyze. Perfusion was set around 90  $\mu$ l/min and, based on previous studies, it was determined that solution exchange occurs in 6 seconds.

#### ***ISOLATION OF ANTIBODY VARIABLE DOMAINS BY POLYMERASE CHAIN REACTION (PCR)***

To isolate antibody variable domains (VL and VH) we performed a PCR with the primers reported in Wang *et al.* (2010) with modifications

<b>Kappa light chain</b>	<b>Primer name</b>	<b>Primer sequence</b>
<b>Forward primer</b>	degKappadir	GAYATTGTGMTSACMCAR WCTMCA
Reverse primer	Kapparev	GGATACAGTTGGTGCAGCA TC
<b>IgG1 heavy chain</b>	<b>Primer name</b>	<b>Primer sequence</b>
Forward primer	degH1dir	CAGGTTACTCTGAAAGWG TSTG
Forward primer	degH2dir	GAGGTCCARCTGCAACAR TC
Forward primer	degH3dir	CAGGTCCAAACTUCAGCA RCC
Forward primer	degH4dir	GAGGTGAASSTGGTGGAA TC
Forward primer	degH5dir	GATGTGAACTTGGAAGTG TC
Reverse primer	IgG1rev	GGAAGATCTATAGACAGAT GGGGGT GTCGTTTTGGC

Table 2 Primers used for the isolation of VL and VH variable domains, from Wang *et al.*, (2000) with modifications.

PCR was performed following the protocol reported as follows:

<b>COMPONENTS</b>	<b>STOCK CONCENTRATION</b>	<b>FINAL CONCENTRATION</b>	<b>VOLUME <math>\mu</math>l</b>
DNA	——	——	1
Forward primer	10 $\mu$ M	300 nM	0,75
Reverse primer	10 $\mu$ M	300 nM	0,75
10X PCR Buffer	10X	1X	4
dNTPs	2.5 mM each	200 mM	4
MgCl <sub>2</sub>	25mM	2,5 mM	5
Phusion High Fidelity Polimerase	——	——	0,2
PCR grade water	——	——	8,95

<u>Steps</u>	<u>Temperature</u>	<u>Time</u>
1	98°C	30 sec
2	98°C	10 sec
3	54°C (VH); 46°C (VL)	30 sec
4	72°C	30 sec
5	72°C	10 min

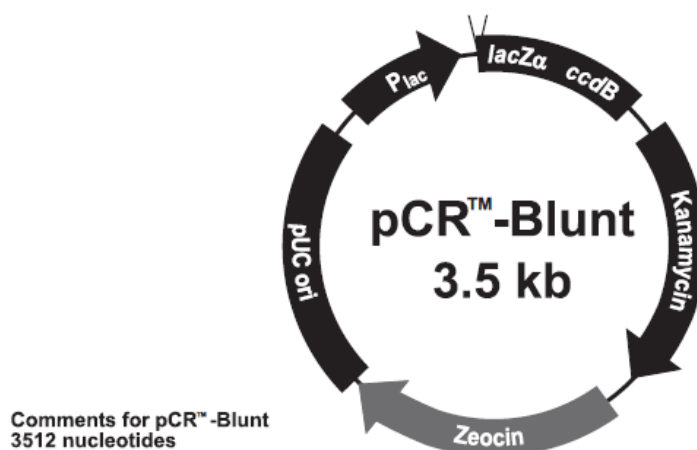
Steps 2-4 were repeated 30 times.

### ***PCR PRODUCT PURIFICATION***

5 µl PCR product of VH and VL (B5 and C4 anti-GluR4 antibody clones) was run on a 1.5% Agarose gel in TAE buffer (Tris, acetic acid and EDTA). 0.04 µl/ml of ethidium bromide, which interacts with DNA and fluoresces under UV-light, was used to visualize the DNA fragments. The electrophoresis was run at 100V, the migration velocity is reverse proportional to the DNA molecular weight. A 2-Log DNA ladder was used as DNA standard for estimating the fragments size. Gel was viewed by a UV illuminator and an image acquired with a digital camera and proprietary software (Kodak 1D LE 3.5). After visualization of DNA bands of a proper weight, consistent with what expected, the rest of PCR product was purified using NucleoSpin® Gel and PCR Clean-up (Macherey-Nagel).

### ***pCRTM -Blunt CLONING OF PCR PRODUCTS***

V<sub>H</sub> and V<sub>L</sub> regions were also cloned in pCRTM -Blunt vector (Invitrogen) which is designed to clone blunt PCR fragments without using any restriction enzymes and without the addition of deoxyadenosine (dA) to the 3' end of PCR products.



After purification from agarose gel, PCR products were cloned into pCRTM - Blunt vector using a 10:1 molar ratio of insert:vector. To estimate the amount of PCR product needed for a 10:1 molar ratio of insert to 25 ng of pCRTM-Blunt vector, was used the following formula:

$X \text{ ng insert} = 10 \times (Y \text{ bp PCR product}) \times (25 \text{ ng linearized pCR}^{\text{TM}} - \text{Blunt}) / (3500 \text{ bp pCRTM} - \text{Blunt})$  where X ng is the amount of PCR product of Y base pairs to be legated for a 10:1 insert:vector molar ratio. Reaction conditions for directional cloning ligation were as follows:

COMPONENTS	STOCK CONCENTRATION	FINAL CONCENTRATION	VOLUME $\mu\text{l}$
pCR <sup>TM</sup> -Blunt	25 ng/ $\mu\text{l}$	25ng	1
VH fragments	4 ng/ $\mu\text{l}$	25ng	5
or			
VL fragments	12 ng/ $\mu\text{l}$	25ng	2
Ligation buffer	10X	1X	1
T4 DNA Ligase	4U/ $\mu\text{l}$	0,4U/ $\mu\text{l}$	1
PCR grade water	—	—	up to 10

The ligation was incubated at 16°C for one hour.

### ***TRANSFORMATION OF COMPETENT *E. coli* CELLS***

DNA was introduced in bacterial cells through heat shock transformation of chemically competent *E.coli*. Cells were thawed on ice for 10 minutes. DNA was added to the cells and incubated on ice for 30 minutes. The mixture was then heat shocked at 42°C for exactly 30 seconds and incubated on ice for 5 minutes. Bacterial cells were resuspended in 950 µl of SOC medium (SOB medium supplemented with 1 mM MgSO<sub>4</sub>, 1 mM MgCl<sub>2</sub> and 0.1% w/v glucose) and then grown at 37°C for one hour in shaking.

#### ***PLASMID DNA PURIFICATION***

Plasmid DNA of colonies grown on the plates were extracted and purified. A single colony was picked up with a sterile toothpick and let to grow in 5 ml of LB supplemented with antibiotic (50 µg/ml) overnight, after which plasmid DNA was purified using the PureYield™ Plasmid Miniprep System (Promega) following the manufacturer's instructions. Extracted DNA was tested for the presence of the insert, quantified (using the NanoDrop™ 2000/2000c, Thermo Fisher Scientific) and sequenced by GATC Biotech.

### 3.2 Production and characterization of anti-scFv-hERG1 antibodies

#### scFv-hERG1 MUTAGENESIS

Mutagenesis was performed on the scFv-hERG1 expression cassette cloned into pPIC9K using the QuikChange® XL Site-Directed Mutagenesis Kit (Stratagene, Agilent Technologies). Suitable primers for the introduction of the Cys amino acid were designed according to the manufacturer's indications and synthesized by Primm Biotech.

COMPONENTS	STOCK CONCENTRATION	FINAL CONCENTRATION	VOLUME $\mu$ l
DNA	13ng/ $\mu$ l	—	1
Forward primer	10 $\mu$ M	125 ng	1,84
Reverse primer	10 $\mu$ M	125 ng	1,5
10X PCR Buffer	10X	1X	5
dNTPs	2.5 mM each	—	1
Quick Solution	—	—	1
<i>Pfu Turbo</i> DNA polymerase	2.5 U/ $\mu$ l	—	1
PCR grade water	—	—	32

<u>Steps</u>	<u>Temperature</u>	<u>Time</u>
1	95°C	1 min
2	95°C	50 sec
3	60°C	50 sec
4	68°C	4 min
5	68°C	7 min

Steps 2-4 were repeated 18 times

After the amplification reaction, 1  $\mu$ l of *DpnI* restriction enzyme (10 U/ $\mu$ l) was added directly to the reaction mixture, that was incubated right after at 37°C for 1 h to digest the parental DNA template.

At this point, bacterial DH5 $\alpha$  ultra competent cells were transformed through heat-shock, following the protocol described in the previous section of Materials and Methods. The following day, several colonies had grown and some of them were picked and DNA was extracted and sequenced to verify the presence of the desired mutation. The construct obtained was labelled scFv-hERG1-Cys.

***scFv-hERG1-G3 AND scFv-hERG1-D8Cys EXPRESSION IN Pichia pastoris***

Linearised scFv-hERG1 and scFv-hERG1-Cys were both digested with *Sall* and transformed into the *Pichia pastoris* strain GS115 by spheroplasting technique, generating Mut<sup>+</sup> transformants. For the transformation we have referred to the Pichia Expression Kit (Invitrogen) indications.

Five days after transformation, single colonies were visible to the naked eye, 92 clones and 4 negative controls were picked and transferred in three different 96-well plates, with different concentration of G418: without G418, 5 mg/ml, 15 mg/ml. G418 selection was performed exploiting the characteristic that pPIC9K contains the bacterial kanamycin gene that confers resistance to Geneticin® in Pichia. The level of Geneticin® resistance approximately depends on the number of kanamycin genes integrated. A single copy of pPIC9K integrated into the Pichia genome confers resistance to Geneticin® to a level of ~0.25 mg/ml. Multiple integrated copies of pPIC9K can increase the Geneticin® resistance level from 0.5 mg/ml (1-2 copies) up to 4 mg/ml (7-12 copies). Due to the genetic linkage between the kanamycin gene and the expression cassette (both under the P<sub>AOX1</sub> promoter), we can infer that Geneticin® resistant clones contain multiple copies of the gene of interest. For this same reason, secreted protein expression may increase because of a gene dosage effect. Thus, the presence of pPIC9K was used as a tool to reveal pPIC9K transformants that harbor multiple copies of the genes of interest, scFv-hERG1 and scFv-hERG1-Cys.

After two days of growth at 30°C, the six best grown clones from the 15mg/ml G418 plates were picked up and evaluated for their capacity to express the protein of interest, yeast cultures were induced according to Pichia Expression Kit protocol (Invitrogen).

Samples from each clone's culture were collected at different time points: 24 h, 48 h, 72 h. After three days of induction with 0.5% final concentration of 100% methanol, supernatants were collected and tested through slot blot.

### ***SLOT BLOT ANALYSIS***

Yeast supernatants were collected and tested for protein expression through slot blot; 200 µl of each supernatant were applied to a PVDF membrane (Amersham) assembled in a slot blot device between two squares of 3MM Whatman paper. The samples were left in incubation for 15 min, then vacuum was applied to dry the samples. The membrane was recovered and washed with T-PBS. Blocking was performed with T-PBS 5% BSA for 45 min and then washed 10 min with T-PBS. The membrane was incubated for 1 hour with anti-6xHis-HRP conjugated antibody (Sigma) diluted 1:2000 in 15 ml T-PBS 5% BSA.

### ***Ni SEPHAROSE PURIFICATION***

Supernatants, obtained from the screening of the clones after yeast transformation, were incubated O/N in rolling with Ni Sepharose 6 Fast Flow (GE Healthcare) according to manufacturer's instructions. After, two wash steps were carried out with 500 µl Wash Buffer (20 mM sodium phosphate, 500 mM NaCl, pH 7.3) and elution was performed using 250 µl Elution buffer (20mM sodium phosphate, 500mM imidazole, pH 7.3).

### ***IMMUNOCYTOCHEMISTRY WITH scFv-hERG1-G3 ANTIBODY***

ICC was performed as previously described, scFv-hERG1-G3 was diluted 1:20 in Ultra V block/PBS and incubated O/N at 4°C.

### ***scFv-hERG1-Alexa488 TEST ON FRESH SURGICAL ESOPHAGEAL BIOPSIES***

Endoscopic mucosal samples from six patients affected by Barrett's esophagus were collected from the Department of Surgery and Translational Medicine, University of Florence, under a protocol approved by the Local Ethic Committee. Two consecutive samples of fresh biopsies of about 2–3 mm in diameter were harvested during endoscopic procedures from the site of BE lesion of each patient, checking each site of biopsy with enhanced endoscopy (NBI – Olympus). Immediately a sample was immersed in PBS 1X and used for experiments with scFv-hERG1-G3-Alexa488 (see

below); the other sample was put in 3.7% formaldehyde for fixation, paraffin embedding and immunohistochemical staining with anti-hERG1 monoclonal antibody (diluted 1:200). Immunohistochemistry was performed, as previously described, without permeabilization and hERG1 expression was evaluated applying, for three areas of BE lesion from each sample, an immunohistochemical score obtained through the combination of the estimate of the percentage of immunoreactive cells (quantity score) with the estimate of staining intensity (staining intensity score). Staining intensity was rated on a scale of 0–3, with 0 = negative; 1 = weak; 2 = moderate, and 3 = strong. The raw data were converted to the combined score by multiplying the percentage and staining intensity values, obtaining a value between 0 and 300 for each area and finally the mean of the three areas was computed for each sample.

Experiments with scFv-hERG1-G3-Alexa488 were performed using a recombinant scFv-hERG1 (patent N° FI2014A000189) directed against the S5-pore region and derived from the anti-hERG1 monoclonal antibody (Duranti, Sette et al, manuscript in preparation). The antibody was labelled as described below. For staining live biopsy samples the following protocol was applied: fresh, non-fixed tissue samples, oriented with the mucosal layer facing upwards, were laid on an agarose liquid surface homogeneously distributed on Cell Culture Chamber Slide (Euroclone; Milan, Italy). Biopsies were incubated in the dark with scFv-hERG1-Alexa488, diluted 1:20 in PBS 1X, at 4°C overnight. The following day samples were washed three times with PBS 1X before and after performing Hoechst staining (1:1000 in PBS 1X) for 30 min. The negative control was considered one of the samples before the incubation with scFv-hERG1-Alexa488. In this study a directed light fluorescence microscope Leica DMR, (Leica; Wetzlar, Germany) was used. During the scanning, after the focus of the sample performed through Hoechst stain, the laser delivers the 488 nm excitation wavelength to measure the scFv- hERG1-Alexa488 signal. The images were captured at the same time of exposure for all biopsies for later analysis and processing. The images were analyzed using ImageJ software (Abramoff M.D. *et al.*, 2004). The image with the strongest fluorescent scFv-hERG1-Alexa488 signal was chosen for each sample and the measure of three different areas was performed. The mean of the three measures, obtained from negative control, was calculated and this value was subtracted in each result of the three different areas of other samples and then for all samples the average was computed.

The association between the value of scFv-hERG1-Alexa488 signal and immunohistochemical score of anti-hERG1 monoclonal antibody was analyzed using the Spearman correlation test.  $P < 0.05$  was considered statistically significant.

### ***ÄKTA PURIFICATION***

Purification of 1 liter yeast supernatant of scFv-hERG1-G3 and scFv-hERG1-D8Cys, respectively, was performed by Affinity Chromatography, using an ÄKTA Protein Purification System (GE Healthcare Life Sciences) with HisTrap HP 1 ml columns. Wash steps and equilibration were performed according to the manufacturer's instructions, using a buffer consisting of 20 mM sodium phosphate, 500 mM NaCl, pH 7.3 and elution was performed utilizing a linear gradient of Elution buffer (20mM sodium phosphate, 500mM NaCl, 500mM imidazole, pH 7.3). Analysis was accomplished using UNICORN 7.0 software.

### ***SEC (SIZE EXCLUSION CHROMATOGRAPHY)***

Samples obtained from purification of both antibodies were gel filtered, using Superdex 75 HR 10/30 (GE Healthcare Life Sciences). Wash buffer composition (20 mM sodium phosphate, 150 mM NaCl, pH 7.3) was adjusted to optimize protocol conditions. Elutions were analyzed through SDS-Page.

### ***Sodium dodecyl sulphate polyacrylamide gel electrophoresis (SDS-PAGE)***

Each sample was applied with the same volume of 15 µl to a stacking gel (400 µl acrylamide (40%)-bisacrylamide (0.8%), 1 ml 0.5 M Tris-HCl, pH 6.8, 40 µl 10% SDS, 20 µl 10% ammonium persulfate, 4 µl TEMED, 2.54 ml H<sub>2</sub>O). Stacking gel were added on the resolving gel (2.6 ml acrylamide (40%)-bisacrylamide (0.8%), 1.75 ml 1.5 M Tris-HCl, pH 8.8, 70 µl 10% SDS, 35 µl 10% ammonium persulfate, 3,5 µl TEMED, 2.55 ml H<sub>2</sub>O). Electrophoretic run were performed at 150 V. Gels were either stained with Coomassie Brilliant Blue or transferred to PVDF membranes for western blotting analysis to assess the presence of the protein (around 30 KDa).

### **WESTERN-BLOT**

After SDS-PAGE gels were transferred to PVDF membrane (Amersham) in transfer buffer (14.4 g, 3.03 g TrisHCl, 200 ml methanol, 800 ml H<sub>2</sub>O) at 100 V for one hour. Membranes were washed in T-PBS (PBS 0.1% Tween) and then blocked with T-PBS 5% BSA over-night (O/N). Membranes were exposed to primary antibody anti-His peroxidase-coupled (Sigma) diluted in T-PBS 5% BSA for one hour at room temperature. After washing the membranes three times for ten minutes, signals were visualized using ECL reagent (Amersham). WB were performed using anti-6xHis-HRP conjugated antibody (Sigma).

### ***scFv-hERG1-G3 and scFv-hERG1-D8Cys QUANTIFICATION AND Biacore ANALYSIS***

scFv-hERG1-G3 and scFv-hERG1-D8Cys were gathered together and dialyzed against PBS 1X using Slide-A-Lyzer™ Dialysis Cassettes (Thermo Fisher). Protein absorbance at 280 nm was measured and Lambert-Beer equation was applied.

Surface plasmon resonance was performed using Biacore

S5-Pore peptide, toward which the antibody is directed, was immobilized, using 20 mM acetate at pH 5.0 as immobilization buffer. After 6 injections (540 sec each one, flow 10 µL/min), the immobilization buffer was exchanged with 10 mM acetate at pH 4.5 (7 injections of 540 sec each, flow 5 µL/min). scFv-hERG1-D8Cys and scFv-hERG1-G3 were flowed over immobilized peptide S5PORO at different concentrations. The conditions employed were: Contact time 120 sec; Dissociation time 600 sec; Flow 30 µL/min; 1<sup>st</sup> regeneration: 100 mM Gly-HCl pH 2.5 for 30 sec; 2<sup>nd</sup> regeneration: 100 mM NaOH for 30 sec.

### **ANTIBODY LABELLING WITH ALEXA 488**

scFv-hERG1-G3 and scFv-hERG1-D8Cys were conjugated with Alexa Fluor® 488 Microscale Protein Labeling Kit (Thermo Fisher Scientific), according to the protocol indications.

### **CELL CULTURE**

HEK 293 cells were cultured as previously described in Materials & Methods. PANC-1, Mia Paca2 (pancreatic ductal adenocarcinoma cell lines), MDA-MB231 (human breast adenocarcinoma) and FLG 29.1 (preosteoblastic leukemia) were cultured in DMEM Dulbecco's Modified Eagle Medium (DMEM) High Glucose (Euroclone) supplemented with 4 mM L-Gln and 10% FBS serum (Euroclone). HCT116 (colon carcinoma cells), as well as, BxPC3 (pancreas adenocarcinoma cells) were cultured in RPMI (Euroclone) supplemented with 4 mM L-Gln and 10% FBS serum (Euroclone).

### **IMMUNOFLUORESCENCE ON FIXED CELLS**

Immunofluorescence (IF) was performed on HEK 293 hERG1 (HEK293 stably transfected with pcDNA3.1-hERG1 cDNA construct) and HEK 293 MOCK (HEK 293 stably transfected with pcDNA 3.1 cDNA), as described in the previous section. scFv-hERG1-G3, scFv-hERG1-D8Cys antibodies were diluted 1:20 in blocking solution and incubated for two and half hours, followed by anti-His (1:250; Abcam) O/N incubation in blocking solution. The following day, cells were washed three times with PBS and incubated with anti-mouse Alexa488 antibody (Invitrogen) for 1 h.

Alexa 488 labelled antibodies, scFv-hERG1-G3-Alexa488 and scFv-hERG1-D8Cys-Alexa488 were diluted 1:20 in blocking solution and incubated O/N at 4°C. Cells were visualized on a confocal microscope (Nikon, C1).

Immunofluorescence quantification was performed using ImageJ software: for each image, we evaluated the fluorescence intensity of three different areas and calculated the mean after subtracting the blue channel values (which refer to nuclei staining). Results were normalized on the control cells fluorescence intensity and results are reported as increment of fluorescence intensity (AU, arbitrary unit).

### **IMMUNOFLUORESCENCE ON LIVE CELLS**

Cells were grown O/N on 60 mm plates (Sarstedt) using an agarose (15 g/L) ring in order to isolate cells and minimize the volume of reagent. Cells were incubated with scFv-hERG1-G3-Alexa488 and scFv-hERG1-D8Cys-Alexa488 diluted 1:20 in complete culture medium in a 37° C incubator with 5% CO<sub>2</sub> for 4 h. Nuclei staining was

performed using Hoechst, as previously described. Cells were visualized on an inverted light microscopy (Nikon, Eclipse TE300).

### ***CELL VIABILITY ASSAY***

Cell viability was evaluated performing a Trypan blue assay. Briefly, cells at a density of  $5 \times 10^3$  cells/well were seeded in a 96-well plate. After 24 h, the medium was replaced with 100  $\mu$ l of fresh medium containing different concentrations of the scFv-hERG1-D8Cys antibody (10  $\mu$ g/ml and 20  $\mu$ g/ml). The complete immunoglobulin, anti-hERG1 monoclonal antibody was tested at a concentration of 100  $\mu$ g/ml. Cells were cultured 24 hours in a humidified incubator at 37°C and 5% CO<sub>2</sub>. After the treatment cells were detached and viable cells were counted. Experiments were performed in triplicate.

Statistical analysis was performed applying Shapiro-Wilk test and Bartlett test to assess data normality and homoskedasticity assumptions respectively. Associations between continuous variables and categorical variables was analyzed through Anova, Welch or Kruskal-Wallis test, depending on assumptions results; subsequently, to determine pairwise statistical significance Tukey test or DSCF (Dwass, Steel, Critchlow-Fligner) test have been applied.

### ***3D SPHEROIDS CELL CULTURE***

$10^3$  PANC-1, Mia Paca2, HEK293 HERG1, HERG1293 MOCK and MDA-MB 231 cells were seeded on an agarose base layer (1,5g/l) in 96 well plate and grown for 72 hours in a humidified incubator at 37°C and 5% CO<sub>2</sub>. Then scFv-hERG1-D8Cys was administered (10  $\mu$ g/ml, 20  $\mu$ g/ml, 40  $\mu$ g/ml), diluted in culture medium, while fresh medium without antibody was added to wells containing cells treated as negative controls. Photos were taken at 24, 48 and 72 hours to monitor cell growth using a Nikon, Eclipse TE300 microscope. A calcein AM assay was performed after 72 hours treatment to evaluate cell death both on cells treated with 40  $\mu$ g/ml scFv-hERG1-D8Cys antibody and negative control cells.

***CELL INVASION EXPERIMENTS***

A cell suspension (200 µl) containing  $2 \times 10^4$  cells was seeded into the upper well of a Boyden chamber (NeuroProbe, Inc., Gaithersburg, MD), in the presence or in the absence of 40 µg/ml scFv-hERG1-D8Cys, separated from the lower compartment (filled with DMEM + BSA) by a porous membrane (8-µm pore diameter) previously overlaid with Matrigel. Boyden chambers were incubated at 37°C in humidified atmosphere containing 5% CO<sub>2</sub> in air for 16 h. Migrated cells, which remained layering onto the lower face of the porous membrane, were fixed with absolute methanol at 4°C overnight and stained with Diff-Quick staining solution (Dade-Behring Holding GmbH, Liederbach, Germany).

### ***3.3 Production and characterization of anti-hERG1- $\beta$ 1 Single Chain Diabody (scDb)***

The construct hERG1- $\beta$ 1-scDb was transformed into GS115 *Pichia pastoris* strain according to the spheroplasting technique previously described.

#### ***CELL ELISA***

Cell ELISA on living cells was performed according to Sette *et al.*, (2013). HEK 293 WT (hERG1-/ $\beta$ 1+) and HEK 293-hERG1 (hERG1+/ $\beta$ 1+) cells were seeded to semiconfluence in 96-well plate in DMEM plus 10 % fetal bovine serum (FBS) and incubated overnight at 37 °C and 5 % CO<sub>2</sub>. After three washes with PBS, anti-hERG1- $\beta$ 1-scDb was diluted at different concentrations into culture medium and added to the cells for two 2 hours at room temperature. The following steps were the same as described above.

#### ***CITOFUORIMETRIC ANALYSIS***

FACS analysis was performed on a panel of human cell lines: HEK 293 WT (hERG1-/ $\beta$ 1+) and HEK 293-hERG1 cells (hERG1+/ $\beta$ 1+). Briefly, cells ( $1 \times 10^5$ ) were incubated for 20 minutes at room temperature with different concentrations (range 0.0-0.2  $\mu$ g) of hERG1- $\beta$ 1-scDb antibody. After incubation, cells were centrifuged and Alexa488 secondary antibody (1:100) was incubated for other 15 minutes. After secondary antibody incubation, cells were centrifuged, resuspended in 300  $\mu$ l of PBS and analyzed using a FACS Canto device (BD Biosciences).

#### ***IMMUNOFLUORESCENCE (IF)***

IF was performed following the protocol which has been previously described. Coverslips were coated with BSA and Fibronectin for two hours. IF was performed on HEK 293 WT (hERG1-/ $\beta$ 1+), HEK 293-hERG1 (hERG1+/ $\beta$ 1+) and GD25 WT cells (hERG1-/ $\beta$ 1-) following the protocol previously described.

## 4. RESULTS

### 4.1 Development and characterization of a monoclonal antibody directed against ionotropic Glutamate Receptor 4 (iGluR4).

Recent evidences have revealed the role of AMPA-type ionotropic glutamate receptors (iGluRs), not only in synaptic plasticity, but also in processes regarding cell migration, proliferation and survival (Ikonomidou *et al.*, 1999; Komuro and Rakic 1993). Moreover, it has been demonstrated (Talos. *et al.*, 2008) that in pathologic conditions, such as TSC (tuberous sclerosis complex), iGluRs are miss-expressed in dysplastic cells, contributing to the increase of cortical network excitability. In particular, iGluR4 has been found to be overexpressed in dysplastic astroglia, one of the characteristic features of TSC. These evidences highlight the importance of exploiting iGluR4 as a tool to target dysplastic neurons and astroglia, setting up new tools to overcome the problems related to the BBB (blood brain barrier) passage.

In this part of the work we have focused on:

- the development and characterization of a monoclonal antibody against the iGluR4 receptor;
- the development of a scFv (*single chain variable fragment*) antibody derived from the monoclonal antibody, anti-iGluR4

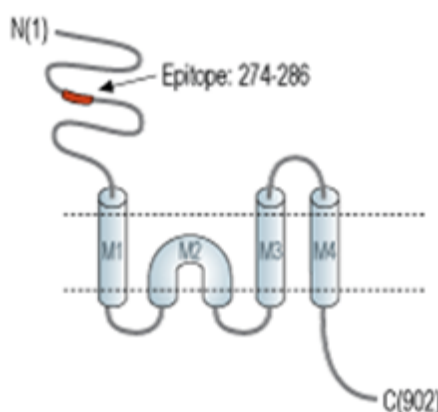


Fig.1 iGluR4 topology (modified from alomone.com)

We have selected an extracellular epitope of the iGluR4 protein, as shown in Fig. 2.

The epitope consists in 13 amino acids and is different in all the four isoforms of the iGluRs with the greatest sequence difference observed between iGluR4 and iGluR2 (Fig. 2). Particularly, iGluR4 and iGluR2 expression has been found to be down- and up-regulated, respectively, in giant dysplastic cells (Talós *et al.*, 2008, Ann. Neurol 63: 454–465).

```

iGluR4 YIIANLGFKDISLERFIHGKANVTGFQLVDFNTPMVKLMDRWKKLDQREYPGSETPP-K
        YIIANLGF D L + GGANV+GFQ+VD++ +V K ++RW L+++EYPG+ T K
iGluR2 YIIANLGFTDGDLLKIQFGGANVSGFQIVDYDDSLVKFIERWSTLEEKEYPGAHTTTIK
iGluR4 YTSALTYDGVLMMAETFRSLRRQKIDISRRGNAGDCLANPAAPWGQGIDMERTLKQVRIQ
        YTSALTYD V VM E FR+LR+Q+I+ISRRGNAGDCLANPA PWGQG+++ER LKQV+++
iGluR2 YTSALTYDAVQVMTEAFRNLRKQRIEISRRGNAGDCLANPAVPWGQGVIEIERALKQVQVE
iGluR4 GLTGNVQFDHYGRRVNYTMDVFELKSTGPRKVGYNWMDKLVL-IQDVPTLGNDTAAIEN
        GL+GN++FD G+R+NYT+++ ELK+ GPRK+GYW+++DK+V+ + ++P+ GNDT+ +EN
iGluR2 GLSGNIKFDQNGKRINYTTINIMELKTINGPRKIGYWSEVDKMVVTLTELPs-GNDTSGLEN
iGluR4 RTVVVTTIMESPVMYKKNHEMFEGNDKYEGYCVDLASEIAKHIGIKYKIAIVPDGKYGA
        +TVVVTTI+ESPYVM KKNHEM EGN++YEGYCVDLA+EIAKH G KYK+ IV DGKYGA
iGluR2 KTVVVTTIILESPVMMKKNHEMLEGNEREYEGYCVDLAAEIAKHCGFKYKLTIVGDGKYGA

```

Fig. 2 Amino acid sequence alignment of iGluR2 and iGluR4

After a bioinformatic study, we have performed an immunological study of the candidate peptide.

To this purpose, we have taken into account the GRAVY INDEX. The GRAVY (Grand Average of Hydropathy) value for a peptide or protein is calculated by adding the hydropathy value for each amino acid residue and dividing by the length of the sequence. The index obtained for the chosen peptide was -2.008. This value is promising, as it is preferable to use for peptide synthesis, conjugation, solubilisation and immunization hydrophilic sequences that have a  $\text{GRAVY} \leq 0$  (Kyte, J *et al.*, 1982).

#### 4.1.1 Monoclonal antibody development

Hybridomas were produced according to Köhler and Milstein protocol (Nature, 1975).

Immunisation was performed using iGluR4 peptide conjugated with ovalbumin (OVA). Three female Balb/c mice were immunized, following the protocol described in Materials and Methods.

Three days after the last immunization mice were sacrificed and splenectomy was performed (Fig. 3, A).

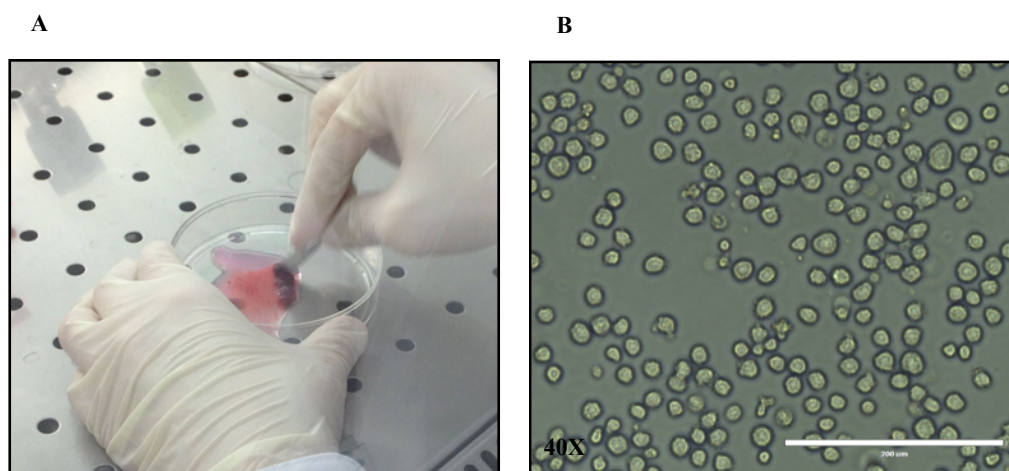


Fig. 3 Picture showing the spleen processing after explant from mice (A); hybridoma cells (B) as they appeared after 14 days from cellular fusion at 40X magnification

B-lymphocytes derived from the spleens of two immunized mice were fused with NS0 myeloma cells.

The product obtained from cell fusion was resuspended in complete medium, in which HAT selective agent was added. The addition of HAT allows the survival of only the hybrids formed by the B-lymphocyte fused to a NS0 myeloma cell. Both spleens derived from two of the three immunized mice (hence named MOUSE 1 and MOUSE 2) underwent the same procedure for cell fusion.

Different dilutions were set up: 1:2; 1:4 and two 1:8 mixtures for each mouse.

Each dilution was aliquoted in a 24-well plate and, subsequently, cells were incubated for about 14 days. After two weeks, colonies were visible to the naked eye. Plates underwent microscopic examination and supernatant was collected from the wells in which cell populations were visible (Fig. 3, B).

Supernatants were analyzed by ELISA assay, as described in Materials and Methods, to assess the ability of the secreted immunoglobulin to recognize the antigen.

Supernatants with an  $OD_{450} > 1.5$  were considered positive. Fig. 4 shows the results obtained from ELISA assay.

MOUSE 1 1:2	1	2	3	4	5	6
A	0,175	0,126	0,951	0,404	0,049	0,050
B	0,546	0,320	0,294	0,275	0,046	0,051
C	0,160	0,089	0,088	0,178	0,099	0
D	0,124	0,072	0	0,058	0,178	0

MOUSE 2 1:2	1	2	3	4	5	6
A	/	1,019	0,526	0,685	/	/
B	0,44	0,68	0,549	0,383	0,379	0,953
C	0,404	0,546	0,32	0,275	0,363	1,115
D	0,318	0,161	1,121	2,265	0,881	/

MOUSE 1 1:4	1	2	3	4	5	6
A	2,241	1,294	1,496	1,148	1,207	2,307
B	1,497	1,32	1,081	1,003	OUT	1,208
C	1,671	0,892	1,049	1,027	0,981	0,833
D	0,127	2,533	1,196	0,902	1,003	1,5

MOUSE 2 1:4	1	2	3	4	5	6
A	/	/	1,553	1,602	/	/
B	1,850	0,188	1,348	/	/	0,257
C	/	/	/	1,267	1,381	0,146
D	/	/	/	2,481	1,745	/

MOUSE 1 1:8A	1	2	3	4	5	6
A	/	0,313	0,312	0,505	0,471	1,417
B	0,221	0,304	0,366	0,568	0,389	/
C	0,049	0,333	0,274	0,273	1,46	0,507
D	0,253	0	0,609	0,295	0,33	0,297

MOUSE 2 1:8 A	1	2	3	4	5	6
A	1,115	OUT	0,734	0,816	1,031	1,417
B	1,386	OUT	1,17	OUT	0,878	0,948
C	0,281	1	OUT	0,956	0,210	1,136
D	/	0,852	0,138	0,749	OUT	0,628

MOUSE 1 1:8B	1	2	3	4	5	6
A	0	0,39	0,269	0	0,264	0
B	0,558	0,419	/	/	0,259	0,317
C	/	0,257	1,178	2,656	0,426	0,244
D	/	0,657	0,515	0,413	0,301	0,205

MOUSE 2 1:8 B	1	2	3	4	5	6
A	1,022	0,694	0,170	0,110	0,738	0,897
B	/	1,076	1,178	2,719	0,059	0,124
C	0,055	1,595	/	1,333	0,122	0,053
D	0,802	/	0,077	0,056	0,861	/

Fig. 4. Tables summarizing the results obtained by ELISA assay screening analyzing the 24 well-plates obtained from cellular fusion. Cut-off for colony positivity was fixed at  $OD_{450} = 1.5$

From screening, we obtained 22 strongly positive populations (Fig. 4), considering both the wells derived from MOUSE 1 and those deriving from MOUSE 2.

Hybridoma populations, positive in ELISA assay, were picked and transferred in a new 24 well-plate and screened separately again by ELISA, during every passage of cell amplification: from wells to flasks (25 cm<sup>2</sup> and 75 cm<sup>2</sup>).

The following summarizing table shows the populations which continuously gave OUT of scale absorbance in ELISA assay. Such results demonstrate to be very promising, as they give evidence of strong binding and/or high yields.

	<u>CLONE</u>	<u>OD<sub>450</sub></u>
<b><u>MOUSE 1 1:4</u></b>	B5	<b>OUT</b>
<b><u>MOUSE 2 1:2</u></b>	D4	<b>OUT</b>
<b><u>MOUSE 2 1:8</u></b>	clA, A2	<b>OUT</b>
	clA, B4	<b>OUT</b>
	clA, C3	<b>OUT</b>
	clA, D5	<b>OUT</b>
	clB, B2	<b>OUT</b>

Table 1. Table summarizing the hybridoma populations which continuously gave OUT of scale absorbance in ELISA assay

Our aim was to select strongly positive hybridoma populations to undergo soft agar cloning. To this purpose, selection was done only between those clones, reported in Table 1, which gave OUT-of-scale absorbance.

B5 anti-iGluR4, derived from MOUSE 1 dilution 1:4, was the population selected for soft agar cloning.

Before performing soft agar cloning, we have tested the hybridoma B5 anti-iGluR4 isotype using IsoQuick (Sigma) (Fig. 5).

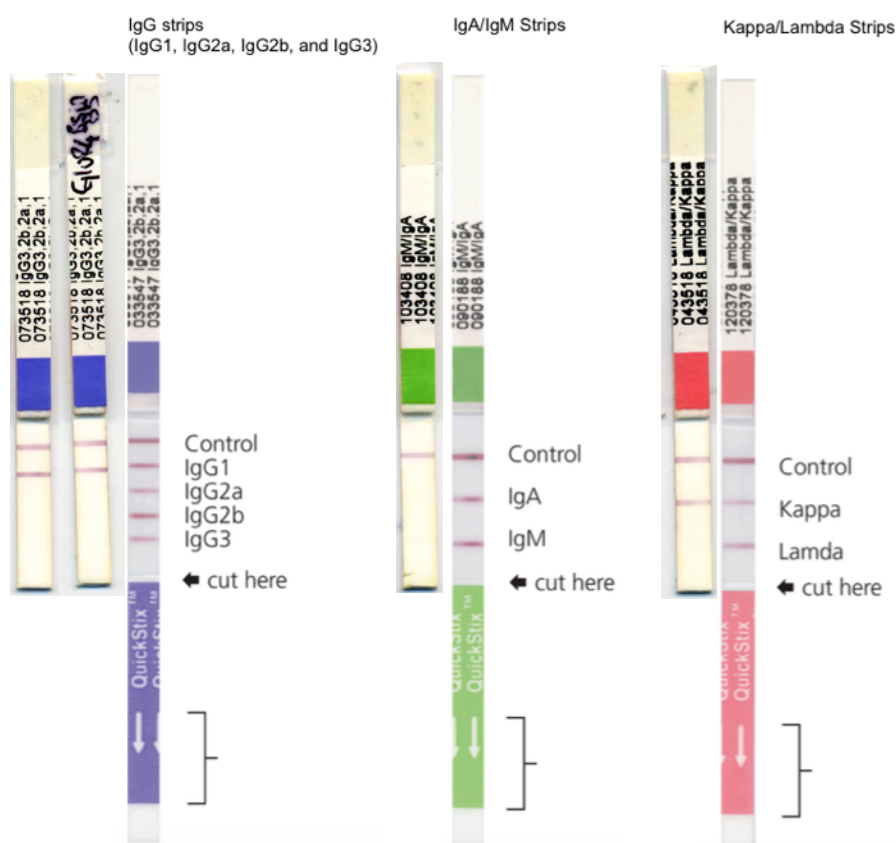


Fig. 5 Isotype test results: strips AI and AII show the presence of a red band, corresponding to an IgG1; the strip in BI shows that no IgMs or IgAs are present, if compared to the control in BII; the strip in CI shows that light chain is a kappa type.

Isotype test revealed that B5 anti-iGluR4 population corresponds to an IgG1 Kappa; the result obtained was quite promising, in fact, as it can be inferred from the Fig 5, bands obtained are single and neat, without resulting in multiple isoforms, thus, perhaps, already indicating the monoclonal nature of the hybridoma population. This result was confirmed after repeating the test, at different time during the screening of the population.

Soft agar cloning was performed according to the protocol described in Materials and Methods.

After 10 days from setting up the soft agar cloning, distinct colonies were visible in the plates. Two representative images of colonies obtained from soft agar cloning, as they appeared with microscopy observation, are reported in Fig. 6.

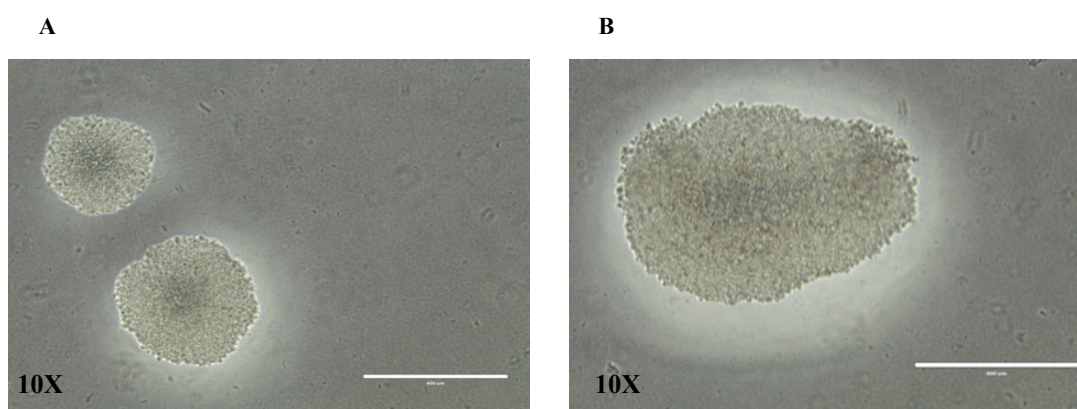


Fig. 6 Pictures showing colonies, as they appeared after soft agar cloning under microscopy examination using 10X magnification.

Colonies were picked and transferred to 96-well plates; then grown colonies were transferred into 24-well plates. Supernatants were taken from wells and analyzed by ELISA assay (Fig. 7).

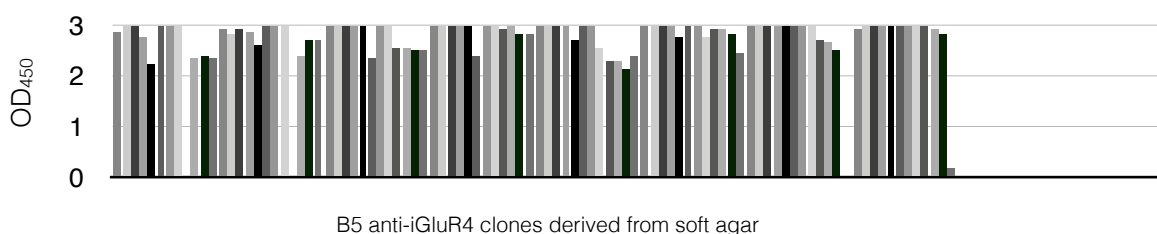


Fig. 7 Histogram showing the results obtained from analysis of the grown colonies after soft agar cloning: the majority of clones showed OUT of scale absorbance.

Results reported in Fig.7 show that most of the clones analyzed gave OUT of scale absorbance. This result was the one we expected because the population cloned in soft agar has been previously sub-cloned by manual picking, as indicated in Materials and Methods.

#### 4.1.2 Anti-iGluR4 clones screening and characterization

Clones which gave OUT of scale absorbance during soft agar screening were amplified, screened and frozen.

We have then started a more detailed characterization of positive clones obtained from soft agar.

To this purpose, we have stably transfected HEK 293 cells using human iGluR4 cDNA, kindly gifted by Prof. Huganir (Johns Hopkins Medicine Brain Science Institute at Johns Hopkins University School of Medicine, Baltimore, USA). iGluR4 cDNA is cloned in pRK5 vector which is not suitable for mammalian cells expression; for this reason it was necessary to set up a co-transfection using two different plasmids: pRK5-iGluR4 and pcDNA3.1, which can be exploited for cell selection. The co-transfection procedure is described in Materials and Methods.

After stable transfection, RNA was extracted from cells, retrotranscribed into cDNA and analyzed by end point-PCR to confirm that stable transfection occurred (Fig. 8).

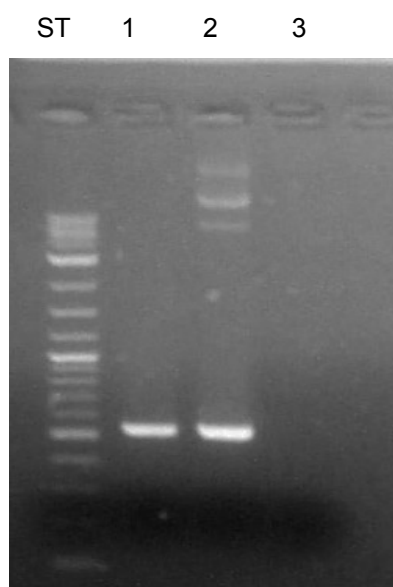


Fig. 8 PCR to assess stable transfection of HEK 293 cells. Lane 1 shows the iGluR4 plasmid cDNA, used as positive control; lane 2 shows the PCR product obtained from the amplification of retrotranscribed cDNA extracted from cells stably transfected with iGluR4; in lane 3 is reported negative control, which corresponds to PCR product obtained amplifying cDNA from HEK 293 WT (control cells).

Promising supernatants from soft agar cloning were screened by cytofluorimetric analysis (FACS). In fact, one of the main goals of the anti-iGluR4 antibody is to be used as a *drug-delivery system* after conjugation with nanoparticles (NPs).

Figure 9 shows the results obtained from FACS analysis performed on HEK 293-iGluR4 cells for the two clones which have given the highest signal: panel A reports the staining obtained for the clone B5 anti-iGluR4, which has demonstrated a good degree of specificity if compared to the staining obtained on the same type of cells after incubation with an unspecific secondary antibody. Panel B, instead, shows the staining obtained after incubation with C4 anti-iGluR4 clone.

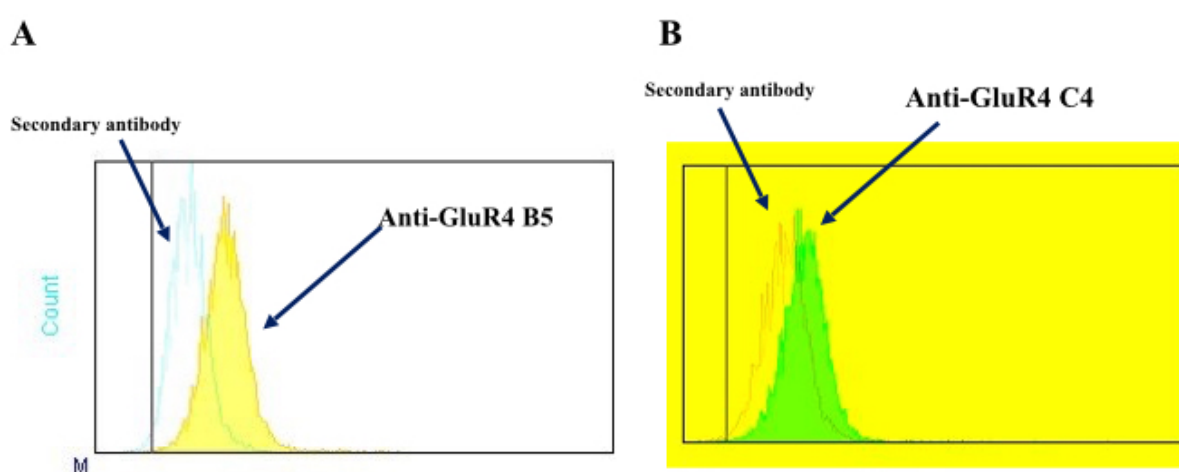


Fig. 9 Results obtained from FACS analysis for B5 anti-iGluR4 antibody, compared to the results obtained using an unspecific secondary antibody. Panel B shows the results obtained for C4 anti-iGluR4 antibody compared to an unspecific secondary antibody.

After FACS analysis, clone B5 anti-iGluR4, one of the most promising supernatant obtained from FACS characterization, was also tested in immunofluorescence on stably transfected HEK 293-iGluR4 and HEK 293 MOCK cells, used as negative control.

Results are reported in Fig. 10; panel A shows negative control HEK 293 MOCK cells treated with B5 anti-iGluR4 supernatant, in which only nuclei staining is detectable; while panel B reports signal obtained on HEK 293-iGluR4, in which the labeling due to the antibody binding is well visible as membranous green staining.

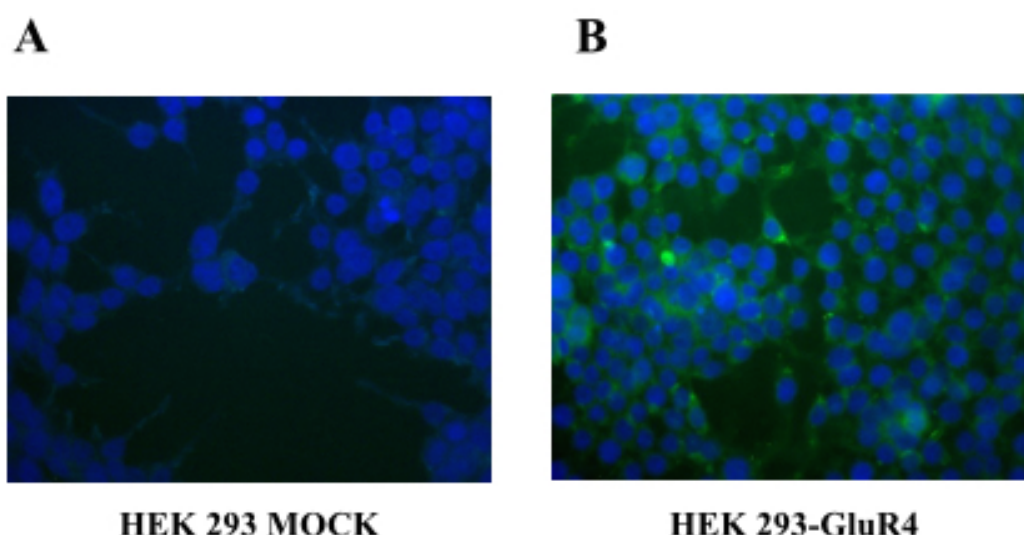
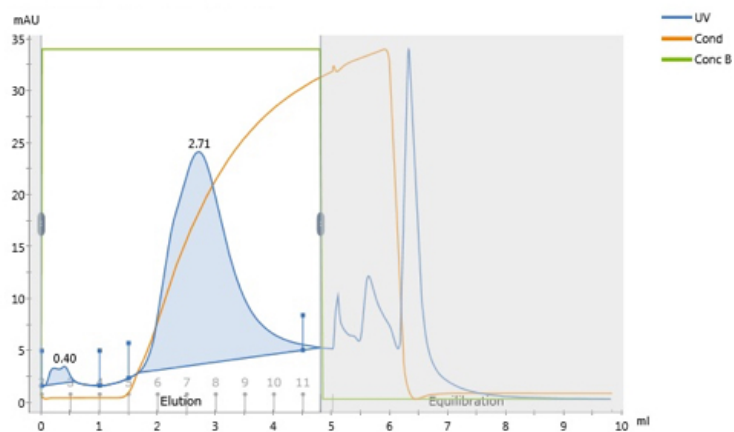
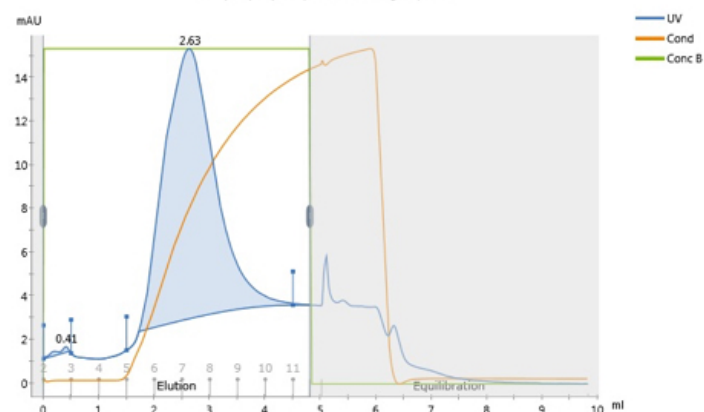


Fig. 10 IF on HEK 293 MOCK cells and HEK 293-iGluR4 cells: panel A shows staining obtained using B5 anti-iGluR4 supernatant on HEK 293 MOCK cells and no signal due to the binding of the antibody can be detected. Panel B shows the signal obtained on HEK 293-iGluR4 cells using B5 anti-iGluR4 supernatant and in this case a clear membranous staining is visible.

Cells from both clones B5 and C4 anti-iGluR4 were adapted to grow without HAT, that has been progressively substituted by HT hypoxanthine-thymidine. HT is used because usually aminopterin remains inside the cells even if HAT is removed from culture medium, continuing to exploit its inhibitory effect on the novo synthesis of nucleotide bases. Thus, aminopterin is diluted from the culture by several passages of the cells in hypoxanthine-thymidine (HT) supplemented medium (approximately 2-3 weeks) before transferring into ordinary hybridoma growth medium DMEM High Glucose added with 4 mM L-Glutamine and 10% FBS FetalClone I (Hyclone).

Cells from B5 and C4 clones were cultured in 75 cm<sup>2</sup> flasks; cells were harvested regularly, supernatant was collected and purified using AKTA Pure (GE Healthcare). Chromatograms obtained from a purification process for both B5 and C4 clone of anti-iGluR4 antibody are reported in fig. 11 panel A; purified antibody was analyzed through SDS-page and Coomassie Brilliant blue staining (Fig. 11, panel B). Chromatograms show two single peaks corresponding to antibody elutions (represented in the chromatograms by the blue areas).

Coomassie staining shows, for each clone, two bands of a molecular weight consistent with the heavy and light chains of the antibody.

**A****B5 clone anti-GluR4****C4 clone anti-GluR4****B****SDS-Page anti-GluR4 antibody****Heavy chain****50KDa****Light chain****25KDa**

B5 anti-GluR4  
6  
B5 anti-GluR4  
7  
B5 anti-GluR4  
8  
C4 anti-GluR4  
6  
C4 anti-GluR4  
7  
C4 anti-GluR4  
8  
C4 anti-GluR4  
9

Fig.11 Panel A Chromatograms obtained from the purification of B5 (upper panel) and C4 (lower panel) anti-GluR4 antibody. For each clone a single peak, represented in the chromatogram by the blue area, is visible. Panel B shows Coomassie staining of fractions eluted B5 and C4 anti-iGluR4 antibody, heavy chain (around 50 kDa) and light chain (around 25 kDa) are indicated in the figure.

### 4.1.3 Anti-iGluR4 antibody testing in immunocytochemistry (ICC) and immunohistochemistry (IHC)

From FACS characterization, two clones emerged to give the highest signal: clone B5 anti-iGluR4 and clone C4 anti-iGluR4.

Thus, we have pursued the antibody characterization of these clones by immunocytochemistry (ICC). To this purpose, we have tested both supernatants on HEK 293- MOCK cells and HEK 293-iGluR4.

Results of ICC experiments are reported in figure 12.

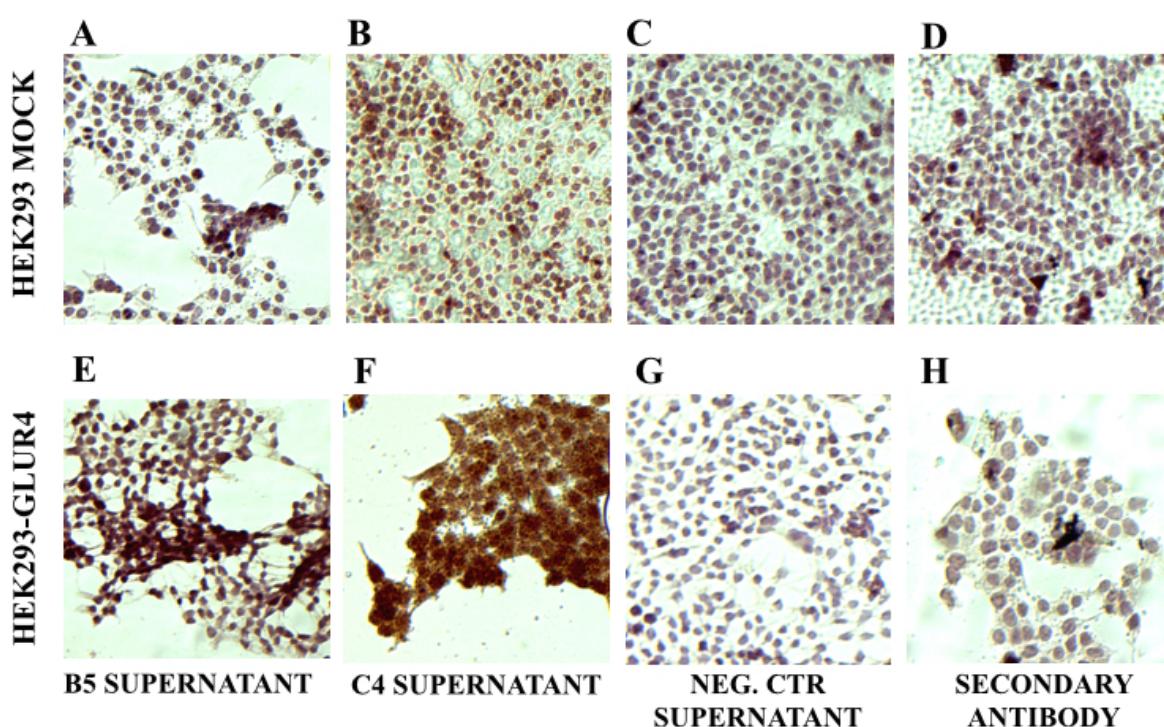


Fig. 12. ICC experiments performed on HEK 293-iGluR4 and HEK 293 MOCK cells with B5 anti-iGluR4 and C4 anti-iGluR4 antibodies diluted 1:10. Experiments were also performed using a negative control supernatant (low values of absorbance in ELISA assay) and an unspecific secondary antibody.

Panel A shows B5 anti-iGluR4 supernatant tested on the negative control cells HEK 293-MOCK, while the panel E below reports the same supernatant tested on HEK293-iGluR4 cells. The staining reveals a stronger signal for HEK293-iGluR4 cells, that express the antigen towards which the antibody is directed, compared to negative control, HEK293 MOCK cells.

Comparable results were obtained using C4 anti-iGluR4 supernatant: stronger signal was obtained for cells overexpressing iGluR4 (panel F), while weak signal was obtained on cells HEK 293-MOCK, used as negative control. Signal specificity was also confirmed by testing, as negative control, one supernatant that was considered negative during all the process of clone screening. The supernatant C6 anti-iGluR4 deriving from the cluster 1:8 of MOUSE 2 was chosen randomly and tested at the same dilution as the B5 anti-iGluR4 and C4 anti-iGluR4 supernatants.

Signal was negative for both HEK 293-MOCK and HEK293-iGluR4, as it can be inferred from panels C and G. The latter results are comparable to those obtained for panels D and H, in which only secondary antibody was used.

B5 and C4 iGluR4 antibody supernatants were also tested in immunohistochemistry on slides derived from patients affected by tuberous sclerosis complex (TSC). Purified antibody from both clones B5 and C4 anti-iGluR4 was tested on slides of TSC patients and on negative control post mortem specimen (kindly provided by Prof. Ingmar Blümcke, University of Erlangen, Germany). In figure 13, we report images taken from the slides of TSC patients (panels A and B) and negative control post mortem (panels C and D).

Staining of cells that represent the peculiar pattern of TSC, giant cells (balloon cells) and dysplastic astroglia, is evident (as highlighted by the arrows).

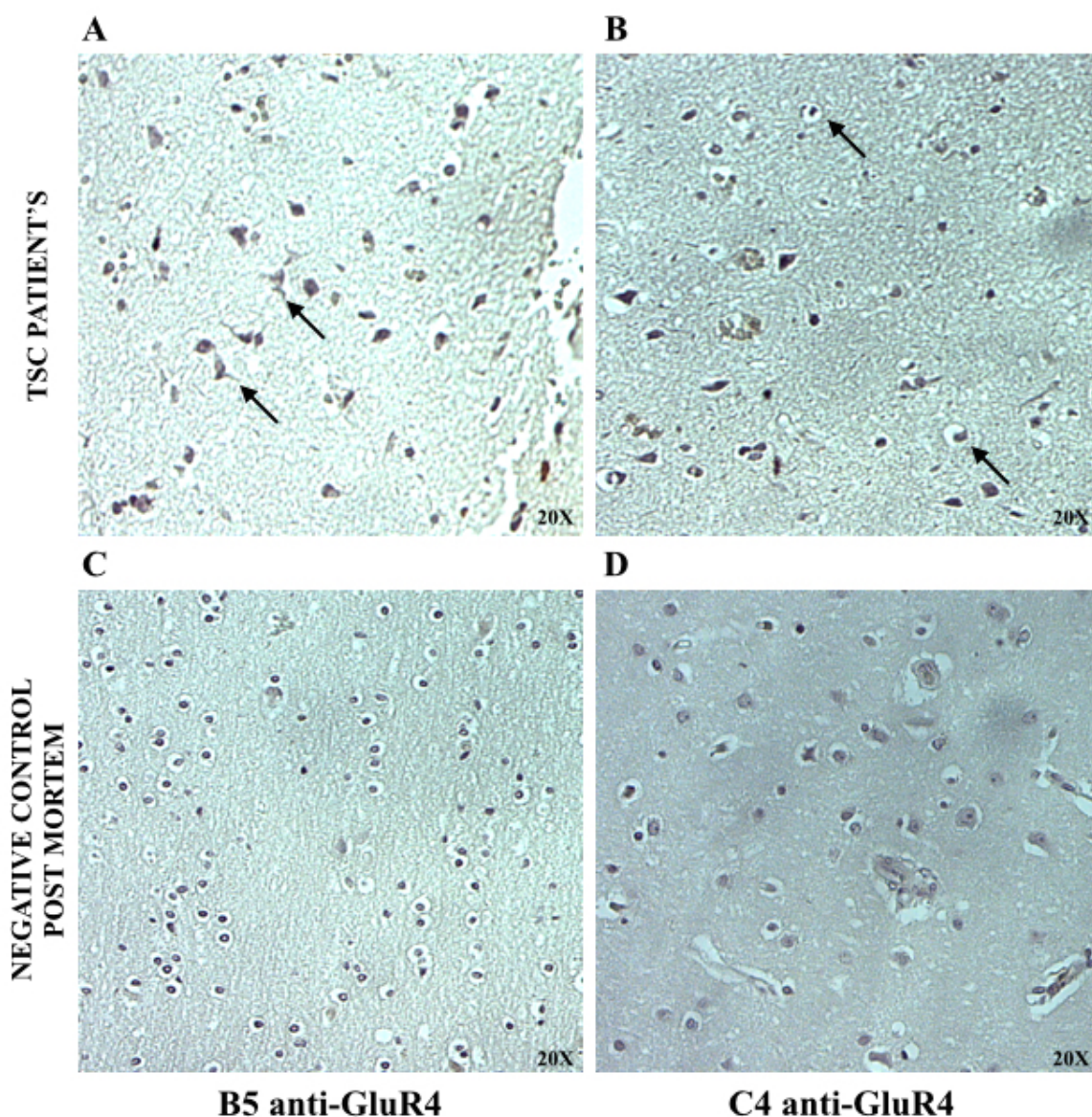


Fig. 13 Panels A and B show staining obtained using purified B5 and C4 anti-GluR4 antibodies on slides derived from TSC patients: staining of peculiar features of TSC are highlighted by the arrows. Panels C and D show IHC performed on negative control post-mortem slides.

In parallel, we have performed functional test in order to further characterize B5 and C4 anti-iGluR4. Cell viability on HEK293-iGluR4 cells and HEK293 MOCK cells was evaluated by Trypan blue assay after 24 hour antibody incubation. Both antibodies induced a slight decrease in cell viability on HEK 293-iGluR4 cells, compared to the control cells (Fig. 14, A). On the other hand, no effect was observed in HEK 293 MOCK cells (Fig. 14, B).

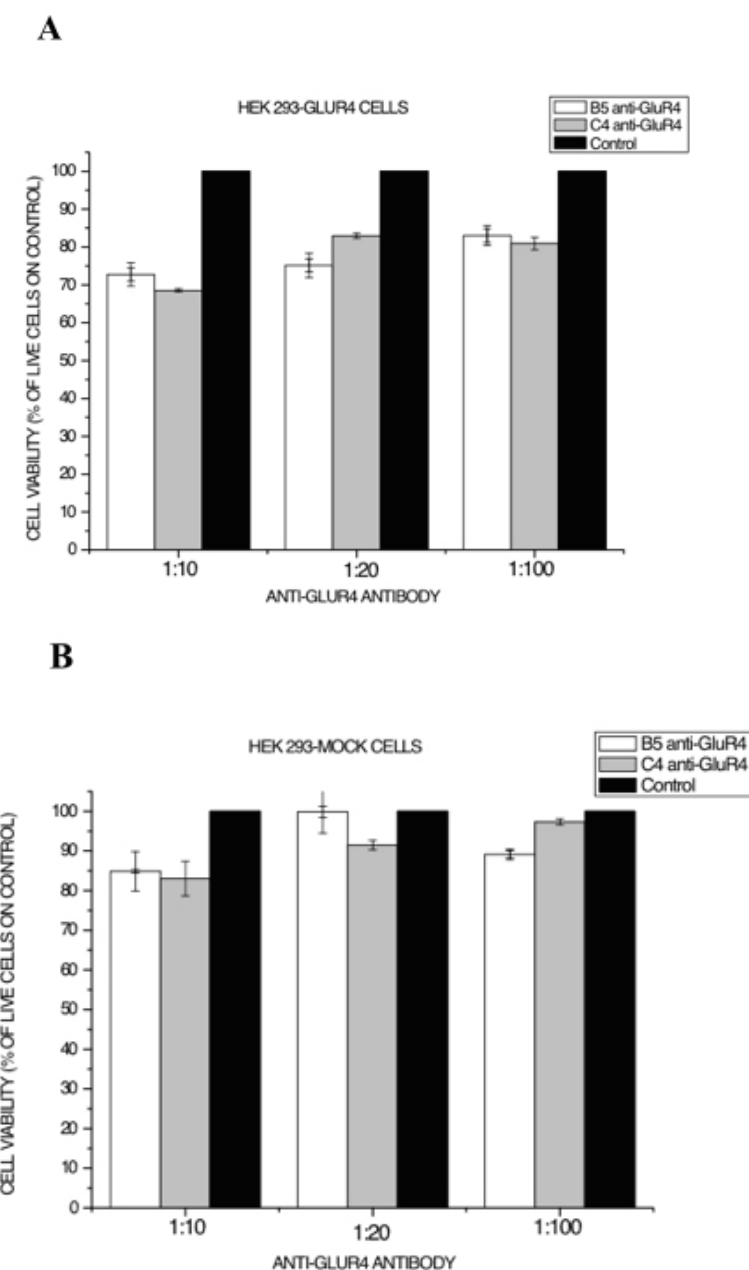


Fig. 14 Cell viability of HEK 293-GluR4 and HEK 293-MOCK cells after treatment with B5 and C4 anti-iGluR4 supernatants.

Furthermore, we have evaluated the effect of the two B5 and C4 anti-iGluR4 clones on Glutamate currents, performing a whole cell patch-clamp analysis. These electrophysiological experiments were led by Dr. Massimo D'Amico. Both antibodies were tested on HEK 293-iGluR4 cells. Glutamate sensitive currents recorded after 15 minutes antibody incubation are reported in Fig. 15, panel B and C .

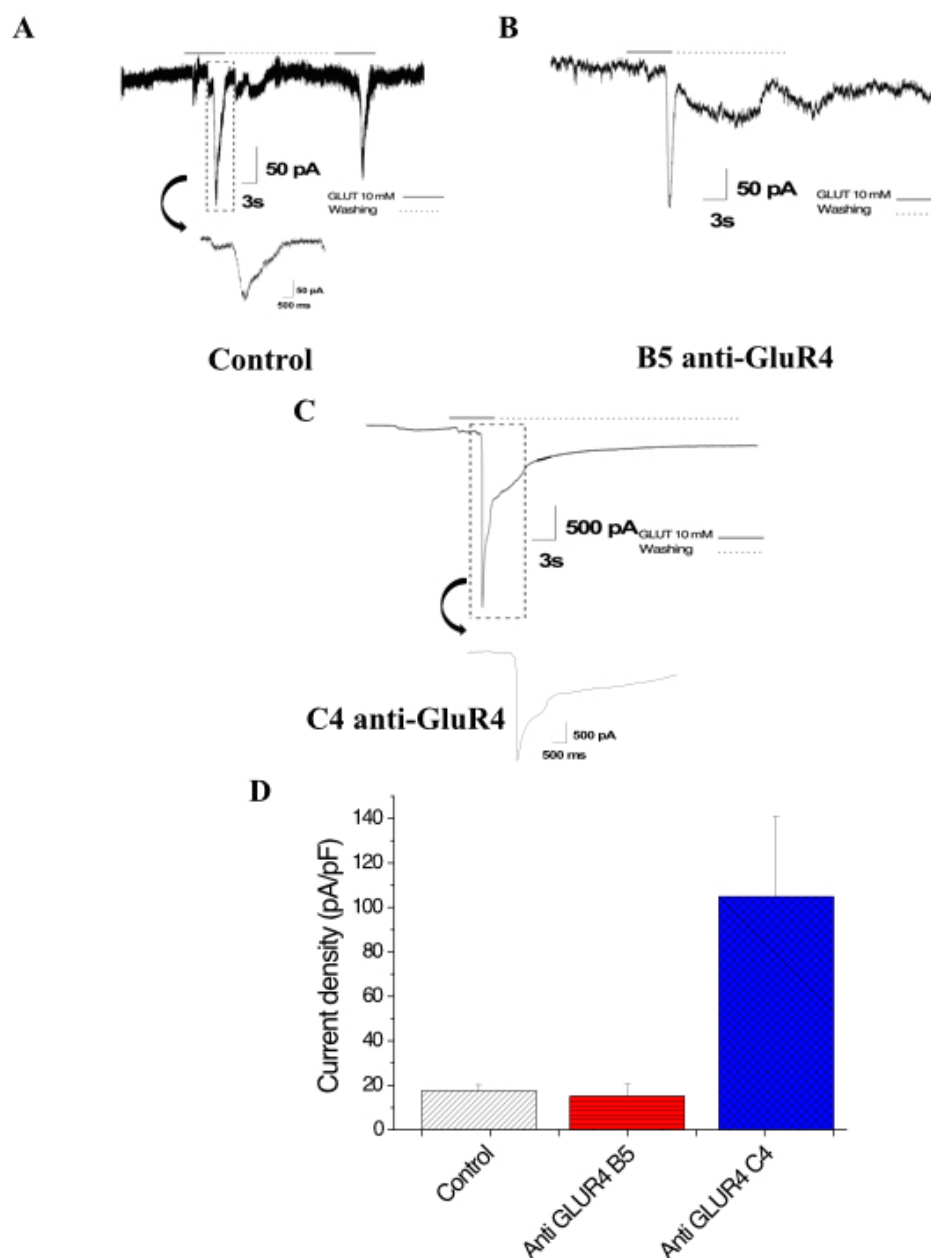


Fig.15 Glutamate sensitive currents in HEK 293-GluR4 cells, after incubation with B5 and C4 anti-GluR4 antibody Panel A. Typical whole cell inward currents evoked by pressure application of 10 mM glutamate. Currents were recorded at a holding potential of -70 mV on HEK 293-GluR4 cells, used as controls. The insert reports a magnification of the peak current. Panel B. Whole cell inward current recorded after 15 min incubation with the B5 anti-GluR4 antibody (dilution 1:2 in PBS). Panel C. Whole cell inward current recorded after 15 min incubation with the C4 anti-GluR4 antibody (dilution 1:2 in PBS). The insert reports a magnification of the peak current, it is worth noting that current scale is different in panel C compared to panel A and B. Time scale is also different in the inserts.

Recordings show that, on the iGluR4 overexpressing cellular model, the typical desensitization of AMPA receptor is slow for glutamate responses (Panel A). Furthermore, the C4 anti-iGluR4 antibody induces a marked potentiation of inward

current and a further reduction of the observed desensitization (Panel C). Such increase is confirmed when calculating the relative current density (Panel D).

Since both clones of anti-iGluR4 monoclonal antibody recognize an important tumor marker, they can also function as important diagnostic tools. To address problems related to targeting dysplastic cell *in vivo*, we have synthesized PLGA-PEG Rhodamine B-G7 nanoparticles (NPs), able to cross an *in vitro* model of BBB. In parallel, we have developed a single-chain variable fragment (scFv-iGluR4), from the already produced monoclonal antibody, which combines small size (around 30 kDa), which is detrimental for NPs conjugation, with antigen specificity.

#### 4.1.4 anti-iGluR4 monoclonal antibody engineering

Total RNA was extracted from frozen B5 and C4 anti-GluR4 cell pellet and retrotranscribed to cDNA for the isolation of VH and VL by PCR. The primers used were modified from Wang *et al.*, 2010, following the protocol described in Materials and Methods.

For each clone, B5 and C4 anti-iGluR4 respectively, five parallel PCR reactions were performed using all the degenerated primers. Couples of primers are reported below:

degH1dir-IgG1rev

degH2dir-IgG1rev

degH3dir-IgG1rev

degH4dir-IgG1rev

degH5dir-IgG1rev

Clones were successfully amplified with the different degenerated primers as shown in the PCR image in Fig. 16.

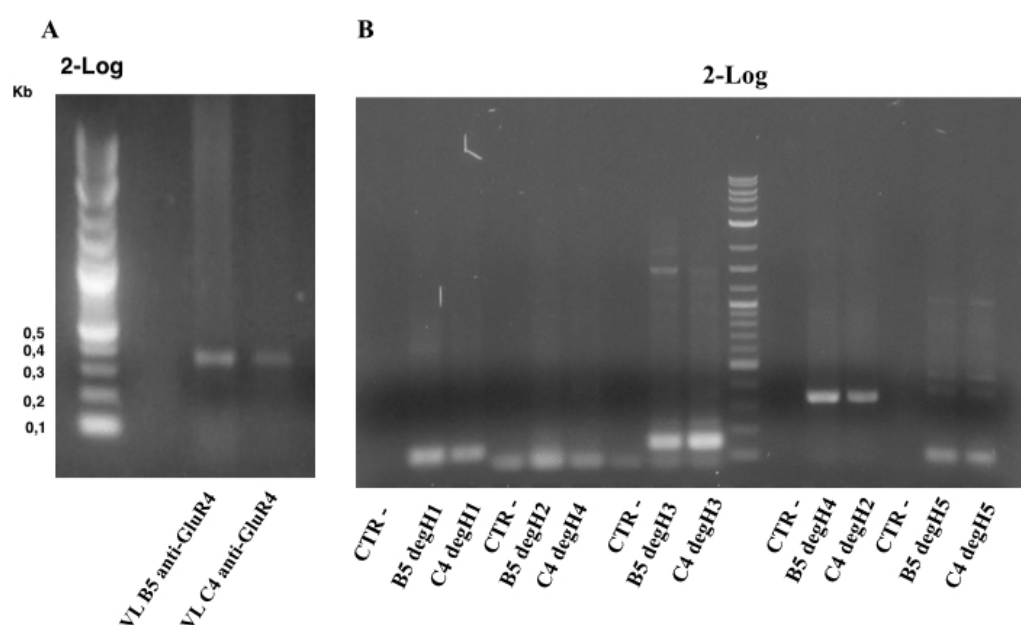


Fig.16 Isolation of VH (panel A) and VL (panel B) chains from B5 and C4 anti-iGluR4 hybridoma cells: a band corresponding to a consistent molecular weight of 350-400 bp is visible. in both pictures after DNA gel electrophoresis.

The correct size of the VH chain is around 350-400 bp; as it can be inferred from the figure (Fig. 16, A), VH isolation was obtained using both degH4dir-IgG1rev and degH2dir-IgG1rev primer pairs, obtaining bands of a consistent weight for both clones, B5 and C4 anti-iGluR4 respectively.

VL chain of both B5 and C4 anti-iGluR4 was isolated using primers as described in Materials and Methods. The electrophoretic run of the PCR product for VL isolation is reported in Fig. 16, B, in which two bands corresponding to the VL of B5 anti-iGluR4 and C4 anti-iGluR4 respectively are visible.

To isolate variable domains we used an high fidelity DNA polymerase Phusion DNA Polymerase (Finnzymes), as described in Materials and Methods.

PCR product were purified and cloned into the pcRBlunt Zero vector, that is a suitable vector for cloning without the using of restriction enzymes. DH5 $\alpha$  bacterial competent cells were thus transformed with the ligation product; the DNA from five colonies of both VH and VL of B5 and C4 anti-iGluR4, respectively, were extracted and sequenced by GATC Biotech.

Electropherograms were analyzed using IMGT Information system software (<http://www.imgt.org>) for determination of CDRs and Framework regions.



## ***4.2 Production and characterization of anti- hERG1 single chain variable fragments antibodies.***

### ***4.2.1 anti-scFv-hERG1-G3 expression and characterization as an in vivo imaging tool***

The second part of the work of this thesis was focused on the expression and characterization of a *single-chain variable fragment* (scFv) antibody directed against the ion channel, hERG1.

hERG1 has emerged in the last decades, not only as a novel regulator of growth and death in cancer cells (Sanguinetti *et al.*, 1995), but also as a new molecular marker for cancer patients' stratification and, more recently, as a target for cancer therapy. Thus, due to the arising interest in hERG1 protein and in order to overcome problems related to the *in vivo* use of murine complete antibodies (immunogenicity and big size of the molecule, preventing an effective penetration of the tumor mass), we engineered the previously produced hERG1-mAb (hERG1-mAb: patented by the University of Florence, n° FI2006A000008), directed against an extracellular epitope of the hERG1 ion channel, located in the pore domain region (S5PORO), to obtain a recombinant single chain variable fragment antibody, scFv-hERG1.

The aim was to develop a new tool for diagnosis and, also, to investigate the potential applications of scFv-hERG1 (named scFv-hERG1-G3) in cancer therapy (patent N° FI2014A000189; "A new immune-based strategy to target hERG1 potassium channel" A Sette, S Crescioli, O Crociani, E Lastraioli, M D'Amico, M Masselli, A Arcangeli. PEGS Europe Protein & Antibody Engineering Summit, November 6-8 2012, Vienna, Austria).

The cDNA of the construct expressing scFv-hERG1 was cloned into pPIC9K vector. Representative models of both the scFv-hERG1 construct and the vector pPIC9K are reported in Figure 18 .

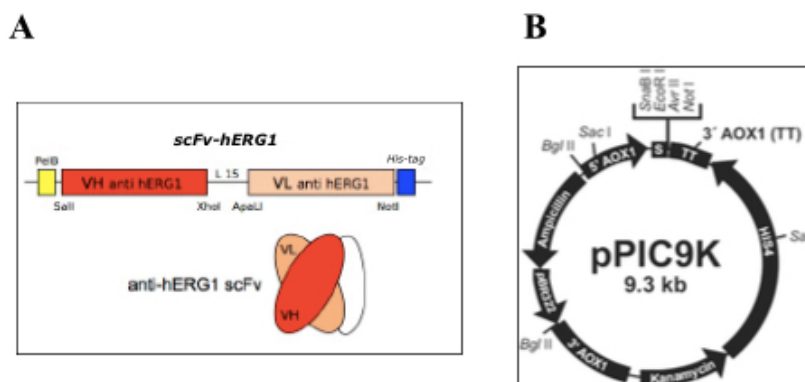


Fig. 18 On panel A is reported the schematic structure of the construct scFv-hERG1, while in panel B is reported the structure of the vector chosen for expression of the scFv-hERG1 antibody.

pPIC9K is a vector suitable for protein expression in yeast host *Pichia pastoris*. The vector has been modified to carry an Histidine tag (His tag), that is useful for antibody purification (Thermofisher Scientific).

Another feature of this vector is to allow the secreted expression of proteins, because of the presence of a  $\alpha$ -factor *signal sequence* in front of the coding sequence.

Secreted expression of heterologous proteins in *Pichia pastoris* is mainly favored by the low levels of secretion of native protein which characterizes the yeast class. Usually, low amount of native protein is secreted into the minimal *Pichia* medium, so that the secreted heterologous protein comprises the vast majority of the total protein in the medium simplifying the first step in purification of the protein (Barr *et al.*, 1992).

Among other advantages offered by the *Pichia pastoris*, as expression system, there is the fact that it is a methylotrophic yeast characterized by ease of genetic manipulation, high levels of protein expression and the ability to perform higher eukaryotic protein modifications, such as glycosylation, disulphide bond formation and proteolytic processing (Cregg JM *et al.*, 2000).

Moreover, *Pichia pastoris* can be grown to very high cell densities using minimal media (Veenhuis M, *et al.*, 1983; Wegner G. 1990) and integrated vectors help genetic stability of the recombinant elements, even in continuous and large-scale fermentation processes (Romanos M. 1995).

The first step for the expression of scFv-hERG1 was *Pichia pastoris* transformation. The protocol we used has been adapted from Pichia Expression Kit (Invitrogen).

Protein expression methodology was acquired at the Molecular Biology laboratory led by Prof. E. Gherardi (University of Pavia), where part of the protein expression experiments were also performed.

The expression cassette sequence of the scFv-hERG1 construct, cloned into the pPIC9K vector, was analyzed using NEBcutter V2.0, in order to choose a proper restriction site, to linearize the construct, as linearization favors DNA uptake during the transformation process.

Analysis is reported in Fig. 19, panel A. The cDNA encoding scFv-hERG1 was linearized, prior transformation, using SalI restriction endonuclease. Digestion with SalI usually generates an integration event that is an insertion at *his4*, thus resulting in a His<sup>+</sup> Mut<sup>+</sup> phenotype in GS115 *Pichia pastoris* strain, which is the strain we have used for expression experiments.

A small portion of the digestion was analyzed by agarose gel electrophoresis to confirm the DNA linearization (Fig. 19, panel B).

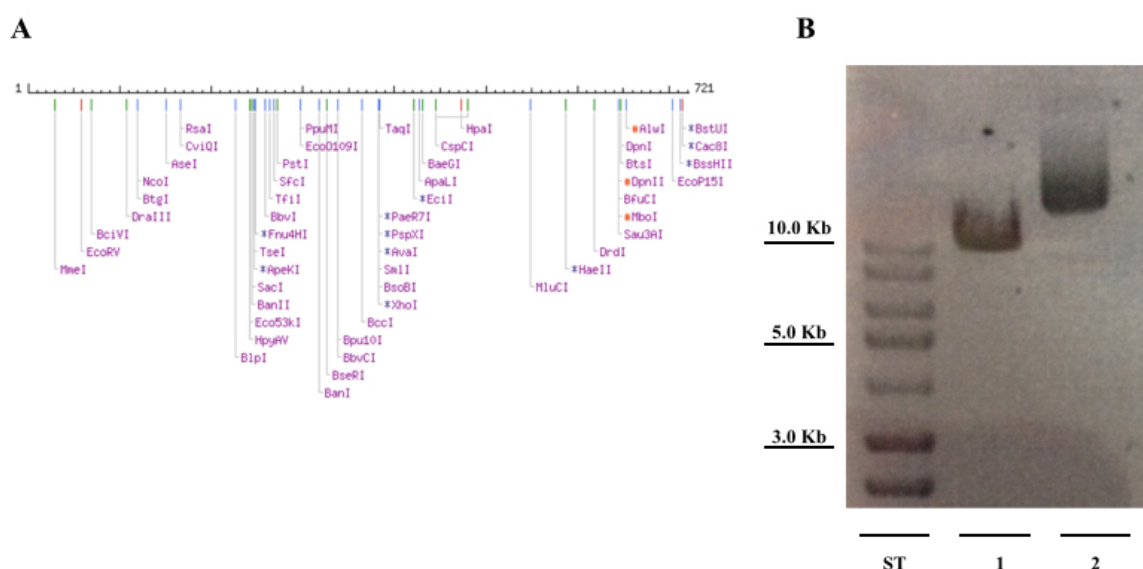


Fig. 19 Panel A. Analysis of the restriction sites of the expression cassette of scFv-hERG1 cloned into pPIC9K. Panel B. Agarose gel electrophoretic run of scFv-hERG1 cDNA: first lane (ST) shows the 2-Log DNA ladder; lane 2 (1) shows the linearized scFv-hERG1 cDNA after digestion with SalI; lane 3 (2) represents uncut cDNA scFv-hERG1.

As it can be inferred from lane 2 in fig. 19, panel B, the DNA was completely digested and was subsequently isolated from gel and purified.

We have chosen to transform yeast cells following the spheroplasting technique, which usually provide the highest efficiency of transformation ( $10^3$  to  $10^4$  transformants per  $\mu\text{g}$  DNA).

In yeast cells, the wall prevents uptake of DNA, thus to enable DNA uptake, it is necessary to partially remove the cell wall. To this purpose is used Zymolyase, an  $\alpha$ -glucanase that hydrolyzes the glucose polymers with  $\alpha 1,3$  linkages in the cell wall. A crucial step is not to overdigest the cell wall, as doing so will cause the death of the cells. The optimal percentage of spheroplasting is 70%, which represents the best condition for the DNA uptake. To achieve the exact percentage of spheroplasting, it is necessary to establish the right time of digestion of zymolase.

Yeast transformation was successful, colonies appeared on the plates after 4 days of incubation at  $30^\circ\text{C}$  (Fig. 20, panel A).

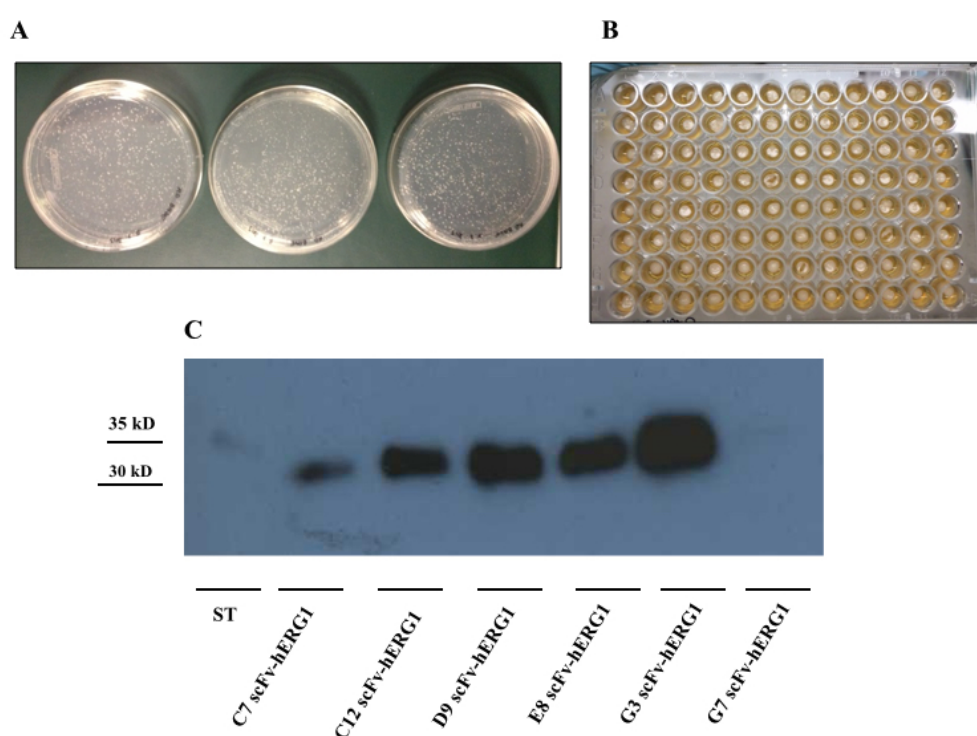


Fig. 20 Panel A shows transformants obtained after yeast transformation with the construct scFv-hERG1; panel B reports transformants grown on YPD agar at 5 mg/ml of G418 concentration; panel C shows WB of purified scFv-hERG1 antibody derived from supernatants of six clones derived from yeast transformation.

Transformants were then picked and screened on YPD-agar containing different concentrations of Geneticin (G418); this kind of selection is possible because pPIC9K

contains the bacterial Kanamycin gene, that confers resistance to kanamycin in *Pichia*. Because of the genetic linkage between the kanamycin gene and the "expression cassette", it is possible to infer that Geneticin® resistant clones contain multiple copies of the gene of interest (Fig. 20, panel B).

Six clones grown on plates, containing G418 for selection, were expressed in small-scale, following induction protocol described in Materials and Methods. Supernatants obtained from these cultures were used for purification and analyzed through western-blot (WB), fig. 20 (panel C), which shows a single band, with a molecular weight of  $\approx$  30 KDa, consistent with the molecular weight of the scFv-hERG1.

We chose the G3 clone (hence named scFv-hERG1-G3), which on WB showed to be the most promising clone in terms of protein production, for high-scale expression (1L *Pichia pastoris* culture). Supernatant was purified using Ni-beads (GE Healthcare) and analyzed through SDS-Page and Coomassie Brilliant Blue staining. For optimization of the purification procedure, elution steps were performed using different imidazole concentrations, as it is reported in Fig. 21, panel A.

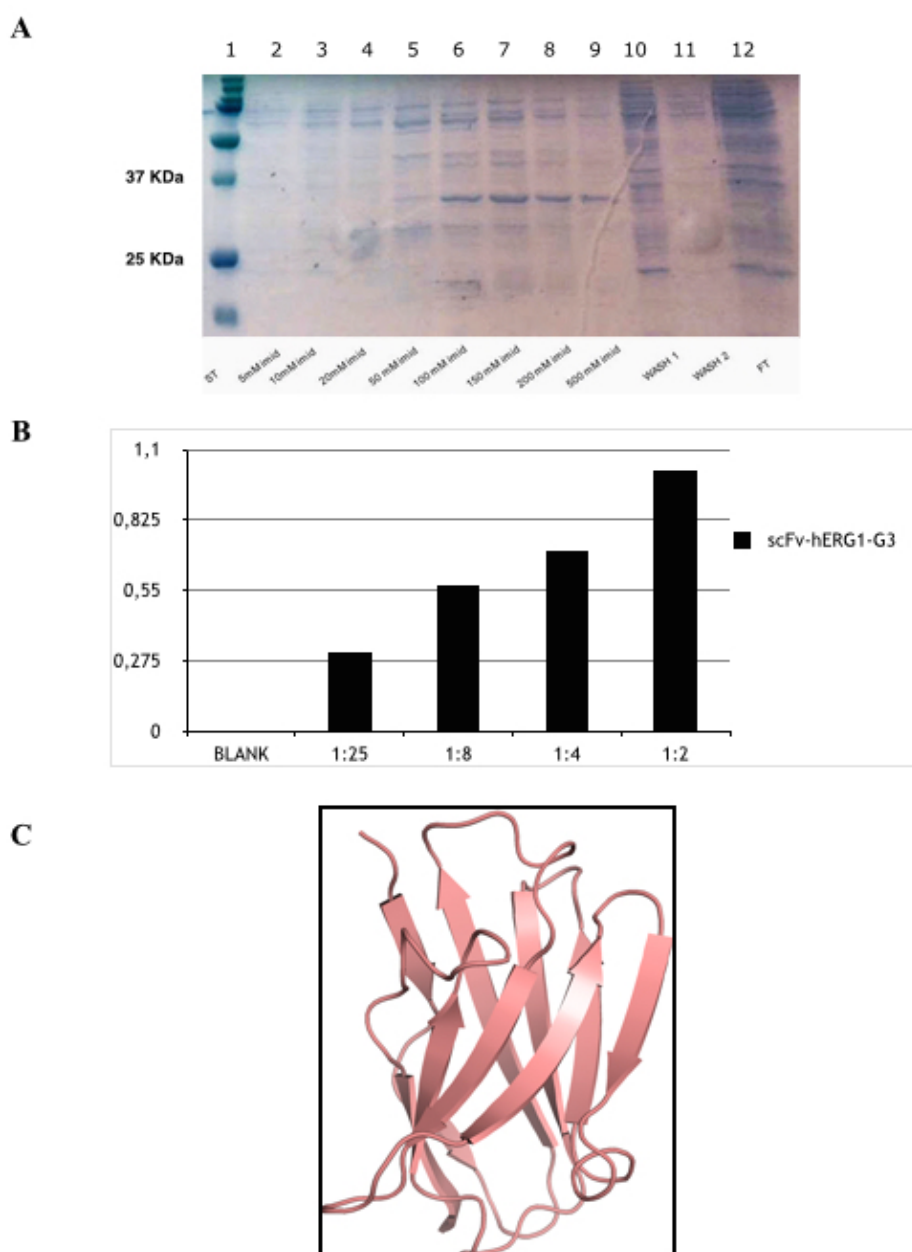


Fig. 21 Panel A shows Coomassie staining in which elutions, obtained using buffer with different imidazole concentrations were tested. A band, consistent with the molecular weight expected for the scFv-hERG1-G3 antibody, around 30 KDa, is detectable in lanes 6, 7, 8 and 9. Panel B reports different dilutions of the scFv-hERG1-G3 antibody tested in ELISA assay, as it can be inferred from the image,  $OD_{450}$  values are proportional to the dilutions tested. Panel C shows the 3D model of the scFv-hERG1-G3 structure.

Coomassie staining shows that scFv-hERG1-G3 protein can be detected in different elutions (molecular weight  $\approx$  30 KDa) as highlighted by the arrows. ELISA test was also performed to assess the binding capacity of the scFv-hERG1-G3 antibody over the immobilized antigen (S5PORO). As it can be inferred from the Fig. 21, panel B, scFv-

hERG1-G3 shows to maintain the capacity to recognize the antigen, in a dose-dependent manner, according to the dilutions tested.

We have also modeled the 3D structure of scFv-hERG1-G3, which is represented in fig. 21, panel C.

As our final goal has been to obtain a molecule to exploit as a diagnostic tool for molecular imaging, we wanted to test scFv-hERG1-G3 with regard to the binding with the native antigen.

Thus, we have performed indirect immunofluorescence (IF) on fixed cells, overexpressing hERG1 (HEK 293-hERG1) and HEK 293-MOCK cells, used as negative control (Fig. 22, PANEL A and B), incubated with scFv-hERG1-G3.

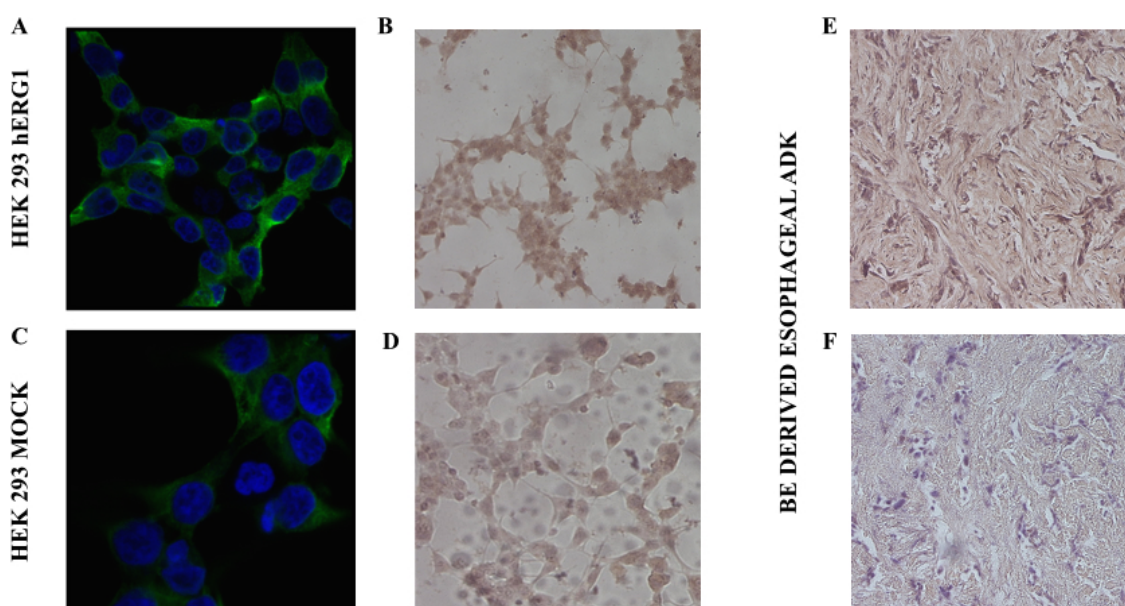


Fig. 22 Indirect IF performed on HEK 293 hERG1 (panel A) and HEK 293 MOCK (panel C) cells using scFv-hERG1-G3 antibody. ICC performed on HEK 293 hERG1 (panel B) and HEK 293 MOCK (panel D) cells using scFv-hERG1-G3. IHC staining obtained on slides of a Barrett's derived ADK patient incubated scFv-hERG1-G3 and anti-His (negative control) is reported in panels E and F, respectively.

As it is possible to infer from the images, there is a good staining on HEK293-hERG1, while there is no staining, with poor background signal for HEK293-MOCK cells, probably correlated to the secondary antibody (anti-His) working conditions. We have

also performed ICC on the same cells (panels B and D), confirming the staining pattern described above.

Recent evidences, given by Lastraioli E. and colleagues (2006) concerning the expression of hERG1 potassium channel in the upper gastric tract, stress that hERG1 protein is not expressed in normal squamous esophageal mucosa and neither in the gastro-esophageal junction mucosa collected below the squamocolumnar junction, when the samples belonged to normal patients, or to patients with inflammatory conditions. On the contrary, hERG1 channels are mis- and overexpressed in the metaplastic mucosa present below the squamocolumnar junction that characterizes BE (Barrett's esophagus) lesions. Moreover, it has emerged that the hERG1 protein is highly expressed in all the dysplasias (Ds) as well as adenocarcinomas (ADKs) arising on a previously diagnosed BE. This fact suggests the hypothesis that the *herg1* gene expression marks an early step along the progression of a normal cell toward a true cancerous cell through a metaplastic and dysplastic stage (Lastraioli et al., 2006).

In this scenario, we have tested scFv-hERG1-G3 in IHC on a section taken from a Barrett's derived esophageal adenocarcinoma, to investigate its potential role as a molecular tool for patients' stratification.

Fig. 22, panel E reports the section stained using scFv-hERG1-G3 in which a clear labelling is detectable; panel F reports the negative control treated only with the secondary antibody anti-His (Abcam).

An essential step for the application of anti-hERG1 *single chain variable fragment* as a molecular probe has been the direct conjugation with a fluorophore. We have labelled scFv-hERG1-G3 with Alexa 488, using Alexa Fluor® 488 Microscale Protein Labeling Kit (Thermo Fisher). The dye used for labelling has a tetrafluorophenyl (TFP) ester moiety that is more stable in solution than the commonly used succinimidyl (NHS) ester. In fact, TFP esters react efficiently with primary amines of proteins to form stable dye-protein conjugates. One of the main problems related to the direct labelling of antibodies, especially single-chain antibodies, whose size is very reduced compared to intact Ig molecules, is the possibility the labelling could compromise the biological properties of the antibodies, decreasing the capacity of antigen binding.

Firstly, scFv-hERG1-G3-Alexa488 was tested in IF on neuroblastoma cells, SH-SY5Y, that have been demonstrated to express hERG1 channel at high levels (Arcangeli *et al.*, 1998).

Results are reported in Fig. 23 (panels A and B) in which a clear staining is detectable, thus showing the maintained capacity of the labelled scFv to bind the antigen.

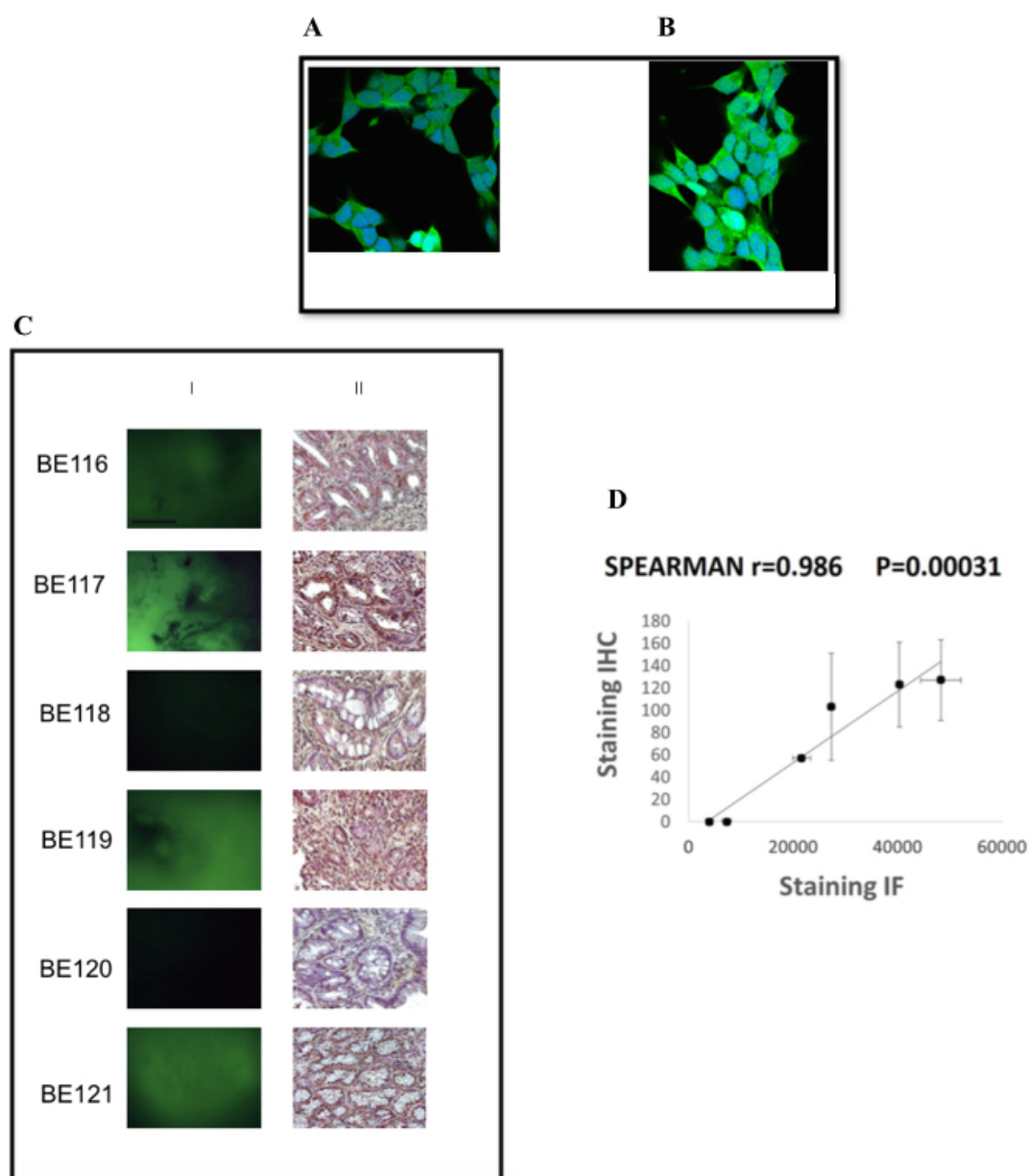


Fig. 23 Panel A and B show direct Immunofluorescence performed on neuroblastoma cells SH-SY5Y, using scFv-hERG1-G3-Alexa488 demonstrating a clear staining and thus assessing the maintained capacity of the antibody directly conjugated with the fluorophore to recognize the antigen. Panel C reports representative images of Immunofluorescence with scFv-hERG1-G3-Alexa488 (C, I) and corresponding immunohistochemical analysis with anti-hERG1 monoclonal antibody (C, II). Panel D shows scatter plot, with standard error, showing the concordance between IHC and IF.

The following part of the work has been focused on the application of scFv-hERG1-G3-Alexa488 in a prospective study on fresh BE samples collected during endoscopy.

In fact, recent data indicate that hERG1 expression could help in identifying patients at higher risk of progressing from BE to adenocarcinoma. Since our aim is to further test the *single-chain variable fragment* in endoscopy to discriminate between hERG1-positive and hERG1-negative BE patients, we have tested scFv-hERG1-G3-Alexa488 on fresh endoscopic mucosal samples from BE patients. At the same time, IHC using anti-hERG1 monoclonal antibody was also carried out on the same sections on paraffin-embedded samples. Figure 23 shows representative images of either fresh samples (panel C, I) or fixed samples (panel C, II). Samples with an intense IHC signal, also displayed a positive IF signal. The mean IHC and IF values were used to perform a statistical analysis, applying the Spearman Correlation Test. A statistically significant value was obtained ( $P=0.00031$ ), with a coefficient of 0.986. Figure 23, panel D shows a scatter plot with the concordance between IHC and IF staining.

### 4.2.2 scFv-hERG1-D8Cys production and characterization as a potential antitumor agent

Considering the potential employment of scFv-hERG1-G3, we wanted to improve protein production, as at a first stage, the protein yield was not completely satisfactory.

For this reason we have analyzed in detail the nucleotidic sequence of the expression cassette of the scFv-hERG1 antibody, that is reported in Fig. 24, panel A. Fig 24, panel B shows the amino acid sequence in which six complementarity-determining region (CDR), identified using the Kabat scheme ([www.bioinf.org.uk](http://www.bioinf.org.uk)), are highlighted.

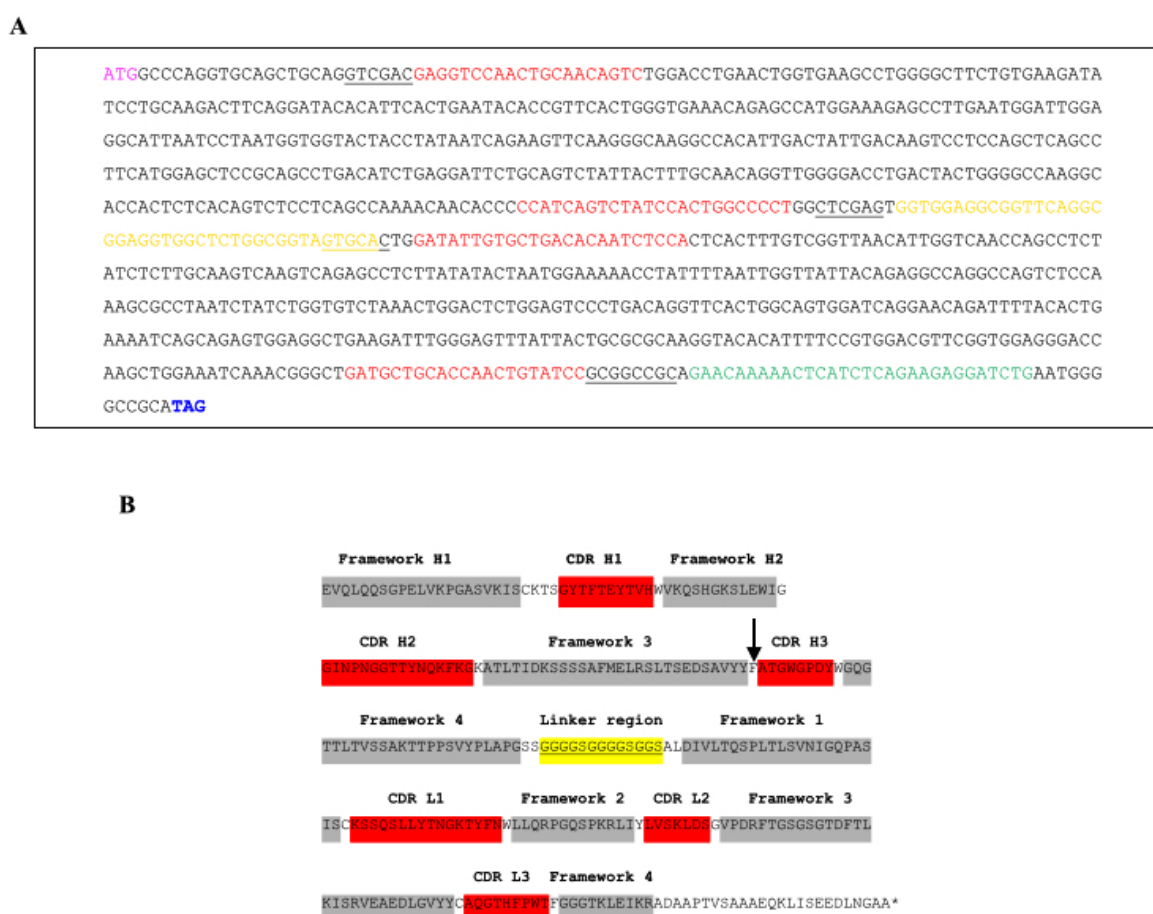


Fig. 24 scFv-hERG1 expression cassette sequence obtained by Automated DNA sequencing service (PRIMM) (A). Underlined are shown restriction sites; in pink is Met start codon; in red are primer sequences; in yellow is peptide linker sequence; in green is myc-tag and in blue is amber stop codon. Highlighted by the square the triplet (TTT) codifying for a Phe amino acid instead of the canonical Cys amino acid (TGT) usually harbored in this position. Amino acid sequence of scFv-hERG1 (B). CDRs were identified using the Kabat scheme. The highlighted sequences in red show the CDRs (heavy and light chain) of the recombinant antibody fragments. The framework regions are highlighted in grey and the glycine-serine linker region is yellow. (Patent application ongoing).

The nucleotide sequence of the scFv-hERG1 unraveled the presence of a Phe in position 95 of the VH domain of the antibody (highlighted in red in panel A). In this position of the VH domain, a T nucleotide was present (see the arrow in fig. 24, B). The substitution of a G was introduced instead of the T in this position, leading to the exchange of the Phe (TTT) with a Cys (TGT) in position 95. This mutation resulted in the introduction of one amino acid (Cys) in the position between Framework 3 and CDR3, which surprisingly resulted fundamental for the formation of the disulfide bond in the immunoglobulin variable domain. The Cys was introduced in the original construct, setting up a mutagenesis protocol (see Materials and Methods). These amino acids are very conserved in all antibodies, just one exception has been previously found in nature (Proba K. *et al*, 1997).

Due the interesting rarity of the structure of our antibody, we wanted to explore the effects that the substitution of a fundamental Cys with a Phe in the VH chain has both on the folding of the protein and on its expression and functionality.

Since the scFv-hERG1 displayed such unusual structure, we reintroduced the missing Cys in the original construct, setting up a mutagenesis protocol, described in Materials and Methods. The cDNA obtained from four mutagenized scFv-hERG1 colonies was sequenced and the sequencing results demonstrated the proper mutation from TTT to TGT, indicative of the desired mutation from Phe to Cys.

Thus, we have expressed also mutagenized scFv-hERG1 (hence named scFv-hERG1-Cys) and transformed it into the GS115 *P. pastoris* host strain, using the spheroplasting technique, as previously described for scFv-hERG1 construct. Six clones (B11, C3, D8, D9, G4, G10), among the scFv-hERG1-Cys transformants, were analyzed. Results of the small-scale expression are shown in Fig. 25, panels A and B. All the clones revealed protein expression after 72 h induction, as shown in slot blot (panel A).

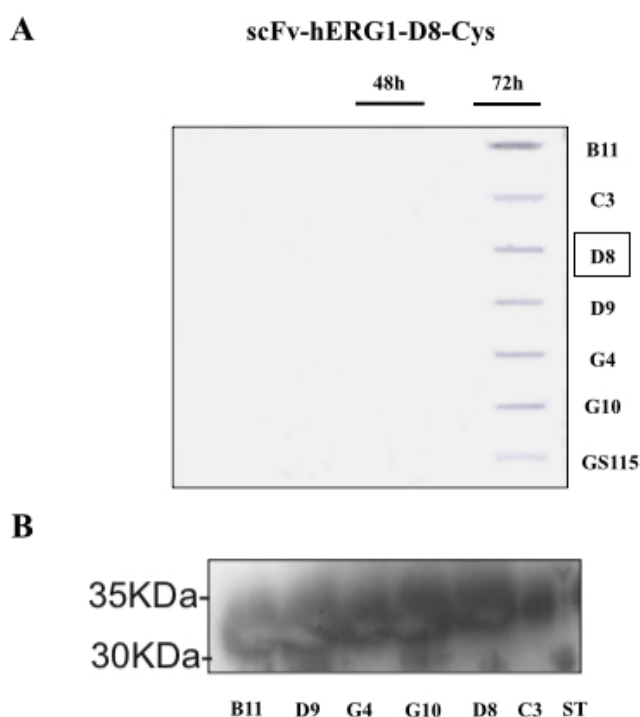


Fig. 25 Slot blot on supernatants collected from induction of scFv-hERG1-D8Cys Pichia pastoris clones at 24 h, 48 h and 72 h (A). Clones B11, C3, D8, D9, G4, G10 and the negative control of non-transformed Pichia strain GS115 were all analyzed. Stained was performed using DAB chromogene. D8 is shown being the best expressing one. Western-blot performed on purified samples of the six clones (B). D8 was the one that showed the highest expression level, while lowest expression was detected for the C3 clone.

After purification, the presence of the protein was assessed through western-blot (panel B). We chose the best expressing clone D8 for scFv-hERG1-Cys (named scFv-hERG1-D8Cys).

Subsequently, we have started a parallel characterization of the native form of the antibody scFv-hERG1 and the form in which the Cys has been restored, scFv-hERG1-Cys.

Larger-scale expression analyses are shown in Figure 27. Chromatograms, obtained after ÄKTA purification, are reported in panel A for scFv-hERG1-G3 and in panel B for scFv-hERG1-D8Cys, respectively. For both antibodies, the protein elution is represented by a single peak (indicated with an arrow in panel A for scFv-hERG1-G3 and in panel B for scFv-hERG1-D8Cys). Fractions 11, 12, 13 (panel A) correspond to scFv-hERG1-G3; fractions 12, 13, 14 (panel B) correspond to scFv-hERG1-D8Cys.

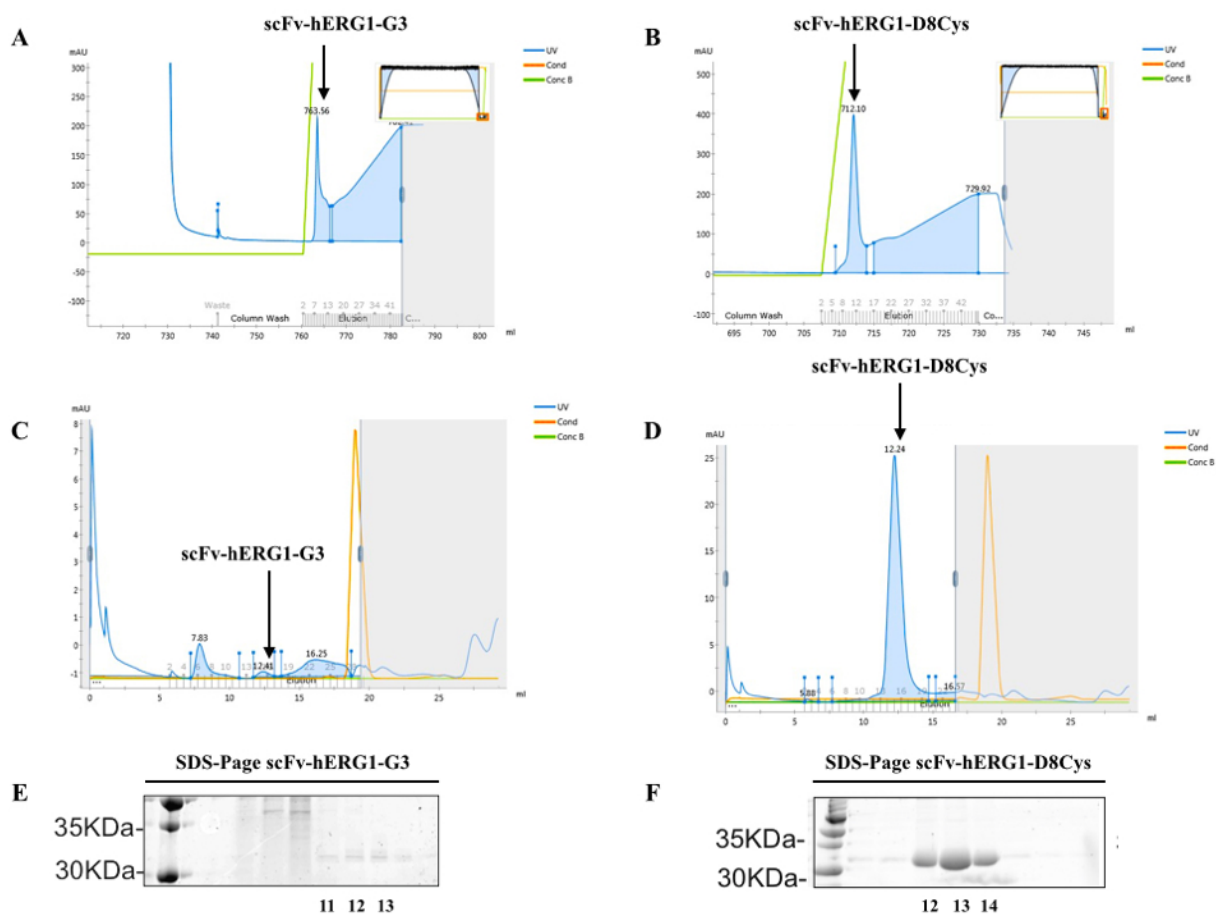


Fig.26 ÄKTA purification through affinity chromatography (A) and gel filtration chromatography (C), using Superdex 75 HR 10/30 (C), of scFv-hERG1-G3. SDS-PAGE of purified scFv-hERG1-G3 elution fractions (E).

ÄKTA purification through affinity chromatography (B) and gel filtration chromatography (D), using Superdex 75 HR 10/30 (D), of scFv-hERG1-D8Cys. SDS-PAGE of purified scFv-hERG1-D8Cys elution fractions (F).

The presence of the protein was assessed through SDS-PAGE and Coomassie Brilliant Blue staining reported in panels E and F for scFv-hERG1-G3 and scFv-hERG1-D8Cys, respectively. Bands corresponding to the molecular size of both antibodies (around 30KDa) are visible.

Comparing the yields of the two proteins, scFv-hERG1-G3 and scFv-hERG1-D8Cys, significant differences were found, as reported in the table below

PROTEIN	YIELD (mg/l)
scFv-hERG1-G3	0,200
scFv-hERG1-D8Cys	1

<sup>a</sup> The yields were normalized to mg protein per liter of *Pichia pastoris* yeast culture.

Thus, we have performed gel-filtration and the resulting chromatograms are reported in Fig 26 (panels C and D). Size-exclusion chromatography (SEC) was performed in order to investigate the possible presence of aggregates which might affect the binding capacities of the two antibodies. Several aggregates are detectable from the analysis reported in panel C that refers to scFv-hERG1-G3; instead scFv-hERG1-D8Cys (panel D) appears in a monomeric form. The characteristic of scFv-hERG1-G3 to form aggregates might deeply affect antibody characteristics, such as yield and binding capacities.

The affinity of the two antibodies towards the immobilized antigen was assessed through Surface Plasmon Resonance (SPR). Fig. 27 shows the sensograms obtained at different concentrations of the scFv-hERG1-G3 and the scFv-hERG1-D8Cys antibodies. KD for scFv-hERG1-G3 is higher ( $3.8\text{E-}07\text{M}$ ) compared to scFv-hERG1-D8Cys ( $6.18\text{E-}08\text{M}$ ). This value is the result of a faster dissociation (lower kd) for the

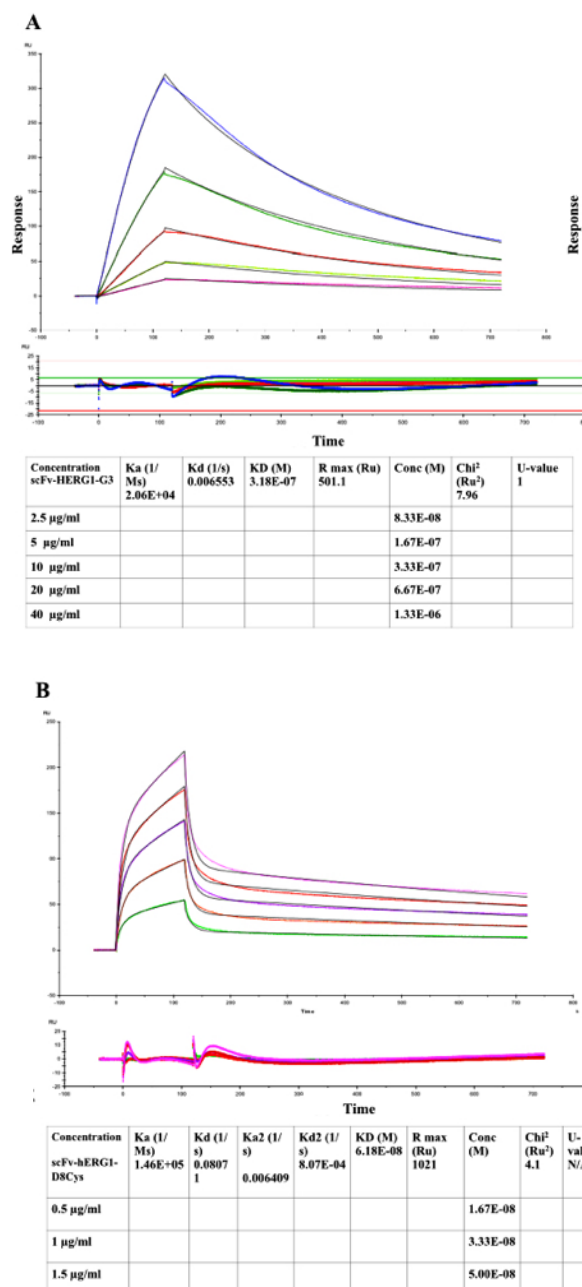


Fig. 27 Sensograms showing the results from SPR (Surface Plasmon Resonance) analysis at different concentrations of the antibodies: scFv-HERG1-G3 (2,5 µg/ml; 5µg/ml; 10µg/ml; 20µg/ml; 40µg/ml) and scFv-HERG1-D8Cys (0,5µg/ml; 1µg/ml; 1,5µg/ml) (B).

scFv-HERG1-D8Cys antibody and a slower association rate (higher Ka) compared to scFv-HERG1-G3 antibody that is also represented by the curve trend.

Moreover, the RU index is 1021 for scFv-HERG1-D8Cys antibody and 501.1 for scFv-HERG1-G3. Such values reinforce the evidence of a better affinity of scFv-HERG1-D8Cys for the immobilized antigen compared to scFv-HERG1-G3 antibody.

We have then performed an immunofluorescence analysis using scFv-hERG1-G3 and scFv-hERG1-D8Cys on fixed cells, to determine the immunoreactivity of the two antibodies towards the native antigen. We used, as cellular model, HEK 293 transfected with the hERG1 cDNA (HEK293-hERG1) and HEK 293 MOCK, that do not express the hERG1 protein, as a control. HEK 293 MOCK cells showed no or weak signal after incubation with both antibodies, while HEK 293 hERG1 showed a good labelling with the scFv-hERG1-G3 and, even better, with the scFv-hERG1-D8Cys (Fig. 28).

Data analysis obtained using ImageJ Software is reported in the graph in figure 28. scFv-hERG1-D8Cys values, corresponding to the IF intensity increment, are significantly higher in cells overexpressing hERG1, if compared to the values of the control obtained in HEK 293 MOCK cells. Moreover, IF signal obtained on HEK 293 hERG1 cells using scFv-hERG1-D8Cys is twofold higher than the value obtained on the same cells using scFv-hERG1-G3 antibody.

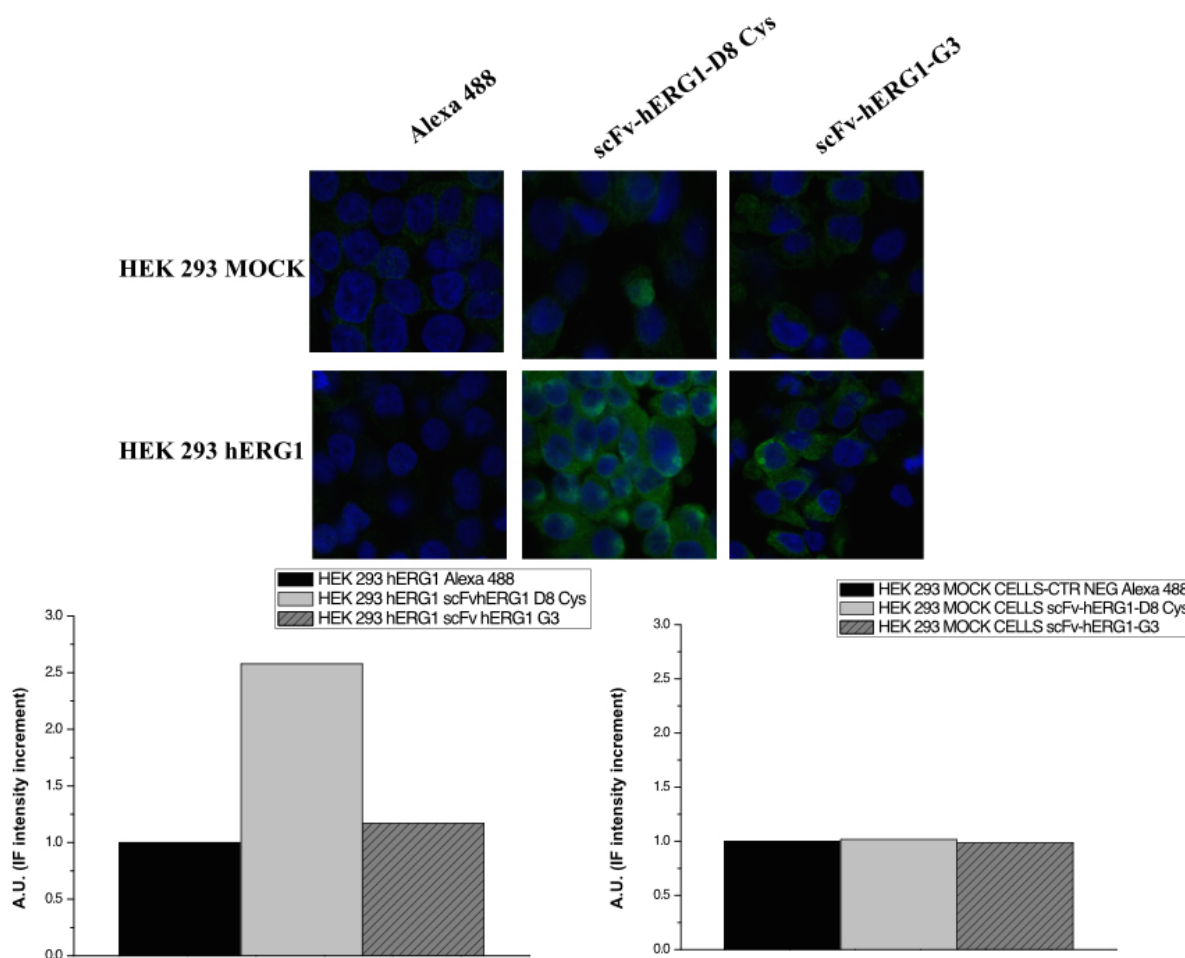


Fig. 28 Immunofluorescence of fixed cells. Cells HEK 293 hERG1 and HEK 293 MOCK were seeded on glass slides and incubated with scFv-hERG1-G3 and scFv-hERG1-D8Cys . Photographs were taken using a C1 confocal microscope (Nikon) . Graphs report the IF signal quantification obtained analyzing the images using ImageJ software. Results were normalized on controls and show the IF intensity increment (AU, arbitrary unit), obtained analyzing three different areas with the same cell density of each IF picture.

We have also tested the immunoreactivity of the two antibodies after direct labelling with the fluorescent molecule Alexa 488. scFv-hERG1-G3-Alexa488 and scFv-hERG1-D8Cys-Alexa488 antibodies were tested in IF on fixed cells (Fig. 29, panels A and B) showing the maintaining of the capacity to recognize the antigen in the native conformation, even after the conjugation with the fluorophore, which, as previously reviewed, might be a detrimental step for antibody functionality (Vira S. *et al.*, 2010) .

IF staining was measured using ImageJ software and results are reported in the graphs below the figures. Signal obtained on HEK 293 HERG1 cells is stronger compared to

the control HEK 293 MOCK cells both for scFv-hERG1-G3-Alexa488 and scFv-hERG1-D8Cys-Alexa488. Values related to HEK 293 HERG1 cells normalized on the respective negative control, show an increase on the fluorescence signal in HEK 293 HERG1 cells for both scFv-hERG1-G3-Alexa488 and scFv-hERG1-D8Cys-Alexa488, respectively.

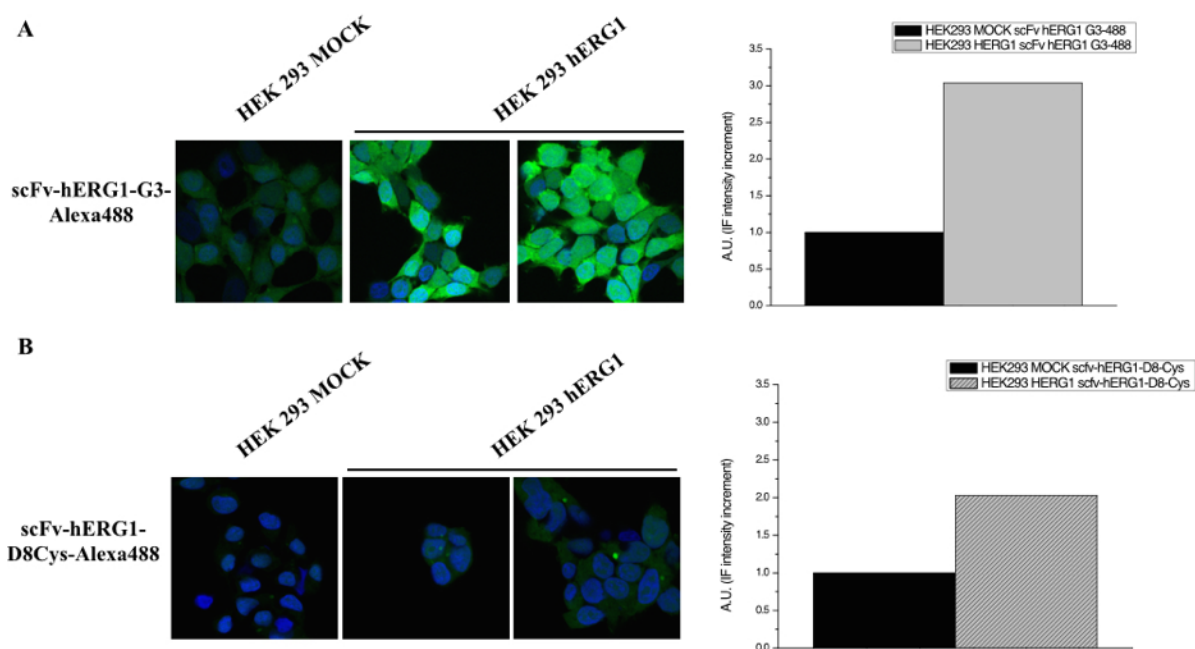


Fig. 29 Immunofluorescence with scFv-hERG1-G3-Alexa488 (A) and scFv-hERG1-D8Cys-Alexa488 (B) antibody on fixed HEK 293 MOCK and HEK 293 HERG1 cells. IF signal was quantified using ImageJ software. As it is possible to infer, both antibodies show to have maintained their functionality after direct conjugation with the fluorophore, with an evident increment of IF intensity, on cells HEK 293 HERG1. Results were normalized on controls and show the IF intensity increment (AU, arbitrary unit), obtained analyzing three different areas with the same cell density of each IF picture.

In order to assess and compare the potential use *in vivo* of scFv-hERG1-G3-Alexa488 and scFv-hERG1-D8Cys-Alexa488 as molecular tools, both antibodies were used in IF on live cells (Fig. 30).

The experiment confirmed the results obtained with the staining on fixed cells; HEK293 hERG1 cells appear to have a stronger signal, if compared with the negative control HEK293 MOCK cells. HEK 293 hERG1 cells appear to have a more specific spotty cellular labelling, while HEK 293 MOCK cells have a non-specific diffuse background. For this reason, we have also included the bright-field image of the same section.

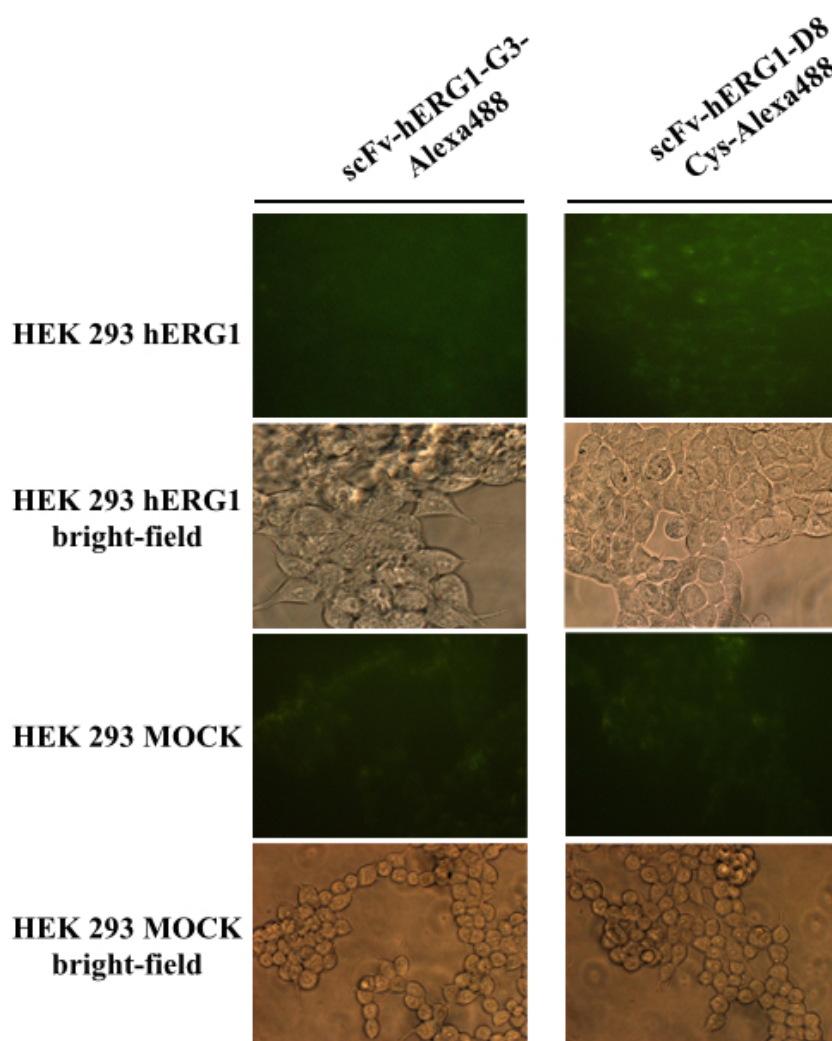


Fig. 30 In-vivo immunofluorescence. scFv-hERG1-G3-Alexa488 and scFv-hERG1-D8Cys-Alexa488 were incubated diluted in the culture medium on live cells HEK 293 hERG1 and HEK 293 MOCK cells.

From the parallel characterization of the two antibodies scFv-hERG1-G3 and scFv-hERG1-D8Cys, it was possible to evaluate that both molecules show the capacity to recognize the antigen, in different biological assays (perhaps with better characteristics for scFv-hERG1-D8Cys antibody). However, substantial differences related to protein production have been found for both antibodies and since protein yield is a crucial parameter to take into account, especially, given the fact that our final goal is to produce a *single-chain* to be exploited for diagnostic and clinical purposes, we have focused on the characterization of scFv-hERG1-D8Cys antibody. The latter has shown to be promising in terms of protein yield. Hence, we have chosen to pursue antibody characterization focusing on cancer cells, as previous studies have reported interesting results related to the action of anti-hERG1 monoclonal antibody on PANC-1 cells (Sette

A. Development of hERG1-targeted nanoparticles for a novel theranostic strategy in pancreatic ductal adenocarcinoma, PhD Thesis, 2013).

Moving from these evidences, we wanted to investigate the possible influence of scFv-hERG1-D8Cys antibody on cancer cell behavior, as the small size of *single chain* recombinant antibodies offers *per se* a valuable advantage for cancer treatment. Fig. 31 shows results obtained from IF on PANC-1 cells stained with scFv-hERG1-D8Cys and the negative control in which only secondary antibodies were incubated. There is a clear membranous signal on cells treated with the scFv-hERG1-D8Cys antibody, compared to the control. Signal intensity has been quantified using ImageJ Software and results are showed in the graph, demonstrating a clear increase in fluorescence intensity.

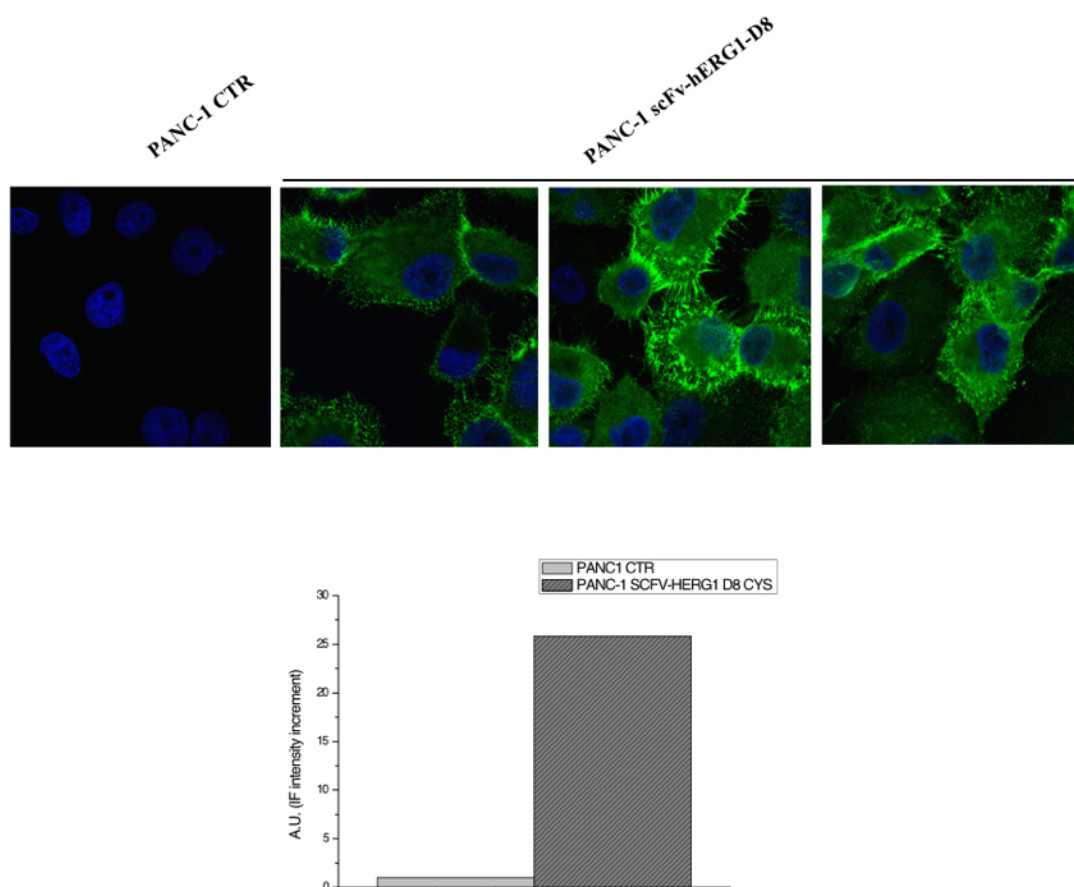


Fig. 31 Indirect IF on PANC-1 cells. A clear membranous staining has been obtained on PANC-1 cells, which express hERG1 channel at high levels, stained with scFv-hERG1-D8Cys antibody, while poor signal was obtained for control cells, treated only with secondary antibodies. IF signal increment (AU, arbitrary unit), obtained normalizing on the control after analysis of three different areas with the same cell density, is reported in the graph. Analysis shows a strong increment of IF intensity for PANC-1 cells stained with scFv-hERG1-D8Cys.

At this stage, we have further explored the effect of scFv-hERG1-D8Cys on a panel of neoplastic cell lines. As reported in Fig. 32 (panel B), a highly significant dose-dependent inhibition of cell proliferation was observed for MDA-MB 231, HEK 293 HERG1 and Mia Paca-2. Moreover, a significant dose-dependent inhibition was observed for FLG 29.1, PANC-1, BxPc3 and HCT 116. All the aforementioned cell lines express hERG1 protein (Lastraioli E. *et al.*, 2015; Bianchi L. *et al.*, 1998; Lansu K. and Gentile S., 2013; Crociani O. *et al.*, 2013). Cells were treated using scFv-hERG1-D8Cys (10; 20 µg/ml). As expected, no significant decrease in cell viability was found in HEK 293 MOCK cells, which do not express hERG1.

Anti-hERG1 monoclonal antibody was also tested at a concentration of 100 µg/ml, as reported in panel A, but no significant effect (except for HEK HERG1 cell line) was observed. We could say that such effect can be attributed to the small size of *single-chain* antibodies, which are fivefold smaller (30 KDa) compared to intact IgG (150 KDa). Moreover, it is worth noting that effect on viability obtained using scFv-hERG1-D8Cys has been achieved at lower antibody concentrations (five to ten-fold lower) compared to the ones tested for the anti-hERG1 monoclonal antibody. Such findings suggest that the small size of scFvs might be crucial to implement antibody effectiveness.

We have thus evaluated the effect of scFv-hERG1-D8Cys on HEK293 HERG1 invasion behavior, as reported in Fig. 32, panel C. It is possible to infer that there is a reduction in the percentage of treated cells able to invade compared to the control.

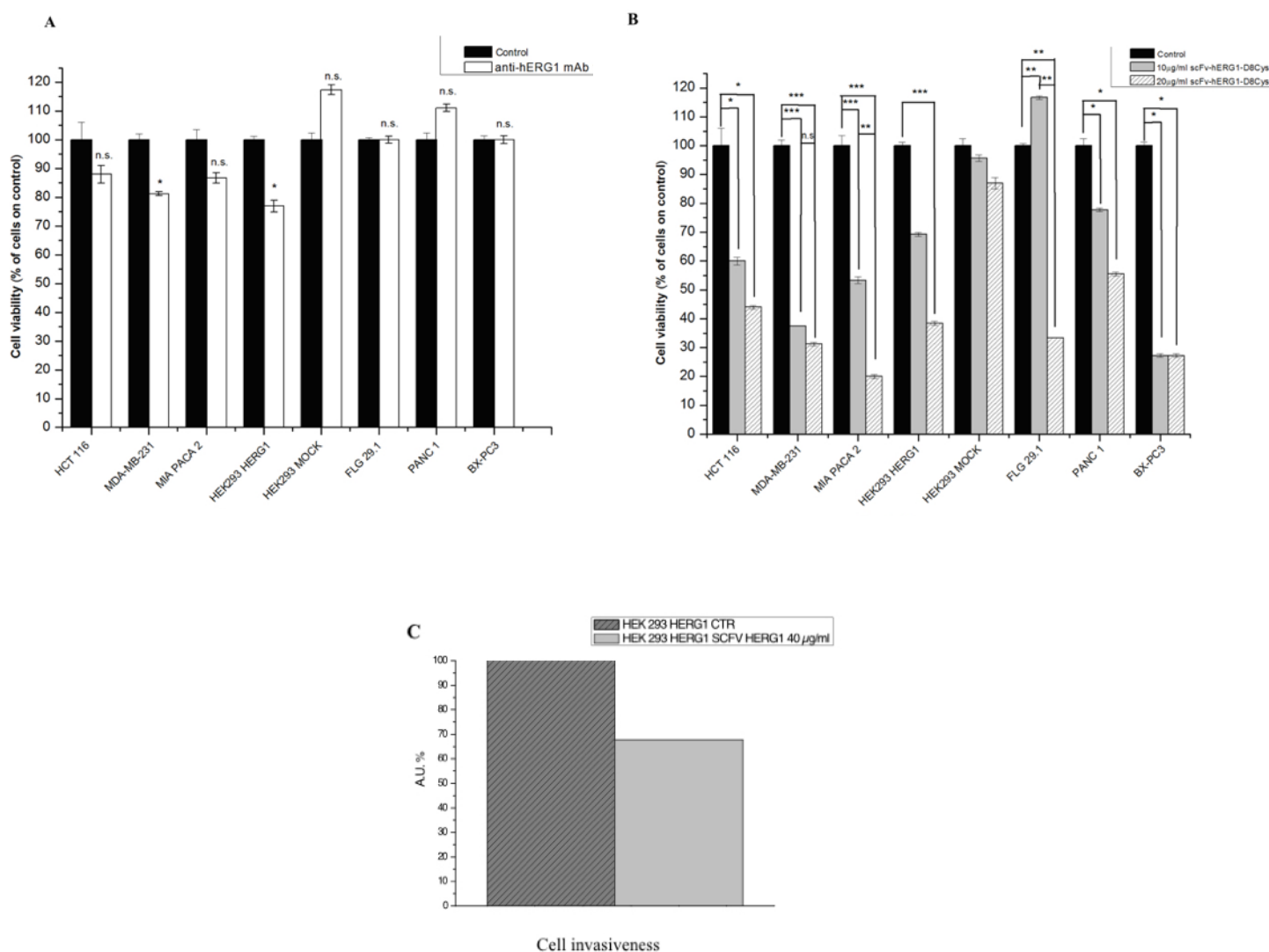


Fig. 32. Trypan blue viability assay performed on HCT-116, MDA MB-231, MIA PACA2, HEK 293 HERG1, HEK 293 MOCK, FLG 29.1, PANC-1, BxPC-3, using anti-HERG1 monoclonal antibody (100 µg/ml, panel A) and scFv-HERG1-D8Cys (10; 20 µg/ml, panel B). All experiments were performed in triplicate. Statistical analysis was performed assessing data normality and homoskedasticity assumptions applying Shapiro-Wilk and Bartlett test respectively, while variance was analyzed through Anova, Welch or Kruskal-Wallis test. Pairwise significance was estimated applying DSFC (Dwass, Steel, Critchlow-Fligner) or Tukey test (\*\* $p < 0,001$ ; \*\*  $p < 0,01$ ; \*  $p < 0,05$ ). Panel C shows results obtained regarding the effect of scFv-HERG1-D8Cys on cell invasiveness. Cells were counted and then values have been reported as the percentage of migrated cells compared to the control (set as 100%). A decrease in the percentage of migrated cells is reported for cells treated with scFv-HERG1-D8Cys.

In order to investigate the effect of scFv-hERG1-D8Cys on a 3D cellular model, we have tested three different concentrations of scFv-hERG1-D8Cys (10; 20; 40  $\mu\text{g/ml}$ ) on spheroids.

In fig. 33 panel A is reported the graph obtained for spheroids generated from HEK293-hERG1. The volume of spheroids treated with 20  $\mu\text{g/ml}$  and 40  $\mu\text{g/ml}$  scFv-hERG1-D8Cys is smaller (see dotted and dash-dot lines, respectively) compared to the control cells (solid line) at each time point. Panel B, instead, shows the growth curve of the HEK 293 MOCK spheroids, in which no difference was found for treated spheroids at the three concentrations of scFv-hERG1-D8Cys tested, compared to the control. Panel A and B also show a representative bright-field image of the control HEK293-hERG1 and HEK 293 MOCK spheroids, respectively, as they appeared after 72 h culture.

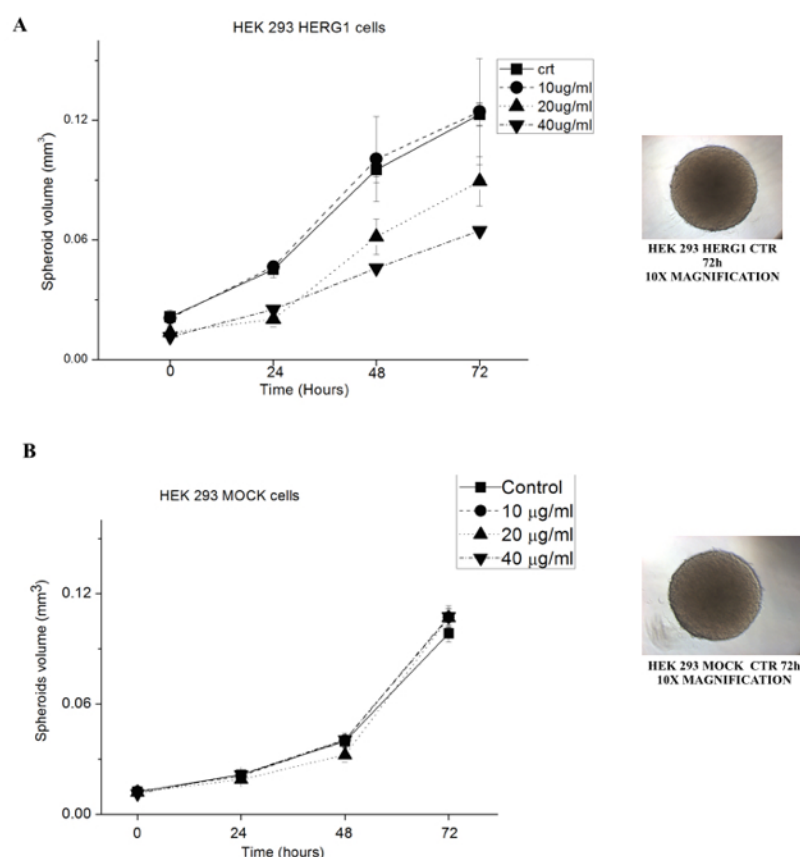


Fig.33. Panel A: HEK 293 HERG1 spheroids 10, 20 and 40  $\mu\text{g/ml}$  scFv-hERG1-D8Cys were tested. Volume of the spheroids treated with 20  $\mu\text{g/ml}$  and 40  $\mu\text{g/ml}$  scFv-hERG1-D8Cys is smaller (dot and dash-dotted line, respectively) compared to the control (untreated cells) at each time point. Panel B, instead, shows the growth curve of the HEK 293 MOCK (not expressing hERG1) spheroids, in which no difference was found for treated spheroids at all the three concentrations scFv-hERG1- D8Cys tested. Representative bright-field image of the control HEK293-hERG1 and HEK 293 MOCK spheroids, respectively, as they appeared after 72 h culture.

Figure 34, panel A shows the effect obtained on pancreatic ductal adenocarcinoma Mia Paca 2 cells. A decrease in the volume of spheroids was observed both for cells treated with 20  $\mu\text{g/ml}$  and 40  $\mu\text{g/ml}$  scFv-hERG1-D8Cys, with a more pronounced effect obtained at the highest concentration tested (dash-dot line) compared to controls, at each time point. Images taken after 72 h, reported on the right part of the figure, show a picture of a control spheroid of Mia Paca 2 taken at 4X magnification; while the right image shows a picture of a Mia Paca2 spheroid treated with 40  $\mu\text{g/ml}$  scFv-hERG1-D8Cys, taken at 10X magnification. In fact, it wasn't possible to acquire pictures of control Mia Paca 2 spheroids after 72 h with 10X magnification, as the volume was too enlarged to allow a proper focusing; while Mia Paca 2 spheroids at 72 h treated with scFv-hERG1-D8Cys can be visualized using 10X magnification, as their volume, compared to control, was strongly reduced.

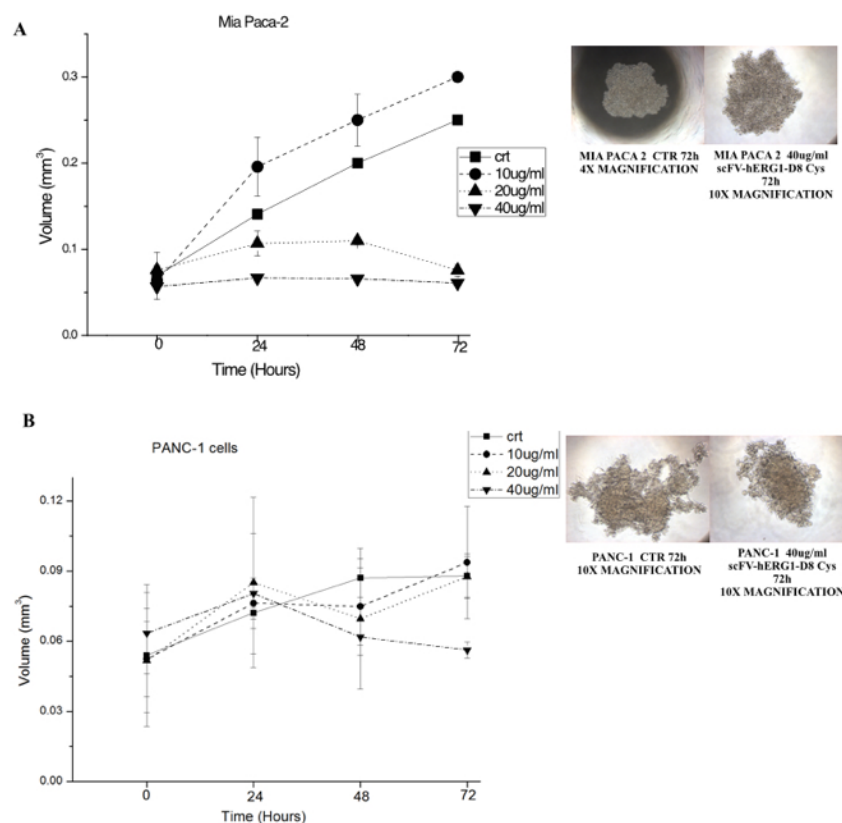


Fig. 34 Pancreatic ductal adenocarcinoma spheroids. Panel A shows the effect obtained on pancreatic ductal adenocarcinoma Mia Paca 2 cells. A decrease in the volume of spheroids was observed both for cells treated with 20  $\mu\text{g/ml}$  and 40  $\mu\text{g/ml}$  scFv-hERG1-D8Cys, with a more pronounced effect obtained at the highest concentration tested (dash-dotted line) compared to the controls, at each time point. A similar effect was observed for PANC-1 spheroids (panel B) with a decrease in the spheroids volume at the highest concentration of the scFv- hERG1-D8Cys antibody tested (see dash-dotted line). Also, pictures taken after 72 h, reported on the right side of the panel, show a substantial decrease in the spheroid volume.

A similar effect was observed for PANC-1 spheroids (Fig.34, panel B) with a decrease in the spheroids volume, compared to the control, after 72 h treatment at the highest concentration of the scFv-hERG1-D8Cys antibody tested (dashed-dot line).

Also, pictures taken after 72 h, reported on the right side of the panel, show a substantial decrease in the spheroid volume for cells treated with the highest concentration of the antibody, compared to the control (see left image).

Fig. 35 shows MDA-MB 231 spheroids: a marked effect of volume reduction is observed for all the three concentrations of scFv-hERG1-D8Cys tested (10, 20, 40  $\mu\text{g}/\text{ml}$ ) compared to the control. Volume reduction can be inferred also from the pictures of MDA-MB 231 spheroids reported on the right side of the figure.

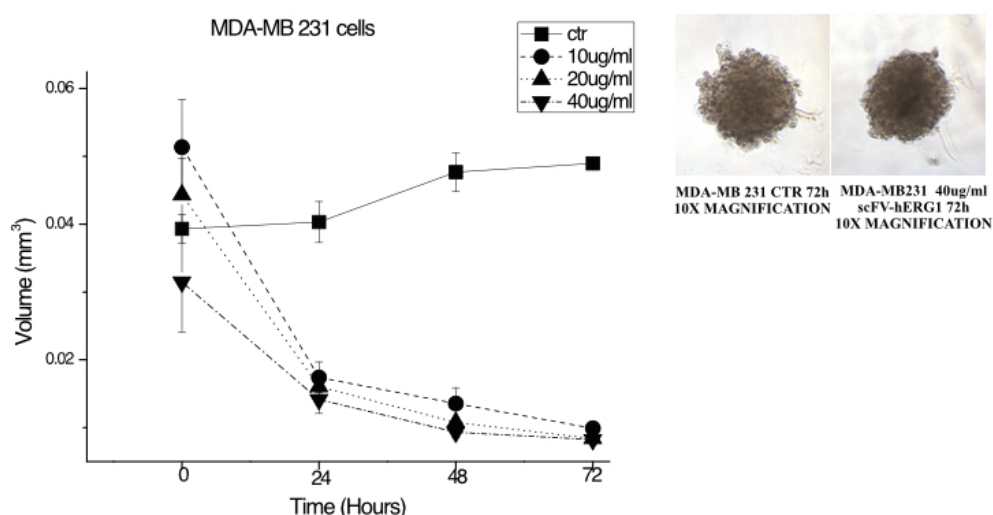


Fig. 35 MDA-MB 231, breast cancer cell spheroids: a marked effect of volume reduction is observed for all the three concentrations of scFv-hERG1-D8Cys tested, compared to the control. Volume reduction can be inferred also from the pictures of MDA-MB 231 spheroids reported on the right side of the figure.

Fig. 36 show the results obtained from the Calcein AM cell viability assay performed on spheroids after 72 h treatment. Green staining represent live cells, while red staining represents dead cells. On the left side of all panels are reported images of controls for each cell line are shown, while on the right side there are images of spheroids treated with 40  $\mu\text{g}/\text{ml}$  scFv-hERG1-D8Cys. It is possible to note a volume reduction for spheroids treated with the antibody, especially for Mia Paca 2, MDA MB-231 and PANC-1 spheroids. Moreover, an increased number of dead cells, especially for MDA MB-231 and PANC-1 spheroids treated with scFv-hERG1-D8Cys is observed.

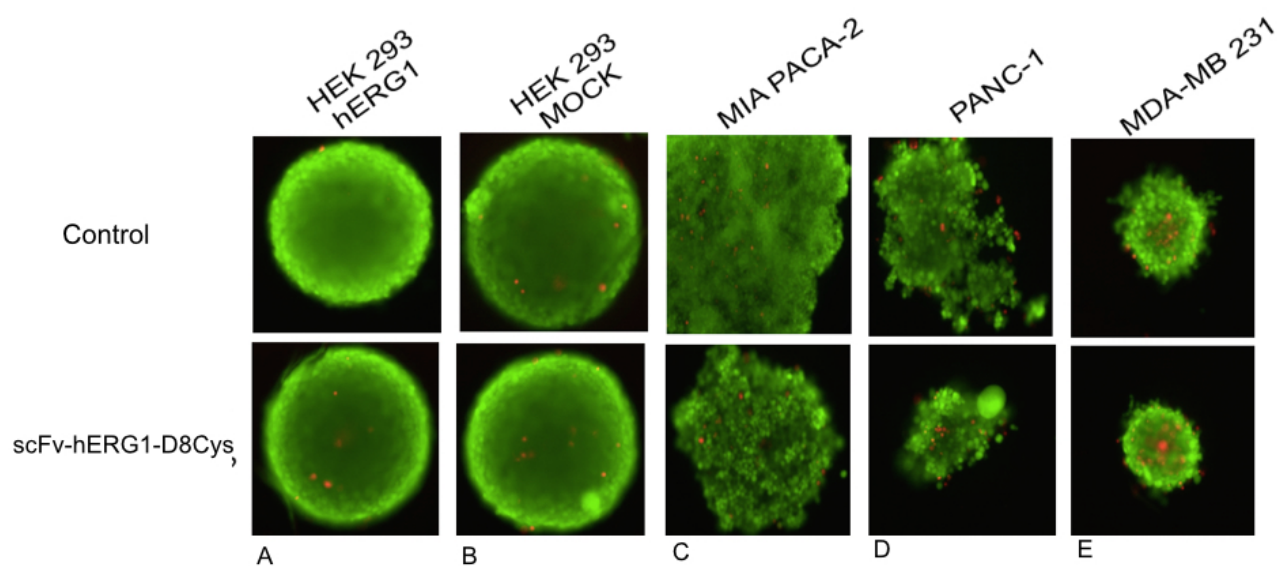


Fig. 36 Calcein AM cell viability assay performed on spheroids after 72 h. Green staining represent live cells, while red staining represent dead cells. Image on the upper panels are pictures of the control for each cell line, while on the lower side there are pictures of spheroids treated with 40  $\mu\text{g/ml}$  scFv-hERG1-D8Cys. From the image it is possible to note the volume reduction for spheroids treated with the antibody, especially for Mia Paca 2, MDA MB-231 and PANC-1 spheroids and, moreover, an increased number of dead cells, especially for MDA MB-231 and PANC-1 spheroids treated with scFv-hERG1-D8Cys.

### 4.3 Production and characterization of hERG1- $\beta$ 1 BISPECIFIC Single Chain Diabody (scDb)

#### 4.3.1 anti-hERG1- $\beta$ 1-scDb antibody production

The construct for the expression of a bispecific antibody composed of the variable domains (VH and VL) of two antibodies, hERG1 mAb (which binds the extracellular domain S5-P of hERG1) and of  $\beta$ 1 integrin mAb TS2/16 (which binds the extracellular domain of  $\beta$ 1 integrin), has been previously assembled in our laboratory by Dr. Silvia Crescioli. In Fig. 37, a schematization of hERG1- $\beta$ 1-scDb is given, showing the variable domains of the anti-hERG1 mAb and the  $\beta$ 1 integrin mAb TS2/16 assembly.

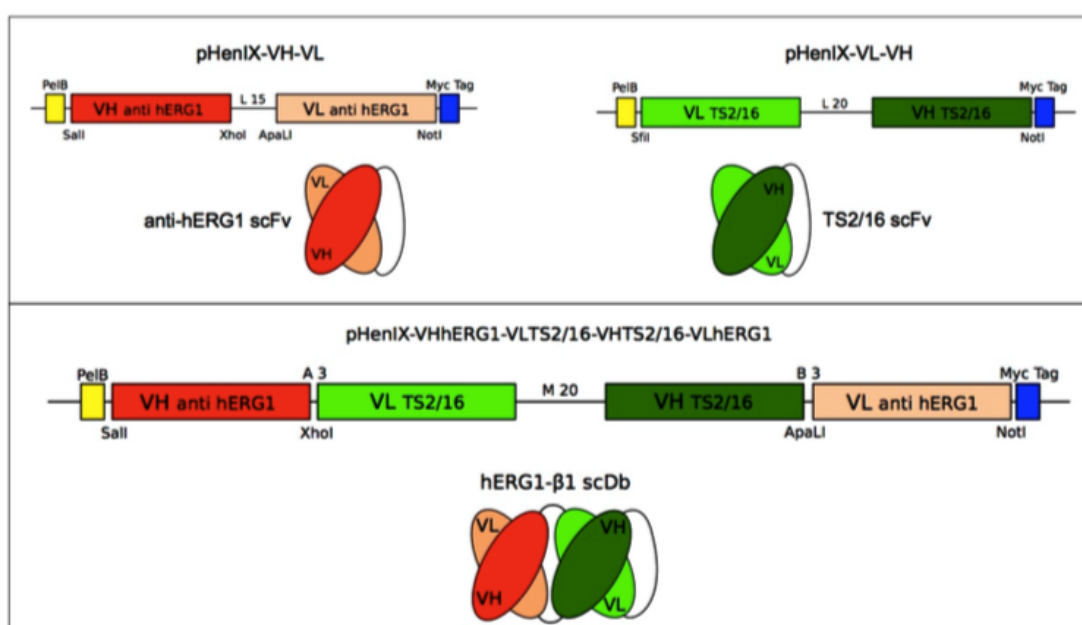


Fig. 37 Schematic representation of anti-hERG1- $\beta$ 1-scDb antibody (Crescioli S., PhD Thesis, 2014)

The construct expressing anti-hERG1- $\beta$ 1-scDb antibody has been cloned into pPIC9K expression vector, which is a vector suitable for expression in *Pichia pastoris* yeast cells.

GS115 *Pichia pastoris* strain was transformed, according to the spheroplasting protocol and 96 clones were screened on YPD-agar plates containing G418 for selection. Six clones were then induced on a small scale and purified using Sepharose Ni beads (GE Healthcare), exploiting the Histidine tag introduced with the pPIC9K vector. Coomassie staining is reported in Fig. 38, panel A, and it shows one band, highlighted by the arrow,

with a molecular weight (around 60 KDa) consistent with the one expected for the anti-hERG1- $\beta$ 1-scDb antibody, corresponding to clone G5.

We have then started large-scale expression of the G5 anti-hERG1- $\beta$ 1-scDb clone, adapting the induction protocol for bigger culture volumes.

Supernatant resulting from 1L *Pichia pastoris* cells culture has been purified using AKTA Pure (GE Healthcare). Results are reported in Fig.38, in which is shown both the chromatogram resulting from the antibody purification (panel B), as well as the Coomassie staining (panel C) in which elutions underlying the blue area have been analyzed. Consistently with what expected a single band, corresponding to the purified anti-hERG1- $\beta$ 1-scDb has been detected for each elution.

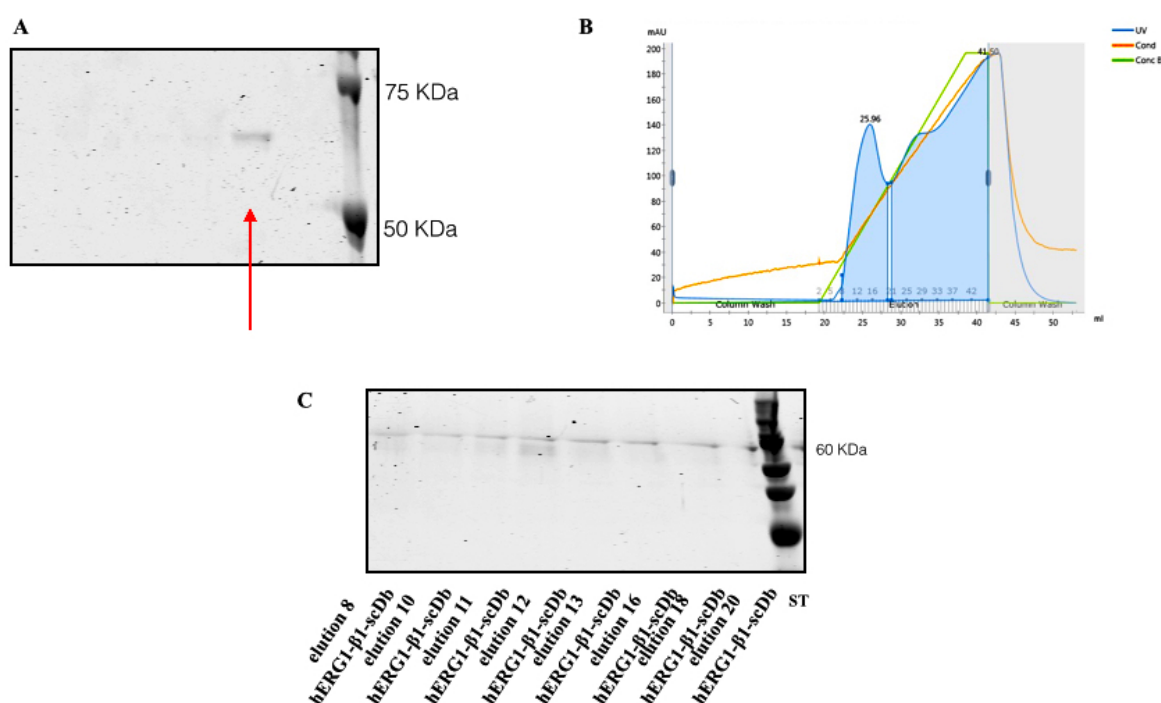


Fig. 38 Panel A shows Coomassie staining of purified supernatants deriving from small scale induction of six clones grown after transformation with anti-hERG1- $\beta$ 1-scDb construct. One band is detectable corresponding to clone G5 with a molecular weight around 60 KDa, consistent with the one expected.

Panel B shows chromatogram generated after purification of supernatant deriving from high- scale expression of G5 clone: one single peak is visible and elutions underlying the blue area have been analyzed and Coomassie staining is reported in panel C, showing bands with proper molecular weight in all the elutions tested.

Anti-hERG1- $\beta$ 1-scDb fractions 8; 9; 10; 11; 12; 13; 14; 15; 16; 18; 20 were gathered together, and dialyzed against PBS 1X. Thus, a detailed characterization of the antibody was started.

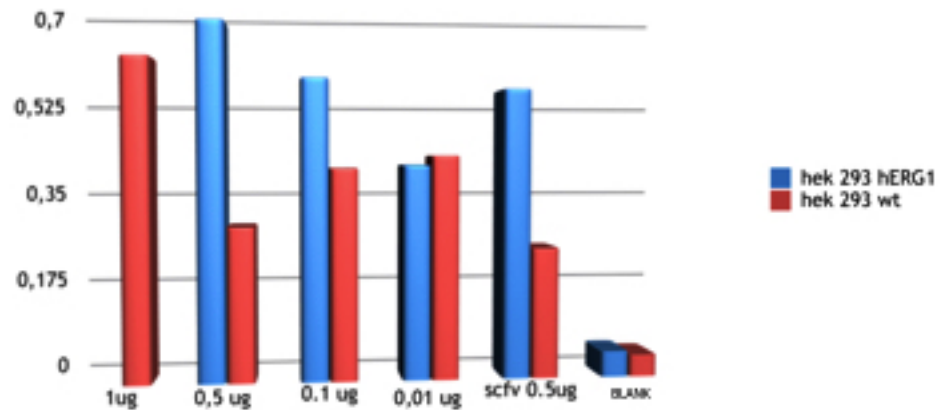
One of the crucial steps was the choice of a proper model to test the anti-hERG1- $\beta$ 1-scDb antibody. The table below summarizes the expression profile related to hERG1 and  $\beta$ 1 integrin of the cell lines, chosen for characterization experiments.

	hERG1 EXPRESSION	$\beta$ 1 integrin EXPRESSION
HEK 293 hERG1	+	+
HEK 293 WILD TYPE	-	+
GD25	-	-

Table 4. HEK 293 hERG1, HEK 293 WT and GD25 expression profile related to hERG1 and  $\beta$ 1 integrin

Bispecific antibody was first analyzed on HEK 293 hERG1 cells which express both hERG1 and  $\beta$ 1 antigens and on cells HEK 293 WILD TYPE cells, which only express  $\beta$ 1 antigen and lack of hERG1 expression. Cell-ELISA was performed and results are reported on Fig. 39, panel A, cell-ELISA showed a certain dose-dependent proportionality for the binding with the native antigen, with higher OD<sub>450</sub>, for cells expressing both hERG1 and  $\beta$ 1 antigens, as expected.

A



B

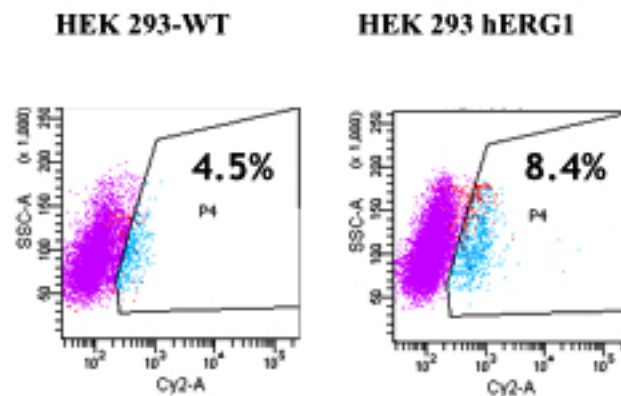


Fig.39 Panel A. Results from cell-ELISA performed on HEK 293 HERG1 and HEK 293 WT cells, using different amounts of anti-hERG1-β1-scDb bispecific antibody. Panel B. FACS analysis on HEK 293 HERG1 and HEK 293 MOCK cells stained using anti-hERG1-β1-scDb.

Moreover, the anti-hERG1-β1-scDb bispecific antibody showed the capacity to bind the antigen in native conditions, as it is for the antigen endogenously expressed by cells. Binding specificity of anti-hERG1-β1-scDb bispecific antibody is also corroborated by the comparison, reported in Fig.39 panel A, between the same amount (0,5μg) of anti-hERG1-β1-scDb and anti-scFv-hERG1-G3, which is one of the two single-chain antibodies that form the bispecific antibody. In fact, the signal obtained after incubating with anti-hERG1-β1-scDb is higher than the one obtained using anti-scFv-hERG1-G3. Such result is in line with what expected, since the signal obtained with anti-hERG1-β1-scDb results from the binding to both antigens, hERG1 and β1; while the signal obtained using scFv-hERG1 results from the binding to hERG1 antigen, only.

In parallel, FACS characterization has been started and results are reported in Fig.39, panel B, specific staining is evident in both cell lines but with a lower extent in HEK 293 WT cells.

We have also performed indirect IF using anti-hERG1- $\beta$ 1-scDb bispecific antibody on HEK 293 hERG1 cells: control cells, treated only with secondary antibodies, anti-Histidine and anti-mouse-Alexa488, clearly show no background signal (Fig.40, panels A and D). Cells HEK 293 hERG1, that express both hERG1 and  $\beta$ 1, have a strong

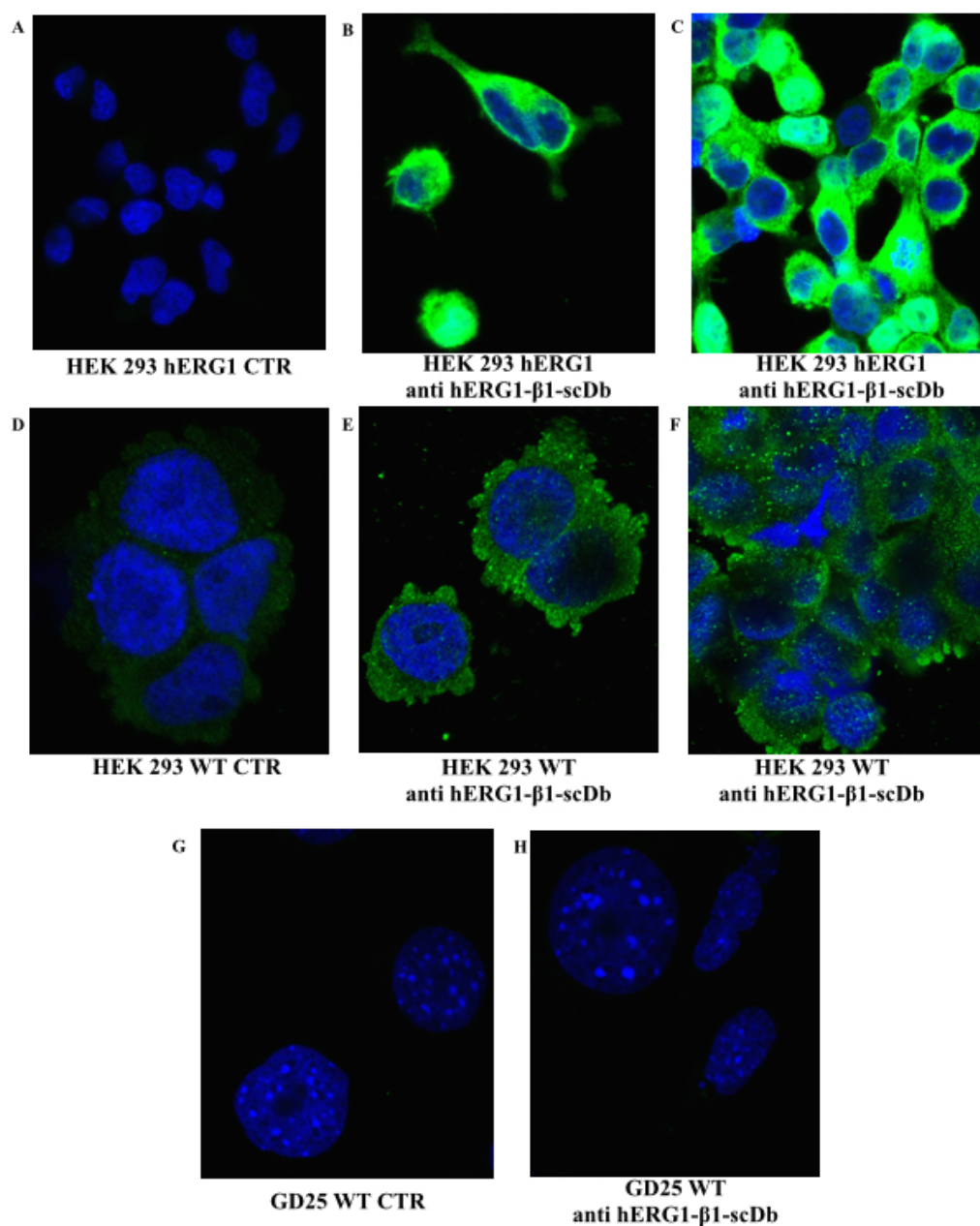


Fig. 40 Indirect IF on HEK 293 hERG1, HEK 293 WT and GD25 WT cells incubated with anti-hERG1- $\beta$ 1-scDb

membranous staining (Fig.40, panels B and C), which is more pronounced if compared to that obtained using anti-hERG1- $\beta$ 1-scDb on HEK 293 WT (hERG1 +;  $\beta$ 1 -) (Fig.40, panels E and F). Panels G and H show negative signal obtained after incubation with anti-hERG1- $\beta$ 1-scDb, such result is consistent with what expected, as GD25 WT cells lack both of the expression of hERG1 and  $\beta$ 1 integrin.

Furthermore, we have evaluated anti-hERG1- $\beta$ 1-scDb staining on cells grown on BSA (Fig. 41 ,panel A and B) and fibronectin (FN) substrates (Fig. 41, panel C and D). In fact, it has been shown that  $\beta$ 1 complex formation is enhanced by FN-dependent integrin activation. As it can be seen from Fig 41, panels C and D, we have a strong membranous signal in cells HEK293-hERG1 seeded on Fibronectin, due to a strict complex formation. The signal has been analyzed using ImageJ software and results are reported in the graph.

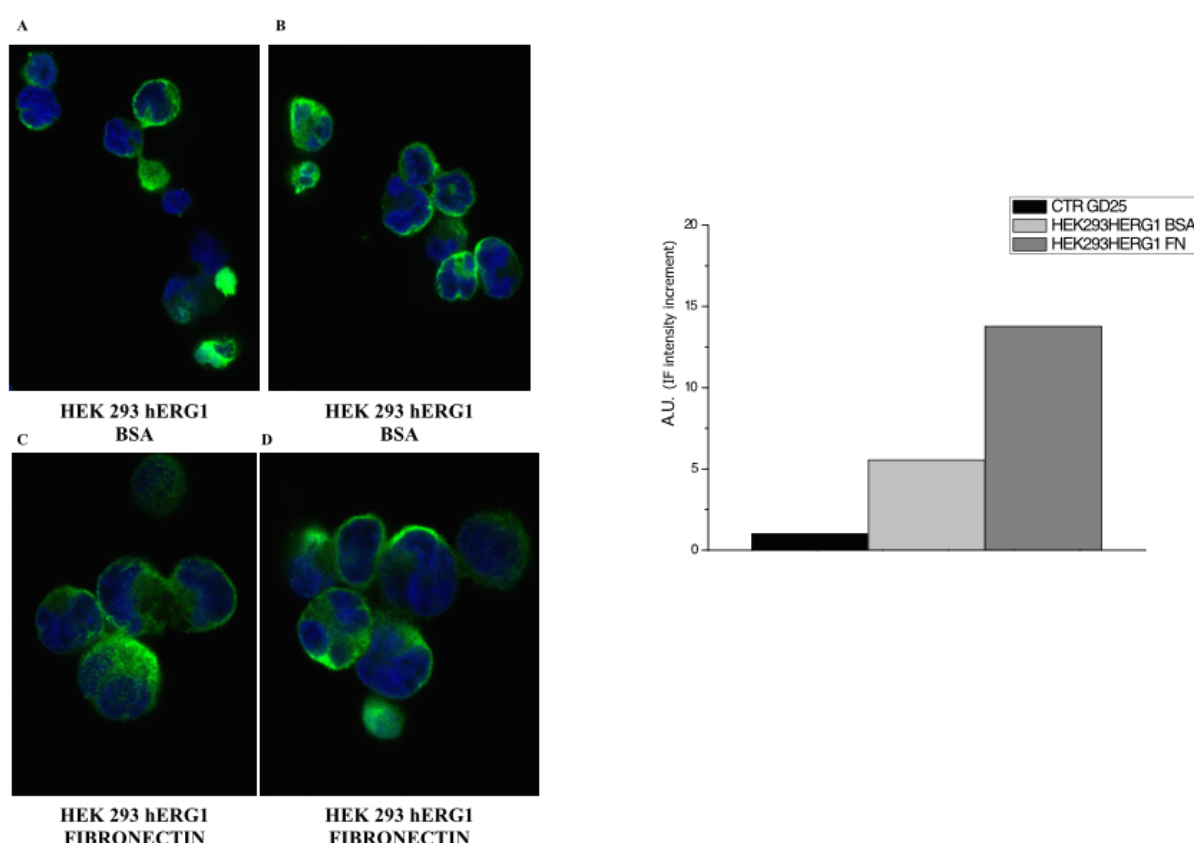


Fig. 41. Indirect IF performed on cells seeded on different substrates, BSA and Fibronectin (FB). IF shows a stronger signal for cells HEK 293 HERG1 coated on FB compared to that obtained for cells coated on BSA.

To further confirm the evidences obtained from previous experiments, we have evaluated the binding of anti-hERG1- $\beta$ 1-scDb, on HEK293-hERG1 cells administering, before antibody incubation, an excess of peptide S5PORO, which is the peptide towards which the scFv-hERG1 antibody is directed. As it can be inferred from Fig. 42, panels A and B, the signal on HEK293-hERG1 cells incubated with anti-hERG1- $\beta$ 1-scDb, due to the binding both to hERG1 and to  $\beta$ 1 integrin, is confirmed. Panel C shows the negative control, while panels D and E show the results obtained after incubation with S5PORO peptide; it is clearly visible that there is a reduction in the signal which is consistent with what we expected. In fact, HEK293-hERG1 cells that are positive for both antigens, after incubation with the peptide show a reduction in staining intensity probably due to the saturation of the antigen binding sites; thus the signal that is visible is the one originated only from the binding to  $\beta$ 1 antigen. Such results are summarized in the graph obtained after ImageJ fluorescence intensity quantification.

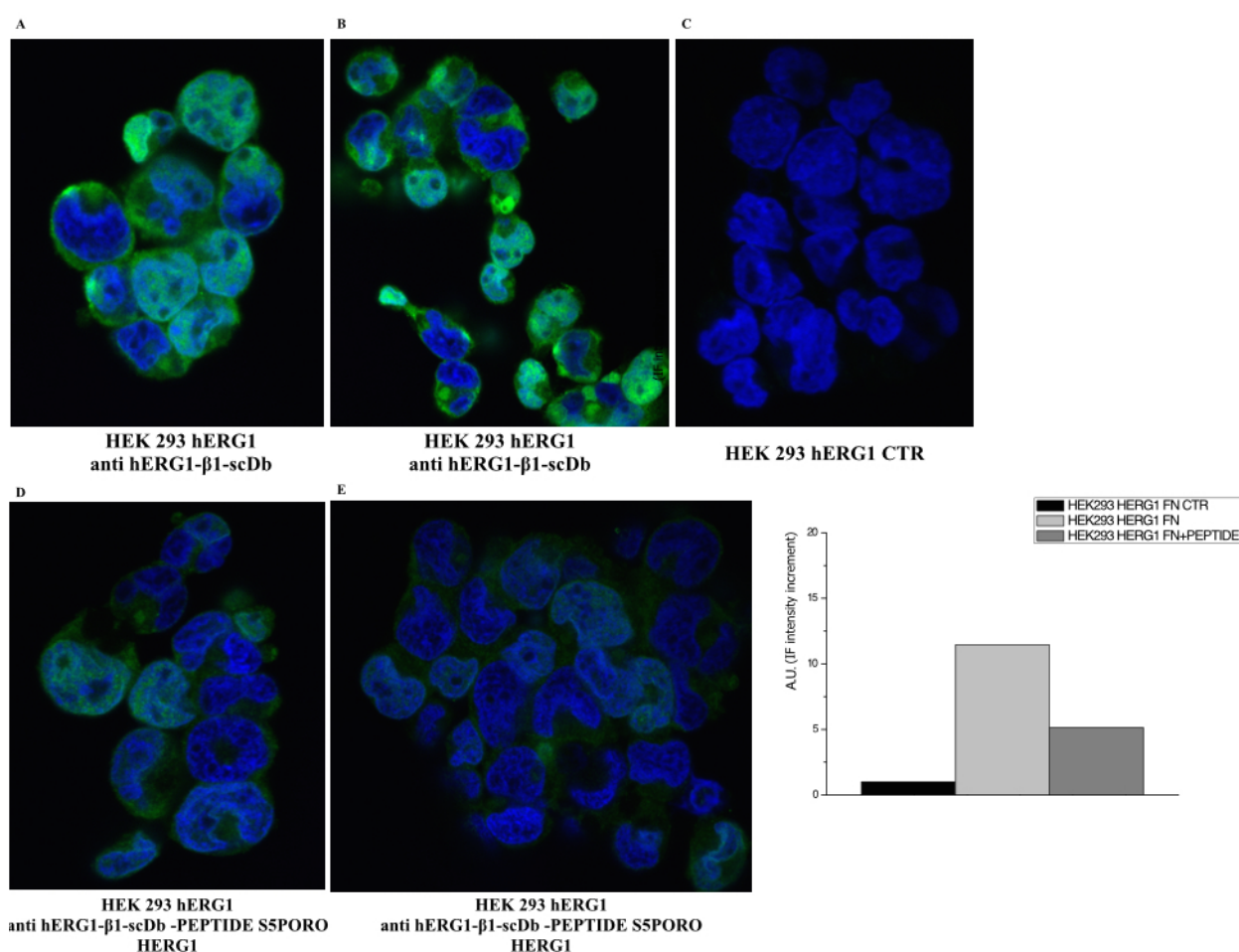


Fig 42 Indirect IF performed on HEK 293 HERG1 cells (panels A and B). Staining of cells after administering of an excess of S5PORO peptide is shown in panels D and E. Panel C reports control cells stained only with secondary antibodies.

## 5. Discussion

### 5.1 Anti- iGluR4 monoclonal antibody development.

In the first part of the work present we have produced two monoclonal antibody populations, B5 and C4, directed against an extracellular epitope of ionotropic Glutamate Receptor 4 (iGluR4).

We have deeply characterized both clones for their capacity to recognize the antigen in native conditions and the data obtained from ICC suggest that the staining is specific for the binding of the anti-iGluR4 antibody; as demonstrated by images of negative control cells shown in Fig. 12, panels G and H, that have confirmed to be strongly negative for the antigen binding.

B5 and C4 iGluR4 antibody supernatants were also tested in immunohistochemistry on slides derived from patients affected by tuberous sclerosis complex (TSC). We have chosen TSC, as a model, because of the central role played by the expression and function of iGluRs in triggering some of the severe symptoms that characterize this pathology. In fact, TSC is associated with inactivating mutations of either TSC1 and TSC2 genes (van Slegtenhorst M *et al.*, 1997). TSC brain lesions are characterized by malformation of cortical development that include cortical tubers, white matter abnormalities, subependymal nodules and subependymal giant cell tumors (Di Mario *et al.*, 2004).

Seizures are one of the symptoms manifested by 70 to 95% of patients very early during childhood (Curatolo P. *et al.*, 2002). Pathogenesis of TSC-related neurological symptoms remains unclear, but iGluRs critically regulate neuronal excitability. Moreover, it has been demonstrated that a higher expression, in particular of iGluR4, is observed in tubers compared to control cortex. iGluR4 has been found to be overexpressed in giant cells, dysplastic astroglia and reactive astrocytes. Results obtained from the IHC staining are consistent with the specific immunocytological profile concerning AMPA-type glutamate receptor expression as we have described above and was reviewed by Talos MD and colleagues (Talos MD *et al.*, 2008).

Moreover, interesting results have emerged from the electrophysiological studies performed using C4 anti-iGluR4, that have demonstrated it acts as a positive allosteric modulator of the iGluR4, in the presence of glutamate.

Taken together, these data should be considered in the light of recent findings about the important role of AMPA-type Glutamate Receptors in cancer. In fact, changes in the levels of expression of complete ionotropic glutamate receptors or receptor subunits were demonstrated to be important for cancer cells proliferation and invasion, thus suggesting the involvement of iGluRs in cancer progression (Stepulak A. *et al.*, 2014). In particular, gene silencing of GluR4 modulated the mRNA expression of various tumor-suppressor genes, oncogenes and other genes involved in invasion, adhesion and metastatic capabilities, resulting in significant increase of cell viability of human rhabdomyosarcoma/medulloblastoma (TE671) and human multiple myeloma RPMI8226 cells. Additionally, silencing of GluR4 stimulated migration of TE671 cells (Luksch *et al.* 2011). In this scenario, it will be crucial to pursue the characterization of anti-iGluR4 monoclonal antibody clones, as their characteristics might be exploited both as diagnostic tools and as channel modulators, perhaps affecting also cancer cell behavior.

Furthermore, the production of a single chain antibody, scFv-iGluR4, stages an important step to tackle problems related to the passage of the blood-brain barrier (BBB), combining the smaller size of the antibody with high antigen specificity. In fact, we have already synthesized PLGA-PEG Rhodamine B-G7 nanoparticles (NPs), which have demonstrated to be able to cross an *in vitro* model of BBB. Functionalization of NPs with scFv-iGluR4 will enhance the system with antigen specificity. Moreover, nanoparticles have the advantage of being able to encapsulate a high dose of cytotoxic drug, thereby reducing systemic exposure and associated side effects, while antibody targeting provides a mechanism to deliver these drugs specifically to the desired site-of-action via endocytosis into the cell cytosol (Mahler S. *et al.*, 2014)

On the whole, these data give evidence that monoclonal anti-iGluR4 B5 and C4 antibodies could be exploited as diagnostic tools and scFv-iGluR4 conjugated with NPs will represent a valid *drug-delivery* system.

## 5.2 Production and characterization of anti scFv-hERG1 antibodies

The role of hERG1 in biological processes involved in cancer development and progression has been extensively explored and more recently an interest has emerged in by its possible exploitation as a novel molecular diagnostic marker and as a therapeutic target in cancer (Gasparoli L. *et al.*, 2015; Pointer KB *et al.*, 2016).

We have given evidence that scFv-hERG1-G3 could be used as a molecular tool for optical *in vivo* imaging for the stratification of patients with high risk to develop from BE (Barrett's esophagus) gastric lesions to gastric ADK (adenocarcinoma) (Lastraioli *et al.*, 2016). The good concordance between IF and IHC (performed with anti-hERG1 mAb), shown in Fig. 23, panel C and D, allow us to propose the use of scFv-hERG1-G3-Alexa488 as a novel tool for optical *in vivo* imaging. After proper testing for safety, the antibody might be used in the future within one of the novel targeted-imaging techniques (Bennett M. *et al.*, 2014). In fact, it has already been reported by Sturm and colleagues that a fluorescently-labelled peptide can be safely administered to patients and revealed by confocal endomicroscopy to successfully identify esophageal dysplasia and esophageal adenocarcinoma. In accordance, the *in vivo* use of scFv-hERG1-G3 has several positive benefits with respect to the use of anti-hERG1 mAb, mainly due to its small size (25-30 kDa), that allows it to penetrate solid tumor mass effectively. Moreover, scFvs are ideal also vectors for the delivery of agents such as radionuclides, enzymes, drugs or toxins *in vivo* (Clark M. *et al.*, 2000; Kim DJ *et al.*, 2002; Xu MY *et al.*, 2004). Moreover, it is worth noting that scFv-hERG1-G3 epitope is located on the extracellular side therefore permeabilization is not required. Overall, these data open new perspectives for the surveillance of BE patients by the *in vivo* use of scFv-hERG1-G3-Alexa488 during standard endoscopy procedures. These results might be transferred to the clinical settings for a new protocol for endoscopic surveillance through the direct, endoscopic detection of hERG1-positive and hERG1-negative BE patients, using the scFv-hERG1-G3-Alexa488.

Given the relevant possible translational applications of the scFv tool; in the present study, we have characterized in detail some attractive features of the scFv-hERG1-G3 molecule. Regarding the structural features, scFv-hERG1-G3 has one tyrosine residue in CDR-H3, which is an important amino acid, creating interactions at the protein-

protein interfaces and has a dominant role in antigen recognition (Koide and Sidhu, 2009).

The CDR-H3 of scFv-hERG-G3 has also two glycine that together represent 37,5% of the amino acid residues in this loop. Moreover, the CDRH3 of scFv-hERG1-G3 is rich in small residues which make it conformationally flexible (Birtalan et al., 2008; Mian et al., 1991). Two serine residues are observed in the CDR-L1 region and these are normally common within tight turns of proteins allowing for flexible movement and binding in the antigen pocket. Tyrosine, in combination with glycine and serine residues have been shown to mediate high affinity antigen recognition (Birtalan, Zhang et al. 2008) and the sequenced scFv-hERG1 fragments possess an abundant level of these residues.

Interestingly, the peculiar presence of a phenylalanine in a position that is usually occupied by one of the two cysteines amino acid, fundamental for the disulfide bond formation, has been previously found only once (Probka et al, 1997; Rudikoff & Pumphrey, 1986). We therefore also made another antibody construct, designated scFv-hERG1-Cys, in which the Cys was restored (patent in preparation).

Regarding the biological properties, both proteins scFv-hERG1-G3 and scFv-hERG1-D8Cys showed to be functional and to maintain the capacity to bind the antigen, as demonstrated in ELISA assay. We could speculate that the maintained capacity to recognize the antigen by both antibodies could be due to the fact that the cysteine has been replaced by a phenylalanine which exhibits a strongly hydrophobic and bulky benzyl side chain, thus maintaining the hydrophobic core formation. In fact, it has been proposed that in domains lacking of the disulfide bridges, cysteine is often replaced by a strong hydrophobic residue, such as phenylalanine, allowing the ability of the protein to accommodate the absence of the cysteine, while maintaining its fold (Halaby D.M. *et al.*, 1999).

Nevertheless, the yield was strongly affected by the reintroduction of the Cys amino acid.

As it has been proposed by Chowdhury S.P. and colleagues (1998), the five-fold improvement of yield of proteins could be due to the improvement in the folding and stability of the mutated scFv forms (Chowdhury Partha S. *et al.*, 1998). These findings could hold true for the scFv-hERG1-D8Cys antibody. Moreover, differences between

the two antibodies have been found also regarding in the binding characteristic obtained from Biacore analysis. In fact, during Surface Plasmon Resonance (SPR), to compare the results obtained from injecting different samples, two kinds of reference points can be considered: the *binding* values that indicate the maximum interaction signal that is revealed at the end of the injection or the *stability* values that indicate the signal registered 20 seconds after the end of the injection.

Binding values were better for scFv-hERG1-D8Cys, resulting in a higher affinity for the antigen (with a lower KD compared to the scFv-hERG1-G3) with a 1.5 fold increase in the affinity.

Such results are in line with what we have shown about the binding with the native antigen in IF both on fixed and live cells; also direct conjugation with the fluorophore Alexa-488 did not affect the capacity of antigen binding, as demonstrated both in IF on fixed cells and in IF on live cells.

The concordance shown between the IF data on fixed and live cells reinforce the evidence already given in our previously published paper (Lastraioli *et al.*, 2016).

Moreover, in this study we have moved further in the characterization of the mutagenized form of the antibody, scFv-hERG1-D8Cys, the latter we have given evidence to maintain the specificity for the antigen with a substantial increase in protein yield.

The data obtained regarding cell viability on cancer cell lines and on 3D spheroid cultures demonstrate that scFv-hERG1-D8Cys has an effect on cell growth, perhaps affecting the proliferation rates, as demonstrated by the results obtained for 3D cultures. Considering the many advantages of employment of scFvs over full-length antibodies, these evidences allow us to propose our scFv, after a proper validation study, as a novel candidate in cancer therapeutics.

### ***5.3 Production and characterization of hERG1- $\beta$ 1 bispecific Single Chain Diabody (scDb)***

The role of hERG1 channel in cancer development is often mediated by its recruitment into plasma membrane functional complexes, in which hERG1 is associated with integrins and growth factor receptors.

It has been demonstrated that hERG1 forms complexes in particular with  $\beta$ 1 subunit of integrin receptors ((Arcangeli A *et al.* 1993), (Hofmann G *et al.* 2001), (Cherubini A *et al.*, 2005), (Pillozzi S *et al.*, 2007), (Pillozzi S *et al.*, 2011), (Crociani O *et al.*, 2013)).

In acute lymphoblastic leukaemia (ALL) hERG1 forms macromolecular complexes with CXCR4 and the  $\beta$ 1 integrin, thus resulting in an activation of extracellular signal-related kinase 1/2 (ERK1/2) and the phosphoinositide 3-kinase (PI3K)/Akt prosurvival signalling pathways (Pillozzi *et al.* 2011). Moreover, in colon adenocarcinoma cell lines, hERG1- $\beta$ 1 integrin complex recruits Focal Adhesion Kinase (FAK) leading to the activation of PI3K and Akt signalling pathways and to activation of Hypoxia Inducible Factor (HIF) with a consequent VEGF-A and other tumor progression genes transcription (Crociani *et al.* 2013). Considering these evidences, the hERG1 and  $\beta$ 1 macromolecular complex can be considered an oncogenic unit. In this scenario, a bispecific antibody able to bind the hERG1- $\beta$ 1 unit, disrupting the complex and preventing downstream signalling, would be a valuable tool. In fact, it is well known that bispecific antibodies could target with strong specificity two different antigens, thus resulting in a better therapeutic efficacy (Grada *et al.*, 2013).

In the present work, we have expressed a bispecific antibody directed against the hERG1- $\beta$ 1 oncogenic unit. We have then characterized the antibody, providing a first body of evidence that the molecule is able to differentially bind hERG1 and  $\beta$ 1 integrin, as it is demonstrated by the results obtained in IF. Such findings are corroborated by those obtained with cells seeded on different substrates (e.g. BSA and Fibronectin). In fact Fibronectin has been demonstrated to enhance complex formation (Crociani O *et al.*, 2013). Other consistent evidences have been provided by the difference of fluorescence intensity that we have obtained also in experiments performed with an excess of S5PORO peptide. Experiments show a proportional decrease of fluorescence

when HEK 293 HERG1 (hERG1 + /  $\beta$ 1+ cells) have been incubated with the peptide, before the staining with the scDb antibody.

Given such promising results, we will pursue the bispecific antibody characterization and the biological effects of the bispecific-scDb will be assessed through hERG1- $\beta$ 1 co-immunoprecipitation and FAK phosphorylation, in HEK293- hERG1 cells treated with hERG1- $\beta$ 1-scDb. Moreover, we want to move from the bispecific antibody to assemble a trifunctional recombinant protein able to target the hERG1- $\beta$ 1 integrin complex and, at the same time, to induce apoptosis through the tumor necrosis factor-related apoptosis-inducing ligand (TRAIL) mediated pathway. We will first produce a recombinant protein composed of our hERG1- $\beta$ 1-scDb N-terminally fused to a single chain TRAIL (scTRAIL). Then the hERG1- $\beta$ 1-scDb-TRAIL antibody will then be tested *in vitro* to evaluate the ability to induce apoptosis (Schneider B. *et al.*, 2010).

## 6. REFERENCES

- Alamae T, Liiv L. Glucose repression of maltase and methanol- oxidizing enzymes in the methylotrophic yeast *Hansenula polymorpha*: isolation and study of regulatory mutants. *Folia Microbiol (Praha)* 1998; 43:443-452.
- Al-Owais, M., K. Bracey and D. Wray. Role of intracellular domains in the function of the hERG potassium channel. *Eur Biophys J*, 2009; 38(5): 569-576.
- Andersen DC, Reilly DE. Production technologies for monoclonal antibodies and their fragments. *Curr Opin Biotechnol*. 2004;15: 456–62.
- Arcangeli A, Rosati B, Cherubini A, Crociani O, Fontana L, Passani B, Wanke E, Olivetto M. Long-term exposure to retinoic acid induces the expression of IRK1 channels in HERG channel-endowed neuroblastoma cells. *Biochem Biophys Res Commun*. 1998; 244(3):706-11.
- Arcangeli, A., O. Crociani, E. Lastraioli, A. Masi, S. Pillozzi and A. Becchetti. Targeting ion channels in cancer: a novel frontier in antineoplastic therapy. *Curr Med Chem*. 2009; 16(1): 66-93.
- Aronica E, Yankaya B, Jansen GH, Leenstra S, van Veelen CW, Gorter JA, Troost D. Ionotropic and metabotropic glutamate receptor protein expression in glioneuronal tumors from patients with intractable epilepsy. *Neuropathol Appl Neurobiol*. 2001; 27:223–237
- Barr, K. A., Hopkins, S. A., and Sreekrishna, K. Protocol for Efficient Secretion of HSA Developed from *Pichia pastoris*. *Pharm. Eng*. 1992; 12, 48-51
- Barrett, D. M., Singh, N., Porter, D. L., Grupp, S. A. & June, C. H. Chimeric antigen receptor therapy for cancer. *Annu. Rev. Med*. 2014; 65, 333–347.
- Bennett M, Mashimo H. Molecular markers and imaging tools to identify malignant potential in Barrett's esophagus. *World J Gastrointest Pathophysiol*. 2014;5:438-449
- Bianchi L, Wible B, Arcangeli A, Taglialatela M, Morra F, Castaldo P, Crociani O, Rosati B, Faravelli L, Olivetto M, Wanke E. hERG encodes a K<sup>+</sup> current highly conserved in tumors of different histogenesis: a selective advantage for cancer cells? *Cancer Res.*; 1998; 58(4):815-22.
- Bird RE, Hardman KD, Jacobsen JW, Johnson S, Kaufman BM, Lee SM, et al. Single-chain antigen-binding proteins. *Science* 1988;242: 426–32.
- Birtalan, S., Y. Zhang, F. A. Fellouse, L. Shao, G. Schaefer and S. S. Sidhu. The intrinsic contributions of tyrosine, serine, glycine and arginine to the affinity and specificity of antibodies. *J Mol Biol*. 2008; 377;1518-1528.

- Bollok M, Resina D, Valero F, Ferrer P. Recent patents on the *Pichia pastoris* expression system: expanding the toolbox for recombinant protein production. *Recent Pat Biotechnol.*; 2009;3(3):192-201.
- Brereton, H.M., Chamberlain, D., Yang, R., Tea, M., McNeil, S., Coster, D.J. and Williams, K.A. Single chain antibody fragments for ocular use produced at high levels in a commercial wheat variety. *J. Biotechnol.* 2007; 129, 539–546.
- Bruenke J, Fischer B, Barbin K, Schreiter K, Wachter Y, Mahr K, et al. A recombinant bispecific single-chain Fv antibody against HLA class II and FcγRIII (CD16) triggers effective lysis of lymphoma cells. *Br J Haematol* 2004;125: 167–79.
- Cavalheiro EA, Olney JW Glutamate antagonists: deadly liaisons with cancer. *Proc Natl Acad Sci USA.* 2001; 98:5947–5948
- Chames P, Baty D. Bispecific antibodies for cancer therapy. *mAbs.* 2009;1(6):539–47.
- Chen HS, Lipton SA. The chemical biology of clinically tolerated NMDA receptor antagonists. *J Neurochem* (2006) 97:1611–1626
- Cherubini, A., Hofmann G, Pillozzi S., Guasti L., Crociani O., Cilia E., Di Stefano P., Degani S., Balzi M., Olivotto M., Wanke E., Becchetti A., Defilippi P., Wymore R., Arcangeli A. Human ether-a-go-go-related gene 1 channels are physically linked to beta1 integrins and modulate adhesion-dependent signalling. *Mol Biol Cell.* 2005; 16: 2972-2983.
- Choi B-K, Bobrowicz P, Davidson RC, Hamilton SR, Kung DH, Li H, Miele RG, Nett JH, Wildt S, Gerngross TU. Use of combinatorial genetic libraries to humanize N-linked glycosylation in the yeast *Pichia pastoris*. *Proc Natl Acad Sci U S A.* 2003; 100:5022-5027.
- Clark M. Antibody humanization: a case of the 'Emperor's new clothes'? *Immunol Today.* 2000; 21: 397-402.
- Couch JA, Yu YJ, Zhang Y, Tarrant JM, Fuji RN, Meilandt WJ, Solanoy H, Tong RK, Hoyte K, Luk W, Lu Y, Gadkar K, Prabhu S, Ordonia BA, Nguyen Q, Lin Y, Lin Z, Balazs M, Scarce-Levie K, Ernst JA, Dennis MS, Watts RJ. Addressing safety liabilities of TfR bispecific antibodies that cross the blood– brain barrier. *Sci Transl Med.* 2013; 5(183):183ra57.
- Cregg JM, Cereghino L, Shi J, Higgins DR. Recombinant protein expression in *Pichia pastoris*. *Mol Biotech.* 2000; 16: 23–52.
- Cregg JM, Madden KR, Barringer KJ, Thill GP, Stillman CA: Functional characterization of the two alcohol oxidase genes from the yeast *Pichia pastoris*. *Mol Cell Biol* 1989; 9:1316-1323.

- Crociani O, Zanieri F, Pillozzi S, Lastraioli E, Stefanini M, Fiore A, Fortunato A, D'Amico M, Masselli M, De Lorenzo E, Gasparoli L, Chiu M, Bussolati O, Becchetti A, Arcangeli A. hERG1 channels modulate integrin signalling to trigger angiogenesis and tumor progression in colorectal cancer. *Scientific Reports*; 2013 3, 3308.
- de Groot J, Sontheimer H. Glutamate and the biology of gliomas. *Glia*. 2011; 59:1181–1189
- De Pourcq K, De Schutter K, Callewaert N. Engineering of glycosylation in yeast and other fungi: current state and perspectives. *Appl Microbiol Biotechnol*. 2010 Aug;87(5): 1617-31.
- Desplancq D, King DJ, Lawson ADG, Mountain A. Multimerization behaviour of single chain Fv variants for the tumor-binding antibody B72.3. *Protein Eng*. 1994; 7: 1027–33.
- Ding, X. W., H. S. Luo, B. Luo, D. Q. Xu and S. Gao. Overexpression of hERG1 in resected esophageal squamous cell carcinomas: a marker. *J Surg Oncol*. 2008; 97(1): 57-62.
- Duranti C., Carraresi L., Crociani O., Iamele L., de Jonge H., Iorio J., Gherardi E., Arcangeli A. Antibody engineering: a mutagenesis tale to investigate structure and expression of scFvs as tools in cancer therapy. PEGS Boston. *The essential protein engineering summit*. 5-9 May 2015
- Ellis LM, Hicklin DJ. VEGF-targeted therapy: mechanisms of anti-tumor activity. *Nat Rev Cancer*. 2008; 8:579-91.
- Ellis SB, Brust PF, Koutz PJ, Waters AF, Harpold MM, Gingeras TR. Isolation of alcohol oxidase and two other methanol regulatable genes from the yeast *Pichia pastoris*. *Mol Cell Biol*. 1985; 5:1111-1121.
- European Chromosome 16 Tuberous Sclerosis Consortium. Identification and characterization of the tuberous sclerosis gene on chromosome 16. *Cell*. 1993;75(7): 1305-15.
- Fan G, Wang Z, Hao M, Li J. Bispecific antibodies and their applications. *J Hematol Oncol*. 2015;8:130.
- Fiske J. L., Fomin V. P., Brown M. L., Duncan R. L., Sikes R. A. Voltage-sensitive ion channels and cancer. *Cancer Metastasis Rev*. 2006; 25(3): 493-500.
- Fournier NM, Lee B, Banasr M, Elsayed M, Duman RS. Vascular endothelial growth factor regulates adult hippocampal cell proliferation through MEK/ERK- and PI3 K/ Akt-dependent signalling. *Neuropharmacology*. 2012; 63:642–652
- Gasparoli L, D'Amico M, Masselli M, Pillozzi S, Caves R, Khuwaileh R, Tiedke W, Mugridge K, Pratesi A, Mitcheson JS, Basso G, Becchetti A, Arcangeli A. New pyrimido-indole compound CD-160130 preferentially inhibits the KV11.1B isoform and produces antileukemic effects without cardiotoxicity. *A.Mol Pharmacol*. 2015;87(2): 183-96

- Gellissen G: Hansenula polymorpha - *Biology and Applications*. 1st edition. Weinheim, Wiley-VCH; 2002 :352.
- Gleeson MA, Sudbery PE. The methylotrophic yeasts. *Yeast* 1988, 4:1-15.
- Goodall S., Jones M. L., Mahler S. Monoclonal antibody-targeted polymeric nanoparticles for cancer therapy – future prospects. *J. Chem. Technol. Biotechnol.* 2015, 90: 1169–1176
- Hackel B, Huang D, Bubolz J, Wang X, Shusta E. Production of soluble and active transferrin receptor-targeting single-chain antibody using *Saccharomyces cerevisiae*. *Pharm. Res.* 2006; 23: 790–7.
- Halaby DM, Poupon A, Mornon J. The immunoglobulin fold family: sequence analysis and 3D structure comparisons. *Protein Eng.* 1999; 12(7):563-71.
- Hamid O, Robert C, Daud A, Hodi FS, Hwu WJ, Kefford R, Wolchok JD, Hersey P, Joseph RW, Weber JS, Dronca R, Gangadhar TC, Patnaik A, Zarour H, Joshua AM, Gergich K, Elassaiss-Schaap J, Algazi A, Mateus C, Boasberg P, Tumeh PC, Chmielowski B, Ebbinghaus SW, Li XN, Kang SP, Ribas A. Safety and tumor responses with lambrolizumab (anti-PD-1) in melanoma. *N Engl J Med.* 2013;369:134-44.
- Hamilton SR, Gerngross TU: Glycosylation engineering in yeast: the advent of fully humanized yeast. *Curr Opin Biotechnol* 2007, 18:387-392.
- Hedley, S. J., Auf der Maur, A., Hohn, S., Escher, D., Barberis, A., Glasgow, J. N., Douglas, J. T., Korokhov, N., Curiel, D. T. An adenovirus vector with a chimeric fiber incorporating stabilized single chain antibody achieves targeted gene delivery. *Gene Ther.* 2006; 13, 88 –94
- Hideyama T, Kwak S When does ALS Start? ADAR2- GluA2 hypothesis for the etiology of sporadic ALS. *Front Mol Neurosci* 2011; 4:33
- Hinoi E, Takarada T, Ueshima T, Tsuchihashi Y, Yoneda Y. Glutamate signalling in peripheral tissues. *Eur J Biochem.* 2004; 271:1–13
- Hodi FS, O'Day SJ, McDermott DF, Weber RW, Sosman JA, Haanen JB, Gonzalez R, Robert C, Schadendorf D, Hassel JC, Akerley W, van den Eertwegh AJ, Lutzky J, Lorigan P, Vaubel JM, Linette GP, Hogg D, Ottensmeier CH, Lebbé C, Peschel C, Quirt I, Clark JI, Wolchok JD, Weber JS, Tian J, Yellin MJ, Nichol GM, Hoos A, Urba WJ. Improved survival with ipilimumab in patients with metastatic melanoma. *N Engl J Med.* 2010; 363:711-23.
- Holliger P, Hudson PJ Engineered antibody fragments and the rise of single domains. *Nat Biotechnol.* 2005; 23: 1126–36.
- Holmes GL, Stafstrom CE. Tuberous sclerosis complex and epilepsy: recent developments and future challenges. *Tuberous Sclerosis Study Group.. Epilepsia.* 2007 ; 48(4):617-30.

- Huston JS, Levinson D, Mudgett-Hunter M, Tai M-S, Novotny J, Margolies MN, Ridge RJ, Brucoleri RE, Haber E, Crea R. Protein engineering of antibody binding sites: recovery of specific activity in an anti-digoxin single-chain Fv analogue produced in *Escherichia coli*. *Proc Natl Acad Sci U S A* 1988;85: 5879–83.
- Ishiuchi S, Tsuzuki K, Yoshida Y, Yamada N, Hagimura N, Okado H, Miwa A, Kurihara H, Nakazato Y, Tamura M, Sasaki T, Ozawa S Blockage of Ca(2+)-permeable AMPA. *Nat Med*. 2002 Sep;8(9):971-8.
- Jain M, Chauhan SC, Singh AP, Venkatraman G, Colcher D, Batra SK. Penetratin improves tumor retention of single-chain antibodies: a novel step toward optimization of radioimmunotherapy of solid tumors. *Cancer Res* 2005;65: 7840–6.
- Johnson MA, Waterham HR, Ksheminska GP, Fayura LR, Cereghino JL, Stasyk OV, Veenhuis M, Kulachkovsky AR, Sibirny AA, Cregg JM: Positive selection of novel peroxisome biogenesis-defective mutants of the yeast *Pichia pastoris*. *Genetics* 1999, 151:1379-1391.
- Kalariti N, Lembessis P, Koutsilieris M Characterization of the glutamatergic system in MG-63 osteoblast-like osteosarcoma cells. (2004) *Anticancer Res* 24:3923–3929
- Kim DJ, Chung JH, Ryu YS, Rhim JH, Kim CW, Suh Y, Chung HK. Production and characterisation of a recombinant scFv reactive with human gastrointestinal carcinomas. *Br J Cancer*. 2002; 87: 405-413.
- Koebel CM, Vermi W, Swann JB, Zerafa N, Rodig SJ, Old LJ, Smyth MJ, Schreiber RD. Adaptive immunity maintains occult cancer in an equilibrium state. *Nature* 2007;450:903-7.
- Koide S, Sidhu SS. The importance of being tyrosine: lessons in molecular recognition from minimalist synthetic binding proteins. *ACS Chem Biol*. 2009;4(5):325-34.
- Kontermann RE. Strategies for extended serum half-life of protein therapeutics. *Curr Opin Biotechnol*. 2011;22(6):868–76.
- Krivoruchko A, Siewers V, Nielsen J. Opportunities for yeast metabolic engineering: Lessons from synthetic biology. *Biotechnol J*. 2011(3):262-76.
- Kunzelmann, K. Ion channels and cancer. *J Membr Biol* , 2005; 205(3): 159-173.
- Kyte J, Doolittle RF. A simple method for displaying the hydropathic character of a protein. *Mol Biol*. 1982;157(1):105-32
- Lansu K. and Gentile S. Potassium channel activation inhibits proliferation of breast cancer cells by activating a senescence program. *Cell Death & Disease*, 2013; vol. 4, no. 6, article e652
- Lastraioli E, Guasti L, Crociani O, Polvani S, Hofmann G, Witchel H, Bencini L, Calistri M, Messerini L, Scatizzi M, Moretti R, Wanke E, Olivotto M, Mugnai G, Arcangeli A.; “Herg1 gene and HERG1 protein are overexpressed in colorectal cancers and regulate cell invasion of tumor cells”; *Cancer Res.*; 2004; 64: 606-611

- Lastraioli E, Taddei A, Messerini L, Comin CE, Festini M, Giannelli M, Tomezzoli A, Paglierani M, Mugnai G, De Manzoni G, Bechi P, Arcangeli A. hERG1 channels in human esophagus: evidence for their aberrant expression in the malignant progression of Barrett's esophagus. *J Cell Physiol.* 2006; 209(2):398-404.
- Lastraioli E, Lottini T, Iorio J, Freschi G, Fazi M, Duranti C, Carraresi L, Messerini L, Taddei A, Ringressi MN, Salemme M, Villanacci V, Vindigni C, Tomezzoli A, La Mendola R, Bencivenga M, Compagnoni B, Chiudinelli M, Saragoni L, Manzi I, De Manzoni G, Bechi P, Boni L, Arcangeli A. hERG1 behaves as biomarker of progression to adenocarcinoma in Barrett's esophagus and can be exploited for a novel endoscopic surveillance. *Oncotarget.* 2016; 13;7(37):59535-59547.
- Lastraioli E, Perrone G, Sette A, Fiore A, Crociani O, Manoli S, D'Amico M, Masselli M, Iorio J, Callea M, Borzomati D, Nappo G, Bartolozzi F, Santini D, Bencini L, Farsi M, Boni L, Di Costanzo F, Schwab A, Onetti Muda A, Coppola R, Arcangeli A. hERG1 channels drive tumour malignancy and may serve as prognostic factor in pancreatic ductal adenocarcinoma. *Br J Cancer.* 2015;112(6):1076-87
- Le Gall F, Kipriyanov SM, Moldenhauer G, Little M. Di-, tri- and tetrameric single chain Fv antibody fragments against human CD19: effect of valency on cell binding. *FEBS Lett.* 1999; 453(1-2):164-8.
- Li, M. and Z. G. Xiong. Ion channels as targets for cancer therapy. *Int J Physiol Pathophysiol Pharmacol.* 2011; 3(2): 156-166.
- Liu SJ, Zukin RS. Ca<sup>2+</sup>-permeable AMPA receptors in synaptic plasticity and neuronal death. *Trends Neurosci.* 2007; 30:126-134
- Luksch H, Uckermann O, Stepulak A, Hendruschk S, Marzahn J, Bastian S, Staufner C, Temme A, Ikonomidou C. Silencing of selected glutamate receptor subunits modulates cancer growth. *Anticancer Res.* 2011;31(10):3181-92.
- Lynch SA, Gill RT: Synthetic biology: new strategies for directing design. *Metab. Eng.* 2012; 14:205-211.
- Ma JKC, Drake PMW, Chargelegue D, Obregon P, Prada A. Antibody processing and engineering in plants, and new strategies for vaccine production. *Vaccine* 2005;23: 1814-8.
- Makvandi-Nejad S, McLean M, HIRAMA T, Almquist K, MacKenzie C, Hall J. Transgenic tobacco plants expressing a dimeric single-chain variable fragment (scFv) antibody against Salmonella enterica serotype Paratyphi B. *Transgenic Res.* 2005;14: 785-92.
- Madden DR. The structure and function of glutamate receptor ion channels. *Nat Rev Neurosci.* 2002;3(2):91-101.

- Mao L, Tang Q, Samdani S, Liu Z, Wang JQ. Regulation of MAPK/ERK phosphorylation via ionotropic glutamate receptors in cultured rat striatal neurons. *Eur J Neurosci* 2004; 19:1207–1216
- Martin CD, Rojas G, Mitchell JN, Vincent KJ, Wu J, McCafferty J, Schofield DJ A simple vector system to improve performance and utilisation of recombinant antibodies. *BMC Biotechnol.* 2006;6: 46.
- Masi A, Becchetti A, Restano-Cassulini R, Polvani S, Hofmann G, Buccoliero AM, Paglierani M, Pollo B, Taddei GL, Gallina P, Di Lorenzo N, Franceschetti S, Wanke E, Arcangeli A. hERG1 channels are overexpressed in glioblastoma multiforme and modulate VEGF secretion in glioblastoma cell lines. *Br J Cancer.* 2005;93(7):781-92.
- Mayfield SP, Franklin SE, Lerner RA. Expression and assembly of a fully active antibody in algae. *Proc Natl Acad Sci USA* 2003;100: 438–42.
- Maynard J, Georgiou G. Antibody Engineering. *Annu Rev Biomed Eng.* 2000;2: 339–76.
- McCafferty J, Griffiths AD, Winter G, Chiswell DJ. Phage antibodies: filamentous phage displaying antibody variable domains. *Nature.* 1990;348: 552–4.
- Merk H, Stiege W, Tsumoto K, Kumagai I, Erdmann VA. Cell-free expression of two single-chain monoclonal antibodies against lysozyme: effect of domain arrangement on the expression. *J Biochem.* 1999;125: 328–33.
- Meyer R, Heinemann SH. Characterization of an eag-like potassium channel in human neuroblastoma cells. *J Physiol.* 1998;508 ( Pt 1):49-56.
- Miller KD, Weaver-Feldhaus J, Gray SA, Siegel RW, Feldhaus MJ. Production, purification, and characterization of human scFv antibodies expressed in *Saccharomyces cerevisiae*, *Pichia pastoris*, and *Escherichia coli*. *Protein Expr Purif.* 2005; 42(2):255-67.
- Moore PA, Zhang W, Rainey GJ, Burke S, Li H, Huang L, Gorlatov S, Veri MC, Aggarwal S, Yang Y, Shah K, Jin L, Zhang S, He L, Zhang T, Ciccarone V, Koenig S, Bonvini E, Johnson S. Application of dual affinity retargeting molecules to achieve optimal redirected T-cell killing of B-cell lymphoma. *Blood.* 2011;117(17):4542–51.
- Morais Cabral, J. H., A. Lee, S. L. Cohen, B. T. Chait, M. Li and R. Mackinnon. Crystal structure and functional analysis of the HERG potassium channel N. *Cell* 1998; 95(5): 649-655.
- Natsume A, Wakitani M, Yamane-Ohnuki N, Shoji-Hosaka E, Niwa R, Uchida K, Satoh M, Shitara K. Fucose removal from complex-type oligosaccharide enhances the antibody-dependent cellular cytotoxicity of single-gene-encoded bispecific antibody comprising of two single-chain antibodies linked to the antibody constant region. *J Biochem.* 2006;140: 359–68.
- Oh MC, Kim JM, Safaee M, Kaur G, Sun MZ, Kaur R, Celli A, Mauro TM, Parsa AT Overexpression of calcium-permeable glutamate receptors in glioblastoma derived brain tumor initiating cells. *PLoS One.* 2012; 7(10):e47846. doi:10.1371/ journal.pone.0047846

- Palmer CL, Cotton L, Henley JM The molecular pharmacology and cell biology of alpha-amino-3-hydroxy-5-methyl- 4-isoxazolepropionic acid receptors. *Pharmacol Rev* 2005; 57:253–277
- Pantoliano MW, Bird, Johnson RE, Asel S, Dodd E.D, Wood S.W; Hardman, K. D. *Biochemistry* 1991; 30, 10117–10125
- Papaioannou NE, Beniata OV, Vitsos P, Tsitsilonis O, Samara P. Harnessing the immune system to improve cancer therapy. *Ann Transl Med.* 2016;4(14):261.
- Pardridge WM, Boado RJ. Reengineering biopharmaceuticals for targeted delivery across the blood-brain barrier. *Methods Enzymol.* 2012; 503:269-92.
- Parpinello G, Berardi E, Strabbioli R: A regulatory mutant of *Hansenula polymorpha* exhibiting methanol utilization metabolism and peroxisome proliferation in glucose. *J Bacteriol.* 1998, 180:2958-2967.
- Patnaik A, Kang SP, Rasco D, Papadopoulos KP, Ellassaiss-Schaap J, Beeram M, Drengler R, Chen C, Smith L, Espino G, Gergich K, Delgado L, Daud A, Lindia JA, Li XN, Pierce RH, Yearley JH, Wu D, Laterza O, Lehnert M, Iannone R, Tolcher AW. Phase I study of Pembrolizumab (MK-3475; Anti-PD-1 Monoclonal Antibody) in patients with advanced solid tumors. *Clin Cancer Res.* 2015; 21:4286-93.
- Perkinton MS, Sihra TS, Williams RJ. Ca(2+)-permeable AMPA receptors induce phosphorylation of cAMP response element-binding protein through a phosphatidylinositol 3-kinase- dependent stimulation of the mitogen-activated protein kinase signalling cascade in neurons. *J Neurosci.* 1999; 19:5861–5874
- Petrecca K, Atanasiu R, Akhavan A, Shrier A. N-linked glycosylation sites determine HERG channel surface membrane expression. *The Journal of Physiology.* 1999; 515(1): 41-8.
- Pillozzi S, Brizzi MF, Balzi M, Crociani O, Cherubini A, Guasti L, Bartolozzi B, Becchetti A, Wanke E, Bernabei PA, Olivotto M, Pegoraro L, Arcangeli A. HERG potassium channels are constitutively expressed in primary human acute myeloid leukemias and regulate cell proliferation of normal and leukemic hemopoietic progenitors. *Leukemia.* 2002;16(9):1791-8.
- Platenik J, Kuramoto N, Yoneda Y Molecular mechanisms associated with long-term consolidation of the NMDA signals. *Life Sci.* 2000; 67:335–364
- Pointer KB, Clark PA, Eliceiri KW, Salamat MS, Robertson GA, Kuo JS. Non-torsadogenic human Ether-à-go-go Related Gene (hERG) inhibitors are associated with better survival for high hERG-expressing glioblastoma patients. *Clin Cancer Res.* 2016 15.
- Porter RR. The hydrolysis of rabbit  $\gamma$ -globulin and antibodies with crystalline papain. *Biochem J.* 1959;73: 119–26.
- Prevarskaya N, Skryma R, Shuba Y. Ion channels and the hallmarks of cancer. *Trends Mol Med.* 2010;16(3):107-21.

- Proba K, Honegger A, Plückthun A. A natural antibody missing a cysteine in VH: consequences for thermodynamic stability and folding. *J Mol Biol.* 1997; 17;265(2): 161-72.
- Pujol M, Ramírez NI, Ayala M, Gavilondo JV, Valdés R, Rodríguez M, Brito J, Padilla S, Gómez L, Reyes B, Peral R, Pérez M, Marcelo JL, Milá L, Sánchez RF, Páez R, Cremata JA, Enríquez G, Mendoza O, Ortega M, Borroto C. An integral approach towards a practical application for a plant-made monoclonal antibody in vaccine purification. *Vaccine* 2005; 23: 1833–7.
- Ren F, Li B, Zhang N, Cao M, Dan W, Zhang S. Expression, purification and characterization of anti-BAFF antibody secreted from the yeast *Pichia pastoris*. *Biotechnol Lett.* 2008;30: 1075–80.
- Ribas A, Puzanov I, Dummer R, et al. Pembrolizumab versus investigator-choice chemotherapy for ipilimumab-refractory melanoma (KEYNOTE-002): a randomized, controlled, phase 2 trial. *Lancet Oncol.* 2015;16:908-18.
- Ribeiro MP, Custódio JB, Santos AE. Ionotropic glutamate receptor antagonists and cancer therapy: time to think out of the box? *Cancer Chemother Pharmacol.* 2017 Feb; 79(2):219-225
- Robert C, Thomas L, Bondarenko I, O'Day S, Weber J, Garbe C, Lebbe C, Baurain JF, Testori A, Grob JJ, Davidson N, Richards J, Maio M, Hauschild A, Miller WH Jr, Gascon P, Lotem M, Harmankaya K, Ibrahim R, Francis S, Chen TT, Humphrey R, Hoos A, Wolchok JD.. Ipilimumab plus dacarbazine for previously untreated metastatic melanoma. *N Engl J Med* 2011;364:2517-26.
- Rogawski MA, Donevan SD. AMPA receptors in epilepsy and as targets for antiepileptic drugs. In: AV Delgado-Escueta, WA Wilson, RW Olsen, RJ Porter, eds. *Jasper's basic mechanisms of the epilepsies*. Philadelphia, PA:LippincottWilliams&Wilkins,1999;947–63.
- Rogawski MA. AMPA receptors as a molecular target in epilepsy therapy. *Acta Neurol Scand Suppl.* 2013;(197):9-18.
- Roggenkamp R, Janowicz Z, Stanikowski B, Hollenberg CP: Biosynthesis and regulation of the peroxisomal methanol oxidase from the methylotrophic yeast *Hansenula polymorpha*. *Mol Gen Genet* 1984, 194:489-493.
- Romanos M. Advances in the use of *Pichia pastoris* for high-level gene expression. *Curr Opin Biotechnol* 1995 6: 527–533.
- Roy JB Vantol, E. A. Cowley, J. Blay and P. Linsdell. Pharmacological separation of hEAG and hERG K<sup>+</sup> channel function in the human mammary carcinoma cell line MCF-7 *Oncol Rep.* 2008; 19(6): 1511-1516.
- Rudikoff S, Pumphrey JG. Functional antibody lacking a variable-region disulfide bridge. *Proc Natl Acad Sci U S A.* 1986 Oct;83(20):7875-8.

- Rzeski W, Turski L, Ikonomidou C. Glutamate antagonists limit tumor growth. *Proc Natl Acad Sci USA* 2001; 98:6372–6377
- Sakai Y, Sawai T, Tani Y: Isolation and characterization of a catabolite repression-insensitive mutant of a methanol yeast, *Candida boidinii* A5, producing alcohol oxidase in glucose-containing medium. *Appl Environ Microbiol* 1987, 53:1812-1818.
- Sakai Y, Tani Y. Cloning and sequencing of the alcohol oxidase- encoding gene (AOD1) from the formaldehyde-producing asporogeneous methylotrophic yeast, *Candida boidinii* S2. *Gene* 1992, 114:67-73.
- Sanguinetti, M. C., Jiang C., Curran M. E. Keating M. T. A mechanistic link between an inherited and an acquired cardiac arrhythmia: HERG. *Cell* 1995; 81(2): 299-307.
- Satta A, Mezzanzanica D, Turatti F, Canevari S, Figini M. Redirection of T-cell effector functions for cancer therapy: bispecific antibodies and chimeric antigen receptors. *Future Oncol.* 2013;9(4):527–39.
- Sette A, Crescioli S, Crociani O, Lastraioli E, D'Amico M, Masselli M, Arcangeli A. A new immune-based strategy to target hERG1 potassium channel. PEGS Europe *Protein & Antibody Engineering Summit*, November 6-8 2012, Vienna, Austria
- Sette A, Spadavecchia J, Landoulsi J, Casale S, Haye B, Crociani O, Arcangeli A. Development of novel anti-Kv 11.1 antibody-conjugated PEG-TiO<sub>2</sub> nanoparticles for targeting pancreatic ductal adenocarcinoma cells. *J Nanopart Res.* 2013;15:2111.
- Schneider B, Munkel S, Krippner-Heidenreich A, Grunwald I, Wels WS, Wajant H, Pfizenmaier K, Gerspach J. Potent antitumoral activity of TRAIL through generation of tumor-targeted single-chain fusion proteins. *Cell Death Dis.* 2010 26;1:e68.
- Skerry TM, Genever PG. Glutamate signalling in non-neuronal tissues. *Trends Pharmacol Sci* 2001; 22:174–181
- Spiess C, Zhai Q, Carter PJ. Alternative molecular formats and therapeutic applications for bispecific antibodies. *Mol Immunol.* 2015;67(2):95–106.
- Stanimirovic D, Kemmerich K, Haqqani AS, Farrington GK: Engineering and pharmacology of blood–brain barrier-permeable bispecific antibodies. *Adv Pharmacol.* 2014;71:301-335.
- Stepulak A, Luksch H, Gebhardt C, Uckermann O, Marzahn J, Siffringer M, Rzeski W, Staufner C, Brocke KS, Turski L, Ikonomidou C. Expression of glutamate receptor subunits in human cancers. *Histochem Cell Biol.* 2009; 132:435–445
- Stepulak A, Luksch H, Uckermann O, Siffringer M, Rzeski W, Polberg K, Kupisz K, Klatka J, Kielbus M, Grabarska A, Mar- zahn J, Turski L, Ikonomidou C. Glutamate receptors in laryngeal cancer cells. *Anticancer Res.* 2011;31:565–573
- Stepulak A, Rola R, Polberg K, Ikonomidou. Glutamate and its receptors in cancer. *C.J Neural Transm.* 2014;121(8):933-44.

- Stewart MQ, Esposito RD, Gowani J, Goodman JM: Alcohol oxidase and dihydroxyacetone synthase, the abundant peroxisomal proteins of methylotrophic yeasts, assemble in different cellular compartments. *J Cell Sci* 2001, 114:2863-2868.
- Sturm MB, Joshi BP, Lu S, Piraka C, Khondee S, Elmunzer BJ, Kwon RS, Beer DG, Appelman HD, Turgeon DK, Wang TD. Targeted imaging of esophageal neoplasia with a fluorescently labeled peptide: first-in-human results. *Sci Transl Med.* 2013;5:184ra61.
- Suryadevara CM, Gedeon PC, Sanchez-Perez L, et al. Are BiTEs the “missing link” in cancer therapy? *Oncoimmunology* 2015;4:e1008339.
- Takano T, Lin JH, Arcuino G, Gao Q, Yang J, Nedergaard M. Glutamate release promotes growth of malignant gliomas. *Nat Med.* 2001; 7:1010–1015
- Grada Z, Hegde M, Byrd T, Shaffer DR, Ghazi A, Brawley VS, Corder A, Schönfeld K, Koch J, Dotti G, Heslop HE, Gottschalk S, Wels WS, Baker ML, Ahmed N. TanCAR: A Novel Bispecific Chimeric Antigen Receptor for Cancer Immunotherapy. *Mol Ther Nucleic Acids.* 2013. 9;2:e105.
- Todorovska A, Roovers RC, Dolezal O, Kortt AA, Hoogenboom HR, Hudson PJ. Design and application of diabodies, triabodies and tetrabodies for cancer targeting. *J Immunol Methods.* 2001; 248: 47–66.
- Traynelis, S.F., Wollmuth, L.P., McBain, C.J., Menniti, F.S., Vance, K.M., Ogden, K.K., Hansen, K.B., Yuan, H., Myers, S.J., Dingledine, R. Glutamate receptor ion channels: structure, regulation, and function. *Pharmacol. Rev.* 2010 62, 405e496.
- van Slegtenhorst M, de Hoogt R, Hermans C, et al. Identification of the tuberous sclerosis gene TSC1 on chromosome 9q34. *Science* 1997 ;277:805–808.
- Veenhuis M, van Dijken JP, Harder W. The significance of peroxisomes in the metabolism of one-carbon compounds in yeast. *Adv Microb Physiol* 1983; 24: 1–82.
- Verhaar M. J., Chester K. A., Keep P. A., Robson L., Pedley R. B., Boden J. A, Hawkins RE, Begent RH. A single chain Fv derived from a filamentous phage library has distinct tumor targeting advantages over one derived from a hybridoma. *Int J Cancer*; 1995; 61(4): 497-501.
- Vira S, Mekhedov E, Humphrey G, Blank PS. Fluorescent labeled antibodies - balancing functionality and degree of labeling. *Analytical biochemistry.* 2010;402(2): 146-150.
- Vogl T, Hartner FS, Glieder A. New opportunities by synthetic biology for biopharmaceutical production in *Pichia pastoris*. *Curr Opin Biotechnol.* 2013 ;24(6): 1094-101.
- Wang Z, Raifu M, Howard M, Smith L, Hansen D, Goldsby R, Ratner D. Universal PCR amplification of mouse immunoglobulin gene variable regions: the design of degenerate primers and an assessment of the effect of DNA polymerase 3' to 5' exonuclease activity. *Journal of immunological methods.* 2000;233(1-2):167-77.

- Warmke J. W. and Ganetzky B. A family of potassium channel genes related to eag in *Drosophila* and mammals *Proceedings of the National Academy of Sciences of the United States of America*, 1994 91, no. 8, pp. 3438–3442.
- Watanabe K, Kanno T, Oshima T, Miwa H, Tashiro C, Nishizaki T. The NMDA receptor NR2A subunit regulates proliferation of MKN45 human gastric cancer cells. *Biochem Biophys Res Commun*. 2008; 367:487–490
- Wegner G. Emerging applications of the methylotrophic yeasts. *FEMS Microbiol Rev* 1990; 7: 279–283.
- Weiss JH. Ca permeable AMPA channels in diseases of the nervous system. *Front Mol Neurosci*. 2011; 4:42
- Weisser NE, Hall JC. Applications of single-chain variable fragment antibodies in therapeutics and diagnostics. *Biotechnol Adv*. 2009;27(4):502-20.
- White R, Hua Y, Scheithauer B, Lynch DR, Henske EP, Crino PB. Selective alterations in glutamate and GABA receptor subunit mRNA expression in dysplastic neurons and giant cells of cortical tubers. *Annals of Neurology* 2001; 49:67–78.
- Wright A, Vissel B. The essential role of AMPA receptor GluR2 subunit RNA editing in the normal and diseased brain. *Front Mol Neurosci*. 2012; 5:34
- Xu MY, Xu XH, Chen GZ, Deng XL, Li J, Yu XJ, Chen MZ. Production of a human single-chain variable fragment antibody against esophageal carcinoma. *World J Gastroenterol*. 2004; 10: 2619-2623.
- Ye Z.C., Sontheimer H. Glioma cells release excitotoxic concentrations of glutamate. *Cancer Res*. 1999; 59:4383–4391
- Yoshioka A, Ikegaki N, Williams M, Pleasure D. Expression of N-methyl-D-aspartate (NMDA) and non-NMDA glutamate receptor genes in neuroblastoma, medulloblastoma, and other cells lines. *J Neurosci Res*. 1996; 46:164–178
- Pardridge WM, Boado RJ. Reengineering biopharmaceuticals for targeted delivery across the blood-brain barrier. *Methods Enzymol*. 2012;503:269-92. doi: 10.1016/B978-0-12-396962-0.00011-2. Review.

**Dottorato di Ricerca in  
SCIENZE BIOMEDICHE**

*sede amministrativa:* Dipartimento di  
Scienze Biomediche Sperimentali e Cliniche  
*coordinatore:* Prof. Persio Dello Sbarba

**Dottorato di Ricerca in Scienze Biomediche**  
**(XXIX ciclo e in proroga al XXIX ciclo)**

Presentazione del candidato : Claudia Duranti  
Curriculum: Oncologia Sperimentale e Clinica  
Ciclo: XXIX

Titolo della tesi: Novel molecular tools in cancer therapy: diagnostic and therapeutic applications of antibodies targeting ion channels and receptors

La Dr. Claudia Duranti, nata a Bagno a Ripoli (FI) il 06/07/1988, laureata in Biologia il 24/07/2013, discutendo una tesi dal titolo “Strategie molecolari per l’assemblaggio di vettori lentivirali utilizzabili per la terapia genica di patologie legate ad alterazioni di canali ionici”.  
con la votazione di 110 e lode/110, è stata ammessa, a partire dal 30/11/2013, al Dottorato di Ricerca in Scienze Biomediche *curriculum* Oncologia Sperimentale e Clinica (XXIX° Ciclo), svolgendo la propria attività di ricerca presso il Dipartimento di Medicina Sperimentale e Clinica, sotto il tutoraggio della Prof.ssa Annarosa Arcangeli

**Descrizione dell’attività di ricerca/Risultati ottenuti:**

L’obiettivo principale della ricerca svolta nei tre anni di Dottorato è stato quello di mettere a punto anticorpi monoclonali e frammenti anticorpali (scFv) da applicare nel trattamento e nella stratificazione diagnostica di neoplasie di diversa istogenesi, aventi come target canali ionici e recettori. A tale proposito, mi sono occupata della produzione e caratterizzazione di quattro anticorpi:  
- un anticorpo monoclonale diretto contro il recettore ionotropico del Glutammato di classe 4, iGluR4;  
un anticorpo ingegnerizzato scFv (*single-chain variable fragment*) diretto contro lo stesso recettore, scFv- GluR4;

- un anticorpo ingegnerizzato scFv, diretto contro il canale ionico hERG1 (produzione e caratterizzazione funzionale);
- un anticorpo bifunzionale, diretto contro la proteina hERG1 e l’integrina  $\beta 1$  (produzione e caratterizzazione funzionale);

L’anticorpo monoclonale diretto contro il recettore ionotropico del Glutammato di classe 4 (iGluR4), è stato prodotto e successivamente caratterizzato in immunoistochimica su un modello di TSC (*tuberous sclerosis complex*), patologia autosomica dominante dell’età pediatrica che presenta, tra le principali manifestazioni cliniche, l’insorgenza di focolai epilettici (sintomatologia caratteristica dei tumori ad

alto grado del sistema nervoso centrale) ed una aumentata espressione del recettore ionotropico del glutammato, GluR4. L'anticorpo monoclonale anti-GluR4 ha dimostrato un pattern di marcatura a carico delle cellule caratteristiche dei quadri istopatologici di TSC, nei quali il recettore GluR4 è stato visto essere iperespresso (e.g. giant cells and dysplastic astroglia) (Talós DM *et al.*, 2008). Parallelamente, l'anticorpo monoclonale è stato testato da un punto di vista funzionale su un modello di cellule iperesprimenti il recettore del GluR4 da me messo a punto, valutandone l'effetto sulla vitalità cellulare ed in esperimenti di patch-clamp. Quest'ultimi hanno messo in evidenza effetti dell'anticorpo anti-GluR4 come modulatore allosterico positivo, in presenza di glutammato. Tale effetto è in corso di approfondimento, dal momento che hanno suscitato particolare interesse recenti ricerche legate al ruolo svolto dai recettori ionotropici del glutammato nella patologia neoplastica (Ribeiro MP *et al.*, 2016). Inoltre, a partire dall'anticorpo monoclonale è stato sviluppato un anticorpo scFv, diretto contro lo stesso recettore GluR4, da impiegare nella messa a punto di un sistema di targeting per il superamento della barriera ematoencefalica (BBB).

Il secondo filone di ricerca di cui mi sono occupata, ha riguardato la produzione su larga scala e la caratterizzazione di un frammento anticorpale scFv-hERG1, diretto contro il canale ionico hERG1. hERG1 è altamente espresso a livello delle lesioni di BE (esofago di Barrett) ed inoltre, esso è espresso in displasie ed adenocarcinomi che hanno origine da lesioni di esofago di Barrett progredite. Queste evidenze rafforzano quindi l'ipotesi che il gene *hERG1* marchi uno step precoce della progressione tumorale (Lastraioli *et al.*, 2006). Da qui la necessità di mettere a punto un tool molecolare (scFv-hERG1) potenzialmente applicabile per la stratificazione dei pazienti affetti da esofago di Barrett. A tal proposito, l'anticorpo scFv-hERG1, dopo una caratterizzazione immunohistochimica ed immunocitochimica, nella quale ha dimostrato una buona specificità di marcatura, è stato coniugato con il fluoroforo Alexa488 ed impiegato in uno studio prospettico effettuato su campioni biotipici freschi prelevati durante endoscopia da pazienti positivi per lesioni di BE. La marcatura ottenuta in IF con l'anticorpo scFv-hERG1-Alexa488 è stata confrontata con quella ottenuta in immunohistochimica su sezioni derivanti dagli stessi campioni, utilizzando l'anticorpo monoclonale intero anti-hERG1. La quasi completa concordanza ottenuta tra le due tipologie di analisi effettuate, ci ha permesso di proporre l'anticorpo scFv-hERG1 come un possibile candidato per l'utilizzo in imaging *in vivo* per la stratificazione di pazienti positivi o negativi per l'espressione di hERG1 e quindi con maggiore o minore rischio di progredire da BE ad adenocarcinoma (Lastraioli E. *et al.*, 2016). L'anticorpo scFv-hERG1 è stato ulteriormente caratterizzato dal momento che da un'attenta analisi della sequenza è emersa la presenza nella catena pesante VH di una fenilalanina (Phe) al posto di una cisteina (Cys) in una posizione fondamentale per la formazione dei ponti disolfuro. La Cys è stata quindi reintrodotta con un protocollo di mutagenesi ed il nuovo anticorpo ottenuto è stato espresso e caratterizzato. Sono state confrontate le rese dei due anticorpi, quello wild type e quello mutagenizzato, la capacità di legare l'antigene immobilizzato mediante analisi con SPR (surface plasmon resonance) e di legare l'antigene nativo mediante IF indiretta, diretta su cellule fissate e su cellule vive. In tutti questi saggi, l'anticorpo scFv-hERG1 mutagenizzato ha dimostrato di presentare caratteristiche migliori, sia in termini di resa, che di riconoscimento antigenico, rispetto all'anticorpo in forma wild type. L'anticorpo mutagenizzato è stato quindi testato su un panel di linee cellulari tumorali, mostrando capacità di riduzione della vitalità cellulare, effetto confermato anche su colture 3D di sferoidi in linee iperesprimenti hERG1, Mia Paca-2, PANC-1, HEK293 hERG1 (C.Duranti *et al.*, manoscritto in preparazione) (scFv-hERG1-Cys- Patent application in corso).

La terza parte del lavoro è stata dedicata alla caratterizzazione di un anticorpo bifunzionale diretto contro hERG1 e l'integrina  $\beta 1$ , con potenzialità da un punto di vista terapeutico, dal momento che hERG1 e  $\beta 1$  esplicano il loro ruolo in diversi tipi di tumore attraverso l'associazione a formare complessi di membrana. L'anticorpo è stato testato in cell-ELISA, dimostrando la capacità di legare

l'antigene in maniera dose-dipendente, su cellule HEK 293 WT (hERG1-/  $\beta$ 1+) e su cellule HEK 293-hERG1 (hERG1+/  $\beta$ 1+). La proteina è stata quindi caratterizzata in citofluorimetria sulle stesse cellule, dimostrando un certo grado di marcatura e, successivamente, in IF indiretta, dimostrando una marcatura selettiva, confermata anche da esperimenti condotti su diversi substrati, tra cui BSA e fibronectina, quest'ultima è nota per la sua funzione promotrice nella formazione del complesso tra hERG1 ed integrina  $\beta$ 1 (Crociani O. et al, 2013).

## Pubblicazioni/Presentazione dati a congressi nazionali e internazionali:

### Pubblicazioni/Presentazione dati a congressi nazionali e internazionali:

- hERG1 behaves as biomarker of progression to adenocarcinoma in Barrett's esophagus and can be exploited for a novel endoscopic surveillance. Lastraioli E, Lottini T, Iorio J, Freschi G, Fazi M, Duranti C, Carraresi L, Messerini L, Taddei A, Ringressi MN, Salemme M, Villanacci V, Vindigni C, Tomezzoli A, La Mendola R, Bencivenga M, Compagnoni B, Chiudinelli M, Saragoni L, Manzi I, De Manzoni G, Bechi P, Boni L, Arcangeli A. *Oncotarget*. 2016 Aug 9. doi: 10.18632/oncotarget.11149.
- “TARGETED DRUG DELIVERY TOOLS USING NANOPARTICLES FUNCTIONALIZED WITH ANTIBODIES”, First Annual meeting, DESIRE Project, Development and Epilepsy - Strategies for Innovative Research to improve diagnosis, prevention and treatment in children with difficult to treat Epilepsy, Azienda Ospedaliero – Universitaria Meyer, Firenze. 20/21 Ottobre 2014
- ANTIBODY ENGINEERING: A MUTAGENESIS TALE TO INVESTIGATE STRUCTURE AND EXPRESSION OF scFVs AS TOOLS IN CANCER THERAPY. Duranti C., Carraresi L., Crociani O., Iamele L., de Jonge H., Iorio J., Gherardi E., Arcangeli A.. PEGS Boston The essential protein engineering summit. 5-9 Maggio 2015
- HERG1 POTASSIUM CHANNEL EXPRESSION IN GI PRENEOPLASTIC LESIONS. Iorio J., Lottini T., Lastraioli E., Duranti C., Munezero Butorano MAG, Taddei A., Vindigni C., Messerini L., Tomezzoli A., Saragoni L., Manzi I., Compagnoni B., Mariella C., Fazi M., Freschi G., Boni L., Salemme M., Villanacci V., Bechi P., Arcangeli A.. INCA Meeting- 9-10 Settembre 2015, Londra
- “IN VITRO BBB MODELS AND FUNCTIONALIZED POLYMERIC NANOPARTICLES”, Third Annual meeting, DESIRE Project, Development and Epilepsy - Strategies for Innovative Research to improve diagnosis, prevention and treatment in children with difficult to treat Epilepsy, Marseille-France October 2016
- Vincitrice di una Fellowship per la partecipazione al congresso PEGS- The essential protein engineering summit. Boston 5-9 Maggio 2015. Poster selezionato per la presentazione: “ANTIBODY ENGINEERING: A MUTAGENESIS TALE TO INVESTIGATE STRUCTURE AND EXPRESSION OF scFVs AS TOOLS IN CANCER THERAPY.”

## Soggiorni di ricerca presso altri laboratori:

Febbraio- Marzo 2015 - Attività di ricerca svolta presso il laboratorio di biologia molecolare e cellulare diretto dal Prof. Ermanno Gherardi- Div. Immunology and General Pathology- Dept. Molecular Medicine- Università di Pavia.

## Seminari:

Attività didattica aa. 2014/2015- 2015/2016- 2016/2017

- Conduzione di seminari ed esercitazioni per l'insegnamento di Immunologia e Tecniche Immunologiche (B007166), Corso di laurea Magistrale in Biotecnologie Molecolari (B108), Scuola Scienze Matematiche Fisiche e Naturali (Università degli Studi di Firenze)
- Presentazione I anno di Dottorato, 30/06/2014 *Presentazione del progetto di Dottorato*
- Presentazione II anno di Dottorato, 16/02/2016 *Novel molecular targets in cancer-therapy: diagnostic and therapeutic applications of antibodies targeting ion channels and receptors*

## Seminari e congressi a cui ho partecipato:

- 24/28 Marzo 2014, Summer School, "Basic and translational oncology", Firenze. Summer School EU ITN 289648 IonTraC and Italian-French Erasmus Intensive Course in Oncology.
- 28/31 Maggio 2014, IX Congresso Nazionale della Società Italiana di Immunologia, Immunologia Clinica ed Allergologia (Firenze).
- 1-3 Luglio 2015 "Cancer biology for cancer therapeutics"- Bender Symposium- ITT meeting- CNR Pisa
- 23-24 luglio 2015 "Second In-vitro Alternatives Workshop" 3D cultures workshop; Area del CNR Firenze - Istituto di Fisica Applicata "Nello Carrara" Sesto Fiorentino (FI)
- 29 Marzo-1 Aprile 2016, Summer School, "Basic and translational oncology", Firenze. Summer School EU ITN 289648 IonTraC and Italian- French Erasmus Intensive Course in Oncology.

Firenze, 14/11/2016

firma del Candidato

Durante il corso di dottorato, il candidato ha seguito con il massimo impegno il programma didattico stabilito dal Collegio dei Docenti ed ha portato avanti con entusiasmo e determinazione le sue ricerche, dando prova di grande inventiva ed intraprendenza, nonché di notevole elasticità nella elaborazione dei dati sperimentali. Nel corso del triennio, il candidato ha inoltre maturato una buona cultura di base ed una vasta esperienza diretta in metodiche sperimentali.

firma del Tutor

Firenze, 14/11/2016

A conclusione del corso triennale del XXIX° Ciclo del Dottorato di Ricerca in Scienze Biomediche (*curriculum* Oncologia Sperimentale e Clinica), il Collegio dei Docenti, facendo propria la relazione presentata dal Prof. Annarosa Arcangeli, in qualità di *tutor*, circa l'attività di ricerca, l'operosità e l'assiduità del candidato, rilascia con parere unanime il seguente giudizio da presentare alla Commissione Giudicatrice ai fini dell'espletamento dell'esame finale.

Per quanto sopra, il Collegio dei Docenti unanime ritiene che la Dr. Claudia Durante possa meritatamente aspirare a conseguire il titolo di Dottore di Ricerca.

Firenze, 14/11/2016

Il Coordinatore del Corso  
(XXIX ciclo)  
Prof. Persio Dello Sbarba

All'Ufficio Dottorato di Ricerca

P.zza S. Marco 4 – 50121 Firenze

**DICHIARAZIONE PER IL DEPOSITO ELETTRONICO DELLE TESI DI  
DOTTORATO DI RICERCA**

*(art. 2, comma 2, del “Regolamento per il deposito della tesi di dottorato dell’Università degli Studi di Firenze” emanato con D.R. 1238 del 20 dicembre 2012 - prot. n. 128377)*

Il/La sottoscritta        CLAUDIA DURANTI matricola 14456 . nato/a BAGNO A RIPOLI.

(prov.) FIRENZE il 06/07/1988 residente in PONTASSIEVE (prov.) FI RENZE

Via LORENZO GHIBERTI .n 120 CAP 50065

Stato di residenza (solo per i cittadini stranieri).....

tel...055 8367614..... e-mail claudia.duranti@unifi.it

cell...333 4251293.....

Domicilio (se diverso dalla residenza).....

.....

presso.....

iscritto/a al corso di dottorato di ricerca in SCIENZE BIOMEDICHE (CURRICULUM  
ONCOLOGIA SPERIMENTALE E CLINICA). (ciclo XXIX.)

Coordinatore Prof. Persio Dello Sbarba

Tutore Prof.ssa Annarosa Arcangeli

Dipartimento sede del dottorato Scienze Biomediche Sperimentali e Cliniche

Titolo della tesi "Novel molecular tools in cancer therapy: diagnostic and therapeutic applications of antibodies targeting ion channels and receptors"

Settore scientifico-disciplinare MED/04

Parole chiave: Recombinant antibodies, oncology, molecular tools, *in-vivo* imaging,

### **DICHIARA**

sotto la propria responsabilità, di essere a conoscenza che:

- ai sensi del DPR 28.12.2000 n. 445, le dichiarazioni mendaci, la falsità degli atti e l'utilizzo di atti falsi sono puniti con le sanzioni previste dal codice penale e dalle Leggi Speciali in materia e che nel caso ricorressero tali ipotesi, il/la sottoscritto/a decadrà fin dall'inizio e senza che sia necessaria nessuna formalità dai benefici conseguiti al provvedimento emanato sulla base di tali dichiarazioni;
- l'Università di Firenze provvederà ad effettuare il deposito degli elaborati di tesi, a norma di legge, presso le Biblioteche Nazionali di Roma e Firenze al fine della conservazione e della consultabilità da parte di terzi;
- l'Università di Firenze ha adottato il "Regolamento per il deposito elettronico delle tesi di dottorato dell'Università degli Studi di Firenze" nel quale si stabilisce che i dottorandi indichino l'accessibilità della tesi di dottorato e gli eventuali limiti della stessa, fermo restando che la tesi non è riproducibile, in tutto o in parte, se non con il consenso scritto dell'autore. Sono comunque fatti salvi i diritti dell'Università degli Studi di Firenze di riproduzione per scopi di ricerca e didattici, con citazione della fonte, fatto salvo quanto indicato in merito di embargo ai sensi degli articoli 3 e 4 del suddetto Regolamento;
- l'Università di Firenze ha aderito alla "*Dichiarazione di Berlino per l'accesso aperto alla Letteratura scientifica*";
- il/la sottoscritto/a dovrà depositare la propria tesi nell'archivio istituzionale ad accesso aperto dell'Ateneo che ne garantirà la conservazione e la pubblica consultabilità;

### **DICHIARA INOLTRE**

- che la copia della tesi depositata nell'archivio istituzionale ad accesso aperto in forma elettronica è del tutto identica alle copie consegnate in formato cartaceo ai Commissari e a qualsiasi altra copia depositata negli uffici dell'Ateneo in forma cartacea o digitale e che di conseguenza va esclusa ogni responsabilità dell'Ateneo stesso per quanto riguarda eventuali errori, imprecisioni o omissioni nei contenuti delle tesi;
- di prendere atto che le copie della tesi, in formato cartaceo o elettronico, depositate presso l'Ateneo, costituiranno le uniche copie alle quali l'Università farà riferimento per rilasciare, su richiesta del/la sottoscritto/a, la relativa dichiarazione di conformità;
- che il contenuto e l'organizzazione della tesi è opera originale e non compromette in alcun modo i diritti di terzi, compresi anche quelli relativi alla sicurezza dei dati personali; che pertanto l'Università è in ogni caso esente da responsabilità di natura civile, amministrativa e penale e sarà tenuta indenne, da parte del/la sottoscritto/a, da qualsiasi richiesta o rivendicazione da parte di terzi;

Data 10/02/2017

(firma) 

#### **DICHIARA ALTRESI'**

*(per coloro che hanno attivato o intendono attivare la procedura di embargo o di tutela brevettuale ai sensi degli artt. 3 e 4 del Regolamento per il deposito elettronico delle tesi di dottorato dell'Università degli Studi di Firenze)*

- che la tesi di dottorato è il risultato di attività rientranti nella normativa sulla proprietà industriale, è stata prodotta nell'ambito di progetti finanziati da soggetti pubblici o privati che vincolano la divulgazione dei risultati, è oggetto di eventuali registrazioni di tipo brevettuale o di tutela;
- che la tesi, in quanto caratterizzata da vincoli di segretezza, non dovrà essere consultabile on-line da parte di terzi per un periodo di 12 mesi a partire dalla data di conseguimento del titolo di dottore di ricerca;
- di impegnarsi, allo scadere del dodicesimo mese a partire dalla data di conseguimento del titolo di dottore di ricerca, qualora non ci siano ulteriori proroghe, a immettere in rete la tesi che sarà resa pubblica e consultabile tramite l'archivio istituzionale ad accesso aperto dell'Ateneo;

- che la tesi di dottorato dovrà altresì essere depositata presso le Biblioteche Nazionali Centrali di Roma e Firenze con il vincolo di non consultabilità da parte di terzi per un periodo di 12 mesi, salvo ulteriori proroghe, a partire dalla data di conseguimento del titolo di dottore di ricerca;
- di indicare qui di seguito le motivazioni dei limiti alla consultabilità.

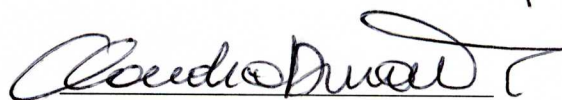
**MOTIVAZIONE DEI LIMITI ALLA CONSULTABILITA':**

Parti di tesi sono già state sottoposte a un editore o sono in attesa di pubblicazione.

La tesi è finanziata da enti esterni che vantano dei diritti su di esse e sulla loro pubblicazione.

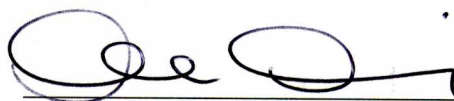
☒ La tesi di dottorato presenta elementi di innovazione per i quali è stata o si intende attivare la procedura di tutela brevettuale.

Data, 10/02/2017



(firma del/della dottorando/a)

Data , 10/02/2017



(firma del tutore)